



**UNESCO-IHE**  
Institute for Water Education

**Deltares**  
Enabling Delta Life  


# **3D Variable-density Groundwater Modelling of the Red River Delta, Vietnam**

Wayangi Lakshani Weerasekera

MSc Number: WSE-GroundwatCH.17.01

Student Number: 48403

August, 2017





# 3D Variable-density Groundwater Modelling of the Red River Delta, Vietnam

Master of Science Thesis  
by  
**Wayangi Lakshani Weerasekera**

Supervisor  
Michael McClain (UNESCO-IHE)

Mentor  
Yangxiao Zhou (UNESCO-IHE)

Examination committee  
Michael McClain (UNESCO-IHE)  
Yangxiao Zhou (UNESCO-IHE)  
Gualbert Oude Essink (Deltires)

This thesis is submitted in partial fulfilment of the requirements for the academic degree of

**Master of Science in Water Science and Engineering**  
UNESCO-IHE Institute for Water Education, Delft, the Netherlands

**Master of Science in Environmental Engineering**  
Instituto Superior Técnico, Universidade de Lisboa, Portugal

**Master of Science in Hydro Science and Engineering**  
Technische Universität Dresden, Germany

MSc research host institution  
[UNESCO-IHE]

Date: August 2017



Although the author and UNESCO-IHE Institute for Water Education have made every effort to ensure that the information in this thesis was correct at press time, the author and UNESCO-IHE do not assume and hereby disclaim any liability to any party for any loss, damage, or disruption caused by errors or omissions, whether such errors or omissions result from negligence, accident, or any other cause.

© W.L. Weerasekera, 2017.

This work is licensed under a [Creative Commons Attribution-NonCommercial 4.0 International License](https://creativecommons.org/licenses/by-nc/4.0/).







# Abstract

The groundwater system of the Red River Delta (RRD), the second largest deltaic plain in Vietnam, is currently under stress due to the rising demand for clean drinking water by the fast growing community. The rapid expansion of industries and intense agricultural activities upsurge the demand on groundwater resources, asking for sustainable groundwater resources management. Henceforth, the current study aims to develop a 3D density dependent groundwater flow and transport model to assist water managers in better understanding the impacts of stresses on their vulnerable groundwater systems. The conceptual model was primarily based on publicly accessible free data and software packages. iMOD-SEAWAT was utilized to assess the potential seawater intrusion in the Red River Delta groundwater system and impacts on it by potential future scenarios.

Paleo-hydrogeologic modelling was executed to evaluate the current salinity distribution status in the deltaic region, which was stated to be influenced by the trapped saline paleo groundwater during eustatic sea level fluctuations. It was tested under two scenarios where one model was assumed to have a uniform sandy aquifer underlying a clay aquitard (SC1). The second model category was implemented with local geology, which was generated with 79 borelogs (SC2). Paleo-reconstruction modelling was simulated for a total duration of 14 kyrs. Hence, final fresh groundwater volumes in the groundwater system were estimated as ~370 and 290 billion m<sup>3</sup> where the paleo-sea water was identified about 70 and 85 km inland in SC1 and SC2 respectively. Comparison of model results with available literature imply a satisfactory correlation with SC2 model.

Groundwater pumping in 1970, 1990 and 2010 was introduced to the model where the groundwater extraction was assumed to be carried out from Pleistocene aquifer. Hence, the depletion of fresh groundwater volume in the Pleistocene aquifer system was calculated to be around 3 billion m<sup>3</sup>. Nevertheless, it developed a serious pumping induced cone of depression under Hanoi.

3D groundwater flow model in the RRD region was then tested for several future scenarios such as keeping a constant pumping rate as in 2010 (FSC1), increasing in pumping rate with the population growth (FSC2), implying mean sea level rise (MSLR) (FSC3) and finally both increasing in pumping rates and MSLR (FSC4). FSC2 model results sum up for a gigantic depletion in groundwater level under Hanoi and other major coastal cities in the Red River area due to tested undue groundwater exploitation. Over exploitation and MSLR together resulted in developing the highest reduction in fresh groundwater volume in aquifers.

**Key words:** Red River Delta, Vietnam, variable-density groundwater flow, 3D model, global data, local geological data, saltwater intrusion, iMOD-SEAWAT, iMOD



# Acknowledgement

I am thankful to Prof. Michael McClain, supervisor of my master thesis for his valuable guidance and instructions provided. I am very much grateful to Associate Prof. Yangxiao Zhou, for his assistant in technical details, dedication, motivated and supervision during the research period. Also, I'd like to extend my sincere gratitude towards Associate Prof. Gualbert Oude Essink, the external mentor from Deltares whom I worked closely with. Special appreciation should be assigned to him for his guidance, motivation and instructions throughout the past 6 months.

I am very much thankful to Daniel Zamrsky and Joeri van Engelen, two PhD researchers from Deltares, Utrecht for their immense assistance in every step and facilitating the necessary data. My project could not have possible without the support and help from Janaka Bamunawala (PhD researcher) and Jeewanthi Sirisena (PhD researcher) from UNESCO-IHE.

My sincerest acknowledgement also goes to the GroundwatCH master programme, its coordinators from IST-Lisbon, IHE-Netherlands and TU-Dresden and also for the ERASMUS MUNDUS scholarship programme to providing me this precious opportunity.

Last but not least, I must express my very profound gratitude towards all my colleagues from UNESCO-IHE and GroundwatCH group.



# Table of Contents

<b>1. Introduction</b>	<b>1</b>
1.1. Background	1
1.2. Problem Statement	2
1.3. Goals and Objectives	3
1.4. Research Questions	3
<b>2. Literature Review</b>	<b>4</b>
2.1. Red River Delta, Vietnam	4
2.1.1. Hydrogeological and Aquifer Properties	6
2.2. Groundwater flow characteristics in Coastal Aquifers	7
2.2.1. Equation of Groundwater Flow	7
2.2.2. Equation of Solute Transport	7
2.2.3. Density of Water	8
2.2.4. Fresh-Saline Interface	10
2.2.5. Consequences of Saline Water	11
2.3. 3D Modelling	12
2.3.1. iMOD-SEAWAT	12
2.4. Paleo Reconstruction Modelling	13
2.4.1. Introduction	13
2.4.2. Sea Level Fluctuation in RRD	13
2.5. Effects of Predicted Mean Sea Level Rise	15
<b>3. Research Methodology</b>	<b>16</b>
3.1. Research Flow	17
3.2. Global Data collection	18
3.2.1. Digital Elevation Model (DEM)	18
3.2.2. Ocean Bathymetry Data	18
3.2.3. Bedrock	19
3.2.4. River Network	20
3.2.5. Land Use	20
3.2.6. Population Density	21
3.3. Local Data Collection	23
3.3.1. Geology	23
3.3.2. Aquifer Property Parameters	24
3.4. Model setup and Simulation	25
3.4.1. Initial Model Setup	25
3.4.2. Paleo – Hydrogeologic Modelling with Only Global Data (SC1)	27
3.4.3. Paleo – Hydrogeologic Modelling with Local Data (SC2)	29
3.4.4. Modelling the Current Status of Delta (SC3)	29
3.4.5. Testing for Future Scenarios (FSC)	29

<b>4. Results and Discussion</b>	<b>31</b>
4.1. Interpretation of Geological Distribution	31
4.2. Development of the Basic Model	34
4.3. Paleo – hydrogeologic Modelling	36
4.3.1. SP0 Model Results	36
4.3.2. SP1 Model Results: 14 - 13 kyrs before present	37
4.3.3. SP2 Model Results: 13 – 11 kyrs ago	38
4.3.4. SP3 Model Results: 11 – 9 kyrs ago	39
4.3.5. SP4 Model Results: 9 – 7 kyrs ago	41
4.3.6. SP5 Model Results: 7 – 4 kyrs ago	43
4.3.7. SP6 Model Results: 4 – 0 kyrs ago	45
4.4. Comparison of Paleo-hydrogeologic Models	47
4.5. Current Status of Red River Delta, Vietnam	49
4.6. Simulation for Future Scenarios	55
4.6.1. Reference Case (FSC1)	55
4.6.2. Increase in Groundwater Extraction Rates (FSC2)	56
4.6.3. Impacts on Predicted MSLR (FSC3)	57
4.6.4. Increase in Groundwater Extraction Rates along with Predicted MSLR (FSC4)	58
4.6.5. Future Scenario Comparison	59
<b>5. Conclusions and Recommendations</b>	<b>61</b>
5.1. Conclusions	61
5.2. Recommendation	63
<b>6. References</b>	<b>61</b>
<b>7. Appendices</b>	<b>64</b>

# List of Figures

Figure 1: Red River Delta, Vietnam.....	5
Figure 2: Density of water as a function of the chlorinity and temperature .....	9
Figure 3: Badon Ghijben-Herzberg principle .....	10
Figure 4: Processes associated with coastal aquifers .....	11
Figure 5: Global eustatic sea level fluctuation during the past 200 kyr .....	14
Figure 6: Effects of the MSLR on coastal aquifers .....	16
Figure 7: Research Flow.....	17
Figure 8: SRTM data on elevation variation in RRD.....	18
Figure 9: Model delta region.....	19
Figure 10: Pumping well locations in the deltaic plain .....	22
Figure 11: Map of borelogs locations.....	23
Figure 12: Variable thickness layers in the model .....	26
Figure 13: Active, inactive and fixed concentration cells in the model domain.....	27
Figure 14: Geology variation along line A-A' a) Winkel et al., 2011 b) 3DSolid-Tool results .....	32
Figure 15: Geology variation along line C-C' a) Winkel et al., 2011 b) 3DSolid-tool results.	33
Figure 16: Geology variation along line D-D' a) Winkel et al., 2011 b) 3DSolid-tool results	33
Figure 17: Improved model boundary conditions; a) IBOUND b) ICBOUND .....	35
Figure 18: a) Velocity distribution of the model with initial conditions b) Velocity distribution of the model with changes .....	35
Figure 19: Concentration variation 14 kyrs ago for a) SC1 b) SC2 .....	36
Figure 20: a) Concentration distribution of SC1 model; 13 kyrs ago b) Saltwater wedge development of SC1 model ( $y = 2190447$ and $y = 2205447$ ) .....	37
Figure 21: a) Concentration distribution of SC1 model; 11 kyrs ago b) Saltwater wedge development of SC1 model ( $y = 2190447$ and $y = 2205447$ ) .....	39
Figure 22: a) Concentration distribution of SC1 model; 9 kyrs ago b) Seawater over topping of SC1 model ( $y = 2206133$ , $y = 2258582$ ) .....	40
Figure 23: a) Concentration distribution of SC1 model; 7 kyrs ago b) Seawater over topping of SC1 model ( $y = 2283955$ ).....	42
Figure 24: a) Groundwater head distribution in SC1 model; 7 kyrs ago b) Groundwater head distribution in SC2 model; 7 kyrs ago .....	43
Figure 25: a) Concentration distribution of SC1 model; 4 kyrs ago b) Seawater over topping of SC1 model ( $y = 2257294$ and $y = 2325446.82$ ).....	44
Figure 26: a) Groundwater head distribution in SC1 model; 4 kyrs ago b) Groundwater head distribution in SC2 model; 4 kyrs ago .....	45
Figure 27: Present day groundwater head distribution a) SC1 b) SC2.....	45
Figure 28: a) Concentration distribution of SC1 model b) Salty paleo water trapped in SC1 model ( $y = 2257294$ and $y = 2325446.82$ ).....	46
Figure 29: Total fresh groundwater volume variation under scenario 1 and 2 .....	48
Figure 30: Freshwater volume variation under scenario 2 .....	48
Figure 31: a) Concentration variation and b) groundwater head distribution in 1970 .....	50
Figure 32: a) Concentration variation and b) groundwater head distribution in 1990 .....	51
Figure 33: a) Concentration variation and b) groundwater head distribution in 2010 .....	51

Figure 34: Area of interest in estimating fresh groundwater volumes .....	52
Figure 35: Total fresh groundwater volume variation in each aquifer type from 1920 to 2010 .....	53
Figure 36: Development of pumping induced cone of depression a) Groundwater head distribution in model layer 7 in 1920 b) Groundwater head distribution in model layer 7 in 2010 c) Head difference in model layer 7 (2010-1920).....	54
Figure 37: a) Concentration distribution in 2110 according to FSC1 b) Head distribution in 2110 according to FSC1.....	55
Figure 38: a) Concentration variation in 2110 under FSC2 b) Groundwater head variation in 2110 under FSC2 .....	56
Figure 39: a) Groundwater concentration and b) head distribution change in FSC2 with respect to FSC1.....	57
Figure 40: a) Concentration variation in 2110 with MSLR b) Groundwater head variation in 2110 with MSLR .....	57
Figure 41: a) Concentration and b) groundwater head distribution change in FSC3 with respect FSC1 .....	58
Figure 42: a) Concentration variation in 2110 with increase in pumping rates and MSLR b) Head variation in 2110 with increase in pumping rates and MSLR .....	59
Figure 43: a) Concentration and b) groundwater head distribution change in FSC4 with respect FSC1 .....	59
Figure 44: Total freshwater volume variation under tested future a) Pleistocene Aquifer b) Holocene Aquifer c) Limestone Aquifer .....	60

# List of Tables

Table 1: Characteristics of aquifer system in the RRD .....	7
Table 2: Water classification.....	9
Table 3: Groundwater pumping rates .....	22
Table 4: Model inputs of hydraulic conductivity, vertical anisotropy factor, specific storage and porosity values .....	24
Table 5: Sources of data collection .....	24
Table 6: Paleo-hydrogeologic model details.....	28
Table 7: Description of tested FSC models .....	30
Table 8: Fresh groundwater volume variation in paleo-reconstruction modelling under SC1 and SC2 .....	49



# Abbreviation

MSLR	Mean sea level rise
IPCC	Intergovernmental Panel on Climate Change
RRD	Red River Delta
TDS	Total dissolved solids
EC	Electrical conductivity
WHO	World Health Organization
FAO	Food and Agriculture Organization
GDP	Gross Domestic Product
DEM	Digital elevation model
PCA	Pleistocene confined aquifer
HUA	Holocene unconfined aquifer
NWL	Neogene water bearing layer
MFZ	Mesozoic fractured zones
HPA	Holocene-Pleistocene aquitard
SRTM	NASA Shuttle Radar Topographic Mission
USGS	United States Geological Survey
HydroSHEDS	SHuttle Elevation Derivatives at multiple Scales
GPW	Gridded Population of the World
GEBCO	General Bathymetric Chart of the Oceans
IDW	Inverse Distance Weighting
AMSL	Above Mean Sea Level
BMSL	Below Mean Sea Level
FAO	Food and Agriculture Organization
MODFLOW	Modular Three-Dimensional Finite-Difference Ground-Water Flow-Model
SEAWAT	Generic MODFLOW/MT3DMS-based computer program designed to simulate three-dimensional variable-density groundwater flow coupled with multi-species solute and heat transport
MT3DMS	Modular Transport Three Dimensional Model Simulator
WGS	World Geodetic System
UTM	Universal Transverse Mercator



# **CHAPTER 1**

## **Introduction**

### **1.1. Background**

Deltaic regions of the world represent only about 1% of the global land area, yet provide habitats for more than half a billion people, creating a very high demand for freshwater in their vicinities (Szabo et al., 2016). Conjunction existence of dense population, intense agriculture and socio-economic developments have created dynamic ecological and social environments in these delta plains. Urbanization and the ever increasing population will certainly intensify the freshwater demands and thus, increase the vulnerability of the fresh groundwater sources within the world's coastal regions.

As a consequence of global climate change(s), sustainability of the world's coastal systems will be directly affected by the predicted mean sea level rise (MSLR) (Brakenridge et al., 2013). These effects will escalate the risks of coastal flooding and storms surges (Yang et al., 2015) and increase the rate of wetland depletions. Further, the combined effect of MSLR and land subsidence (often caused by large overexploitation, e.g. Minderhout et al., 2017) will exacerbate the pressures exert on delta regions and it will subsequently impact the groundwater resources (Szabo et al., 2016). Moreover, changes in precipitation and evaporation will lead to more uncertainties in river discharges, resulting in significant fluctuations of salinity levels within these deltaic regions (Nohara et. al., 2006; Yang et al. 2015). Combined effect of the aforementioned multiple threats on the fresh groundwater resources of the world's deltaic regions is substantial and could easily result in drastically diminishing its freshwater quantity and quality.

According to the IPCC 5th assessment report, water resources scarcity is identified as an emerging threat in Asia (Hijioka et. al., 2014). Moreover, predicted MSLR will affect the coastal inhabitants of South and South-East Asian regions. Further, they have also clearly identified that most of these large deltaic systems are contemporary sinking as a result of intense groundwater extractions (Minderhout et al., 2017).

Numerical modelling of groundwater systems in coastal deltas under various environmental and anthropogenic impacts is an approach that can be adopted to investigate the behaviour of

deltaic systems under different scenarios. Given the aforementioned environmental and social-economic concerns, development of a numerical model that can estimate the extent of seawater intrusion into groundwater systems in deltaic areas will enable water managers, engineers and scientists to scrutinize the probable anthropogenic and environmental impacts on groundwater resources. Outcomes of such models have an integral role in developing sustainable coastal zone or environmental management plans.

## 1.2. Problem Statement

Red River Delta (RRD) in Vietnam is one of the largest deltas in Southeast Asia region, spanning over 21,000 km<sup>2</sup> (Tran et al., 2012). Despite the fact that this region has ample amounts of surface water, the insufficiency of infrastructures like dams, reservoirs, sewage systems have already created massive amounts of water quality issues and high levels of suspended deposits in rivers and inland water bodies. Most of the fresh surface water bodies in major cities of the delta plain have already exceeded the threshold concentration level of heavy metal (e.g. Arsenic), making use of those surface water bodies unreliable, difficult or expensive (Nguyen et. at., 2011). Therefore, the present water demands for agriculture, domestic and industrial usage in the region are been satisfied by groundwater extraction (Tran et al., 2012).

Further, rapid industrialization, urbanization and intensified agricultural practices have created a greater demand on freshwater, forcing these groundwater extractions to be carried out at unprecedented magnitudes. Thai Binh and Nam Dinh, two provinces in the northern Vietnam, located within the territory of RRD are already suffering the consequences of these massive groundwater extractions. They have recorded significantly depleting groundwater tables (in a range of 4 to 8 m) and drying up of shallow wells (Van Pham and Lee 2014). The declination of groundwater levels have ultimately resulted in saltwater intrusion (Van Pham and Lee 2014).

Besides these anthropogenic activities, owing to its relatively flat and low-lying geographic layout of these areas, MSLR is also likely to play an integral role in saltwater intrusion to the RRD. During the past 15 years, sea-level has risen up at a rate of 3 mm/year, while the future predictions indicate a staggering 100 cm of sea level rise by 2100 (Van Pham and Lee 2014). Most importantly, researchers have identified the probable saline intrusion extent in RRD region to be as high as 30 – 50 km by considering only the probable groundwater extractions (Van Pham and Lee 2014). This condition is likely be further exacerbate with the MSLR predictions (Dasgupta et al., 2009, Dzung et al., 2014 and Neumann et. al., 2015). Meanwhile, it is also known that the saltwater intrusion rate in groundwater systems in RRD is affected considerably by the relatively high land subsidence rate of the area (~1 mm/year) and reduced fluvial sediment supply to the delta (Tran et al., 2012).

### **1.3. Goals and Objectives**

The main goal of this study is to develop a 3D variable-density groundwater flow and coupled salt transport model that can demonstrate the current status of the aquifer system at Red River Delta in terms of its groundwater quality and quantity and to use it for assessing the effect of climate and anthropogenic changes driven responses of the aquifer system.

The specific objectives of the research study are as the following:

- Characterizing the hydrogeology of the Red River Delta plain
- Analyzing and conceptualizing of the groundwater flow system in relation to seawater intrusion
- Constructing a 3D variable density saline intrusion model using global data
- Paleo reconstruction modelling
- Improving the model accuracy by implementing the local data
- Formulating and simulating climate change and groundwater extraction scenarios

### **1.4. Research Questions**

This research study targets to explore and address the following main questions:

1. How does the eustatic sea level variation affect Red River Delta from a groundwater point of view?
2. Is it reasonable to utilize global data for modelling in a data scarce region; and what is the quality of the product/result?
3. What is the current state (baseline scenario) of the fresh-saline distribution in Red River Delta?
4. What is the impact on saltwater intrusion with respect to mean sea level rise and an increase in groundwater pumping on the system?
5. Which scenario has the highest impact on saltwater intrusion

## **CHAPTER 2**

# **Literature Review**

## **2.1. Red River Delta, Vietnam**

Vietnam is the easternmost country on the Indo-China Peninsula in Southeast Asia (Nguyen, 2008). According to the World Bank statistics published in 2015, Vietnam has a population of 91.7 million with a GDP of \$193.6 billion and a GDP growth rate of 6.7%. Currently, Vietnam's GDP per capita growth rate is among the fastest in the world, categorizing Vietnam into a lower-middle income country (World Bank Group, 2016).

On the other hand, Vietnam has also been ranked as one of the top five most vulnerable countries to climate change (Hijioka et. al., 2014). The exposure to climate change driven pressures will have numerous adverse consequences to the country's groundwater resources (Van Pham and Lee 2014). Average annual temperature of the country has increased by 0.5 to 0.7 °C over the past 50 years. Furthermore, the average annual precipitation has also been increased within the northern parts of Vietnam over the same time period. Additionally, the World Bank reports have also reported the fact that Vietnam is highly vulnerable to climate change, where economic losses have been estimated around 1 -1.5 percent of GDP over the past two decades (World Bank Group, 2016). Thus, country's ecosystems need much more attention for its sustainability against these multiple threats.

The Red River Delta (RRD) or Song Hong Delta is located in the north of Vietnam, centring the Red River as shown in Figure 1. It originates in Yunnan Province, China and drains across an area of 160,000 km<sup>2</sup>, nourishing about 19.8 million inhabitants and finally falls into the Gulf of Tonkin (Gulf of Bac Bo) (Tran et al. 2012 and Li et al. 2006). It is the second largest river system in Vietnam, which provides significant contributions to the country's economy. Annual discharge of river water to the estuary is about 84 billion m<sup>3</sup>, which varies significantly over the dry and wet seasons (Hien et al., 2010).

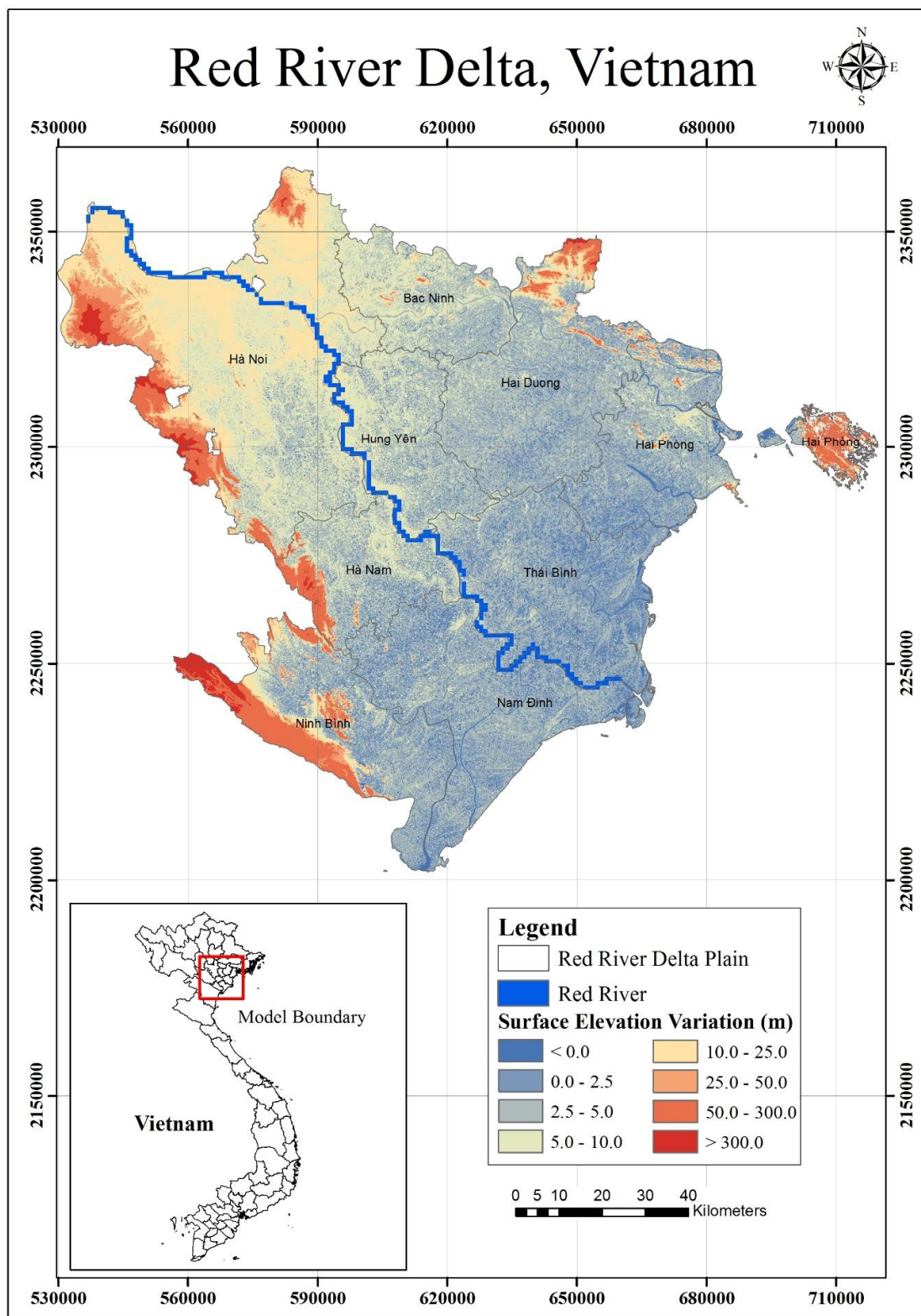


Figure 1: Red River Delta, Vietnam

RRD has a relatively flat terrain, where the land areas below 2 m are often flooded during the rainy seasons (Van Pham and Lee 2014). Further, the delta is characterized by tropical monsoonal climatic system with a noticeable maritime influence. The average annual rainfall of this area varies around 1300 – 1800 mm, where 85% of that rainfall is received during the summer rainy season (April to October). Thus, RRD has warm and humid summer with average temperatures fluctuating from 27° C to 29° C, where winter season is relatively cool and dry with an average temperature of about 16° - 19° C. The mean tidal range of the area varies in between 1.9 – 2.6 m, whereas the maximum tidal range is recorded to be around 3.2 – 4 m on average (Li et al. 2006).

Paddy fields dominate the region's land cover, accounting for about 68%. Urban and rural areas account for 16% the total area, while surface water bodies accounts for about 11% of the land. RRD plain also has fish and shrimp aquacultures in smaller scales (5%). Four major rivers flow through the RRD plain, namely Red River, Dao River, Ninh Co River and Day River. Water levels in these rivers have strong spatial and seasonal signals (Van Pham and Lee 2014).

### **2.1.1. Hydrogeological and Aquifer Properties**

RRD plain composes of five distinguishable hydrogeological units, where only two of them play an economical role in terms of groundwater resources (Van Pham and Lee 2014). Holocene unconfined aquifer (HUA) is the top most aquifer, which is distributed over an area of about 11,450 km<sup>2</sup>, accounts for about 88% of the delta. This aquifer is followed by a confining aquitard layer aging from Holocene to Pleistocene (HPA), is sandwiched between HUA and Pleistocene confined aquifer (PCA). HPA is mostly under the HUA and only exposed to the surface around the northern border of the delta. PCA is generally placed under both HUA and HPA and distributed almost entirely in the delta region. At the border of the delta, exposed Mesozoic bedrocks create mountainous areas, which develop the Mesozoic fractured zones (MFZ). Geological cracks and erosion in Mesozoic bedrock are capable of storing and transmitting water and recharge the aquifer systems. Neogene water bearing layer (NWL), which is lying directly over the bedrock contains cleft and karst water aging from the Neogene period of the Cenozoic era to the Triassic period of the Mesozoic era (Bui et al., 2011). Among all the available hydrogeological units, HUA and PCA play an integral role in groundwater storage and provide economical values to the groundwater resources.

Table 1: Characteristics of aquifer system in the RRD

Source: Bui et al., 2011

Aquifer system	Geological ages	Hydrogeo-logical conditions	Depth to the layer's top (m)	Thickness (m)	$q$ (L/s/m)	TDS (g/L)	$T$ (m <sup>2</sup> /day)	$S_y/S$	Materials	Groundwater potential	Groundwater storage capac-ity (billion m <sup>3</sup> )
HUA	Holocene	Unconfined aquifer	0	0–60	0.3–20.87	0.02–19.83	10–2,123	0.09–0.1	Clay slurry, sandy dust, and gray sand	High potential	10
HPA	Holocene-Pleistocene	Aquitard	0–60	0–40	No data	No data	No data	No data	Silty clay, clay sand, clay	No potential	No data
PCA	Pleistocene	Confined aquifer	0–70	0–80	0.04–71	0.01–23.39	1–6,720	0.00004 –0.145	Mediumcoarse sands, gravel, cobble Cemented gravel, cemented clay, arkosic sand-stone, argillite, and clay carbon	Highest potential	13
NWL	Neogene	Discontinu-ous aquifer	0–100	0–1,000	0.1–15.1	0.1–12.2	1–3,724	No data	Sandstone and porphyry	Medium potential	No data
MFZ	Mesozoic	Fractured zones	No data	No data	0.12–6.15	0.15–0.293	64–305	No data		Low potential	No data

## 2.2. Groundwater flow characteristics in Coastal Aquifers

Salinity concentration levels in groundwater result in water densities different from freshwater (1000 kg/m<sup>3</sup>), which ultimately cause serious impacts on flow systems. This phenomenon of variable-density groundwater flow and coupled salt transport has to be accounted properly in developing sustainable coastal aquifer management plans.

### 2.2.1. Equation of Groundwater Flow

Groundwater flow in aquifer systems is facilitated by pores medium with interconnected pores or openings. Generally, voids in pores mediums are occupied by either water or air or both. Availability of these fluid phases in pores medium obscure the studies on groundwater flow systems. However, groundwater flow is calculated by considering the equation of continuity and equation of motion (Oude Essink, 2001). Equation 1 discloses the groundwater flow equation, which considers Darcy's Law, continuity equation, sources, sinks and transient flow to calculate the relevant groundwater flow.

$$\frac{\partial}{\partial x} \left( K_{xx} \frac{\partial h}{\partial x} \right) + \frac{\partial}{\partial y} \left( K_{yy} \frac{\partial h}{\partial y} \right) + \frac{\partial}{\partial z} \left( K_{zz} \frac{\partial h}{\partial z} \right) - W = S_S \frac{\partial h}{\partial t} \quad \text{-----Equation 1}$$

### 2.2.2. Equation of Solute Transport

Groundwater flow primarily depends on density differences, where the presence of solutes can alter the flow quite significantly. Coastal aquifers signify the above-described phenomenon, where solute transport in groundwater is described by the two-dimensional advection-dispersion equation. Advection-dispersion equation can be stated for a conservative solute (such as chloride ion) as shown in Equation 2 (Oude Essink, 2001).

$$\frac{\partial C}{\partial t} = \frac{\partial}{\partial x_i} \left( D_{ij} \frac{\partial C}{\partial x_j} \right) - \frac{\partial}{\partial x_i} (C V_i) + \frac{(C - C') W}{n_e D} \quad \text{Equation 2}$$

Where C - Concentration of the dissolved solids

$D_{ij}$  - Coefficient of hydrodynamic dispersion

$V_i$  - Effective velocity of the groundwater in the direction of  $x_i$

$C'$  - Concentration of the dissolved solids in a source or sink

W - Sources and sinks

D - Saturated thickness of the aquifer

Equation 2 is a combination of the impacts on hydrodynamic dispersion and advection taking place due to the changes of solute concentrations. Hydrodynamic dispersion consists of mechanical dispersion and molecular diffusion. Mechanical dispersion is caused by the velocity variations at microscopic scale. Solute dispersion depends on both fluid flow and the characteristics of the pore system. On the other hand, molecular diffusion is caused by the random movements of the molecules in fluid, which depends on the concentration gradients and the properties of the fluid and the soil. Under normal conditions, molecular diffusion is negligible compared to the hydrodynamic dispersion. Further, exact determination of hydrodynamic dispersion is a non-trivial task due to the scale dependency, fingering, transient effects, aquifer heterogeneity and anisotropy effects (Oude Essink, 2001).

### 2.2.3. Density of Water

Under the normal conditions, the influence of pressure and temperature on water density can be neglected, especially when compared with the influence caused by dissolved solids concentration (Figure 2). Thus, density of water is often considered to be related to the amount of total dissolved solids (TDS). Further, in coastal groundwater aquifers, Chloride (Cl) is the predominant negative ion to be considered when estimating the groundwater density and salinity level. Salinity concentration can be expressed by different ways, such as;

- concentration in milligrams of chloride per litre of water (mg Cl/l)
- measuring TDS concentration (mg/l)
- assessing the Electrical Conductivity (EC) (mS/cm)

EC can be converted into salinity using the following equation (Equation 3) (Faneca Sanchez et al., 2015).

$$Cl \text{ (g/l)} = EC \text{ (mS/cm)} \times 0.36 - 0.45 \quad \text{Equation 3}$$

Water can be classified into several categories in terms of EC and salinity concentrations levels. One such classification, published by the Food and Agriculture Organization (FAO) is given in Table 1 (Rhoodles *et. al.*, 1992).

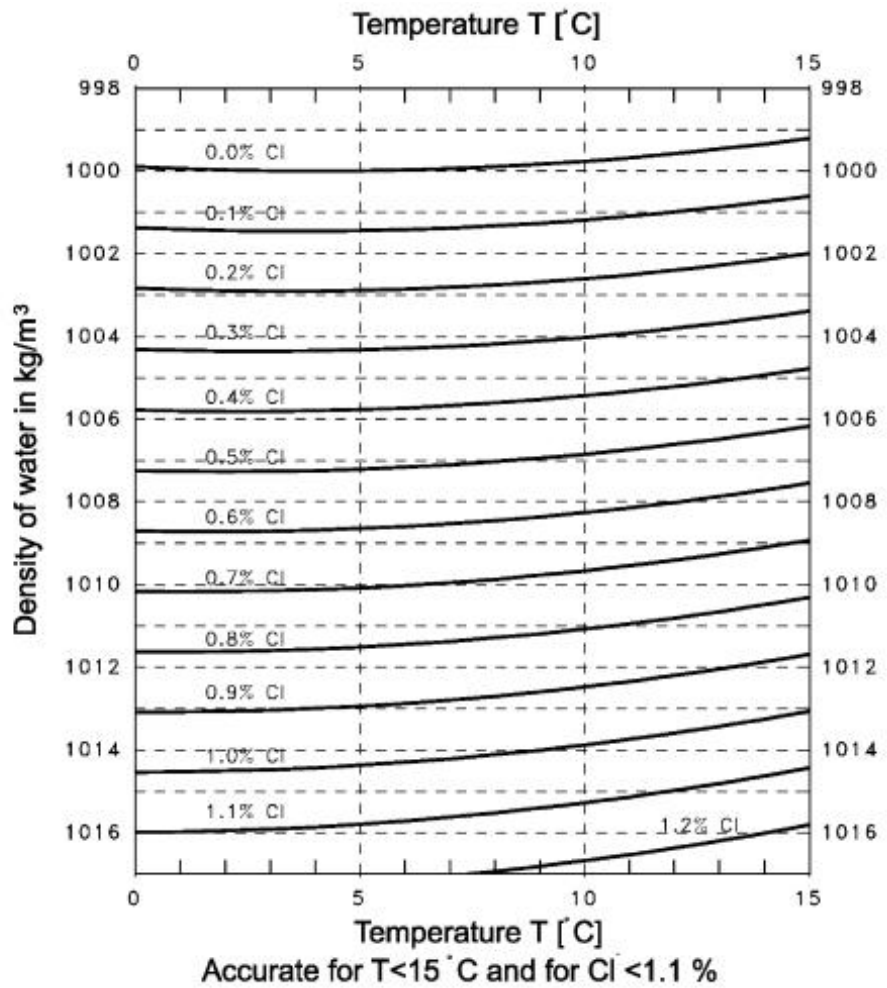


Figure 2: Density of water as a function of the chlorinity and temperature  
Source:(Oude Essink, 2001)

Table 2: Water classification

Water Class	EC (dS/m)	Salt concentration (mg/l)	Type of water
<b>Non-saline</b>	< 0.7	< 500	Drinking and irrigation water
<b>Slightly saline</b>	0.7 – 2	500 - 1500	Irrigation water
<b>Moderately saline</b>	2 – 10	1500 – 7000	Primary discharge water and groundwater
<b>High saline</b>	10 – 25	7000 – 15000	Secondary discharge water and groundwater
<b>Very high saline</b>	25 – 45	15000 – 35000	Very saline groundwater

<b>Brine</b>	> 45	> 35000	Seawater
--------------	------	---------	----------

#### 2.2.4. Fresh-Saline Interface

The fresh-saline interface is a complex, sensitive and dynamic interface and being closely scrutinized the coastal groundwater management frameworks (Kim et al., 2007). Although the density difference is small, it is very important in estimating groundwater flow in coastal aquifer systems. The Badon Ghijben-Herzberg principle (BGH) is a straightforward concept used to estimate the position of fresh-saline interface (Oude Essink, 2001).

$$\text{Pressure saline groundwater} = \text{Pressure fresh groundwater}$$

$$\rho_s hg = \rho_f (H + h)g$$

$$h = \alpha H$$

$$\text{Where; } \alpha = \frac{(\rho_s - \rho_f)}{\rho_f} \text{-----Equation 4}$$

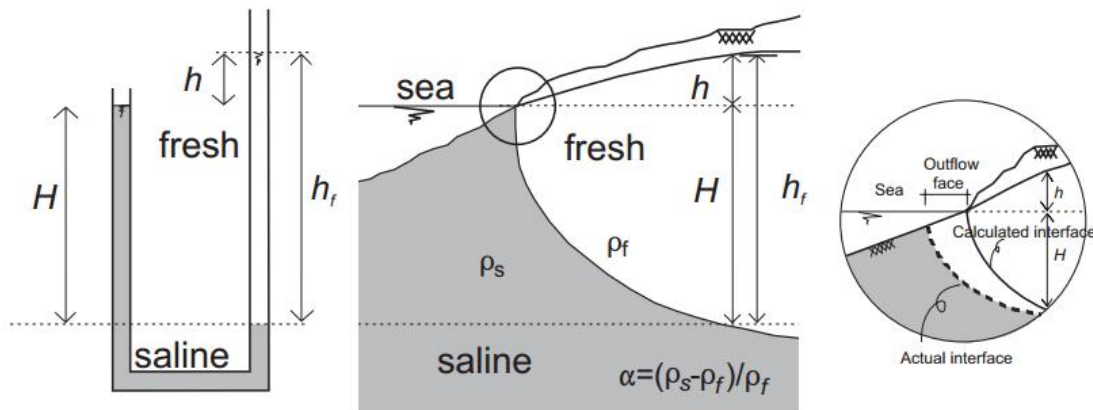


Figure 3: Badon Ghijben-Herzberg principle

Source (Oude Essink, 2001)

Equation 4 is valid only with horizontal flow in the freshwater zone and stagnant saltwater and its application is valid under the following conditions.

- The aquifer is homogeneous
- Hydrodynamic dispersion is negligible
- Vertical flow in the aquitard, horizontal flow is negligible
- Horizontal flow in the aquifer, vertical flow is negligible
- Salt groundwater is at rest

Figure 4 expresses the processes associated with coastal aquifer systems that determine the stability of the fresh-saline groundwater interface.

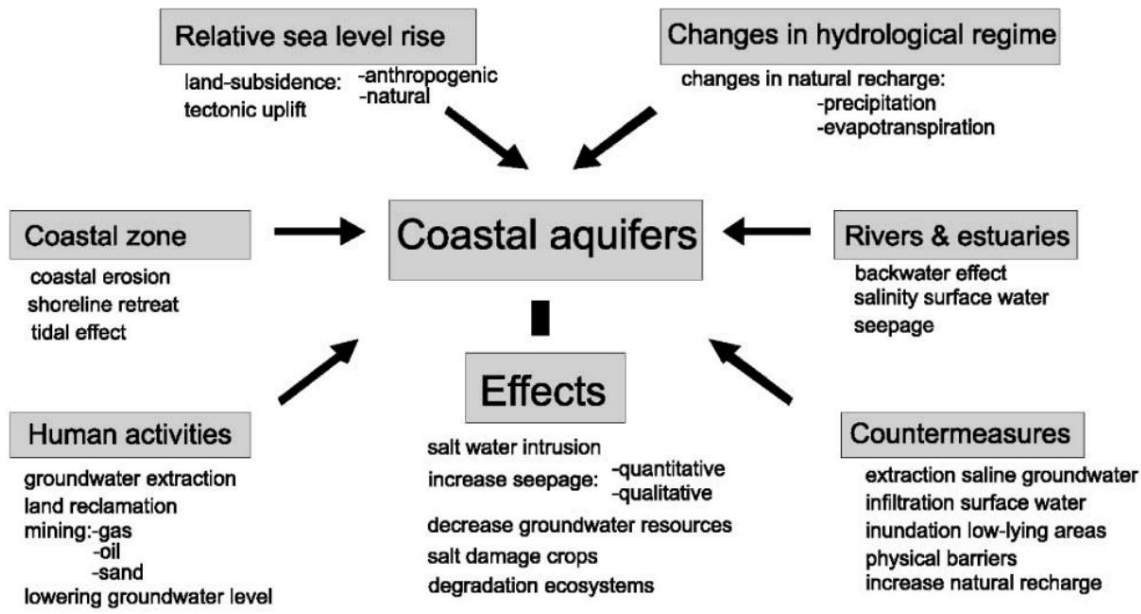


Figure 4: Processes associated with coastal aquifers

Source (Oude Essink, 2001)

## 2.2.5. Consequences of Saline Water

According to the guidelines published by the World Health Organization (WHO), taste of drinking water is affected with the chloride concentrations of water exceed 250 mg/l (WHO, 1996). Further, higher salt concentrations may produce a laxative effect and may dehydrate the human body. Dehydration can also occur in plants via the plant osmosis process, which may reduce the plant's yield or even cause its death at higher concentrations. Higher salt concentrations can deplete the ecological health of the streams and estuaries, which have direct implications on the riparian zones as they occupy the lowest parts of the landscape, where most of the saline groundwater is released to the surface. High salinity levels also lead to accelerate soil erosion processes as well.

Salinity can have direct implications on human through;

- cost to rural communities of declining population
- loss of business
- cost of rural restructure when farms become unprofitable
- increase health problems due to stress on families affected by the changes

Further, salinity may also indirectly affect people by reducing the quality of the natural environment (Queensland Government, 2016).

## 2.3. 3D Modelling

This study estimates the dynamics of the fresh-saline groundwater distribution through a 3D model developed by the use of iMOD-SEAWAT. It is a modified version of SEAWAT v4.00.05, which couples MODFLOW and MT3DMS including variable-density into a user-friendly version of modelling the groundwater flow systems. Further, iMOD facilitates the construction of models with SEAWAT and the visualisation and edition of input and output model data. iMOD-SEAWAT output files can also be visualize and analyse with Tecplot.

### 2.3.1. iMOD-SEAWAT

Variable-density groundwater flow is estimated in SEAWAT through the equation given below (Langevin et al., 2007).

$$\nabla \cdot \left[ \rho \frac{\mu_0}{\mu} K_0 \left( \nabla h_0 + \frac{\rho - \rho_0}{\rho_0} \nabla_z \right) \right] = \rho S_{s,0} \frac{\partial h_0}{\partial t} + \theta \frac{\partial \rho}{\partial C} \frac{\partial C}{\partial t} - \rho_s q'_s \quad \text{Equation 5}$$

Where;

$\rho_0$  – Fluid density at the reference concentration and the reference temperature

$\mu$  – Dynamic viscosity

$K_0$  – Hydraulic conductivity tensor of the material saturated with the reference fluid

$h_0$  – Hydraulic head measured in terms of the reference fluid of a specified concentration and temperature

$S_{s,0}$  – Specific storage

$t$  – Time

$\theta$  – Porosity

$C$  – Salt concentration

$q'_s$  - Source or sink of fluid with density  $\rho_s$

Further, the general equation for the state for fluid density can be expressed as;

$$\rho = \rho_0 \exp [\beta_C (C - C_0) + \beta_T (T - T_0) + \beta_P (P - P_0)] \quad \text{Equation 6}$$

Where  $\beta_C$ ,  $\beta_T$  and  $\beta_P$  are defined as expansion coefficients for solute concentration, temperature and pressure.  $\beta_C$ ,  $\beta_T$  and  $\beta_P$  are to be estimated with following equations.

$$\beta_C = \frac{1}{\rho} \left( \frac{\partial \rho}{\partial C} \right)_{T,P} \quad \beta_T = \frac{1}{\rho} \left( \frac{\partial \rho}{\partial T} \right)_{C,P} \quad \beta_P = \frac{1}{\rho} \left( \frac{\partial \rho}{\partial P} \right)_{C,T}$$

In case of existence of multiple solute concentrations that can affect the fluid density, Equation 5 is modified with the exception of pressure term. In SEAWAT, the equation used

to describe the state is as Equation 7. Further, the current study considers the density differences derived on the salinity distribution.

$$\rho = \rho_0 + \sum_{k=1}^{NS} \frac{\partial \rho}{\partial C^k} (C^k - C_0^k) + \frac{\partial \rho}{\partial T} (T - T_0) + \frac{\partial \rho}{\partial l} (l - l_0) \text{ -----Equation 7}$$

where;

NS - Number of solute species

$l$  - Height of a water column

## 2.4. Paleo Reconstruction Modelling

### 2.4.1. Introduction

Variable density groundwater flow modelling is one of the strategies that can be used to assess coastal freshwater resources for management and planning frameworks. Therefore, it is essential to have proper initial salinity concentration distribution for the model due to the density feedback of salinity concentration on variable-density groundwater flow. In general, steady state simulation with current boundary conditions provides the initial quantitative inputs for the variable-density groundwater models. Yet, a coastal groundwater system is rarely in equilibrium and often reflects the events that have occurred thousands to sometimes millions of years ago.

Paleo reconstruction modelling or transient modelling is therefore a possible way to develop the initial salinity concentrations. This process involves starting a model at a reference point in time where salinity distribution is either more or less known or certain to be non-influential to the present day salinity distribution. Paleo hydrogeologic modelling is a comparatively challenging task due to the lack of data on paleo-boundary conditions within the considered time scales. Furthermore, it is impossible to validate the models on historical time frames (Delsman et al., 2014). Nevertheless, Delsman et al, 2014 also shows that the end result of paleo reconstruction modelling over the Holocene, viz. the salinity distribution, matches pretty well with present day salinity distributions in some coastal zones. This demonstrates that the present salinity distribution is a function of past historical time frames.

### 2.4.2. Sea Level Fluctuation in RRD

The geological and geomorphological developments of the RRD plain were predominantly controlled by the eustatic sea level changes in the South China Sea. It has direct implications on the Pleistocene and Holocene sedimentation in the region. Therefore, paleo-hydrogeologic modelling in RRD plain will be beneficial for the variable-density groundwater flow model in the current study. The largest regressive phase of the eustatic sea level changes during the Quaternary period has taken place during the middle to upper Pleistocene and the maximum transgression has occurred during the middle Holocene. Figure 5 illustrates that before 20

kyrs, sea level used to be 120 m below its present level, mainly due to the pressure exerted by the massive ice caps on the continental shelves.

From its lowest point recorded, sea level has gradually increased over the time and a stable sea level state was reached about 8.5 kyr ago. Yet, the sea level remained escalating continuously and has achieved a state of about 3 – 5 m above the present MSL. This phenomenon has taken place around 6 – 4 kyr ago and then the sea level has started declining to reach the present sea level. Therefore, near surface layers with marine sediments are dominated by fine sand and clays. They are known as marine terraces, which are the dominant sediment type in the RRD flood plain. During the Holocene period, flood plain progressed inland as far as the present location of Hanoi where the estimation of aforementioned phenomenon is beneficial to the current study. The most inland Holocene marine terraces must have been deposited during the last sea level high stand. Further, the older near surface marine deposits are possibly placed during the lower or middle Pleistocene age. They reveal that the sea in the Quaternary period must have submerged larger areas of the flood plain. Later, rivers have eroded the marine terraces and subsequently deposited the coarse grained fluvial deposits and form the near surface sediments (Tran et al., 2012 and Larsen et al., 2017).

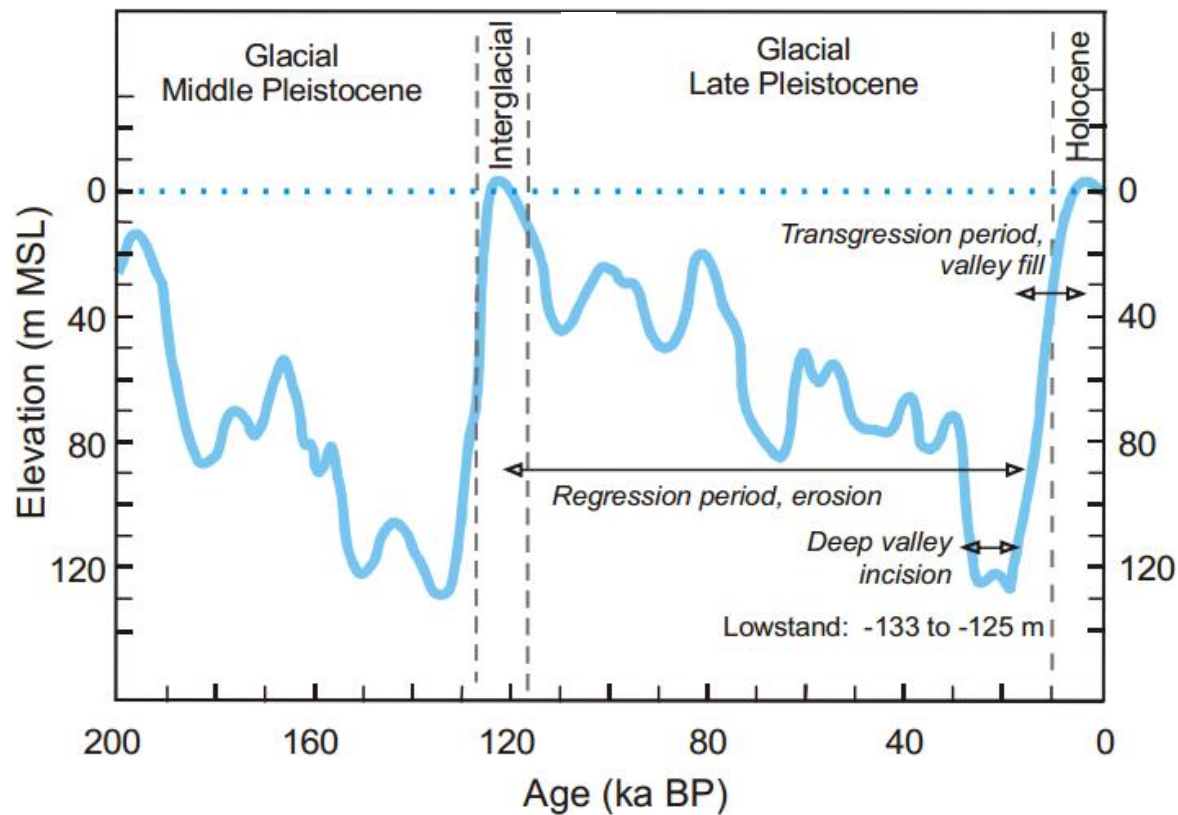


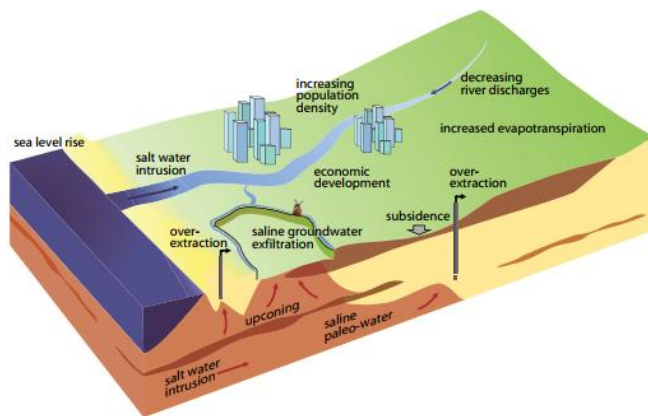
Figure 5: Global eustatic sea level fluctuation during the past 200 kyr

Source: (Waelbroeck et al., 2002)

## 2.5. Effects of Predicted Mean Sea Level Rise

As shown in Figure 6, MSLR has been identified as a serious issue for global coastal groundwater systems. The rate of MSLR has been increased during the past century, pressurising the groundwater resources. Ocean thermal expansions, glacier melt and the changes in terrestrial storages are listed as the driving forces towards MSLR (Dasgupta et al., 2009).

Coastal surface water resources are directly influenced by the MSLR with storm surges, wave attack, flooding and collapse of coastal protection systems. Further, MSLR can cause coastal erosion extending to shoreline retreat. This will directly affect the groundwater aquifer systems. Moreover, anthropogenic activities have reduced the sediment transport in rivers, which in combined with MSLR results in increasing the saltwater intrusion process. Increased salinity levels in rivers, estuaries and deltas are a threat to the sustainability of underlying groundwater aquifers. Coastal aquifers within the zone of influence of MSLR have a higher possibility to encounter saltwater intrusion. Seepage will increase the aquifer salinity level, while decreasing the fertility of the soil. The fresh-saline groundwater mixing zone and the interface will also move further inland. Finally, the groundwater pumping wells, which were previously situated outside the salinization zone will then be situated inside the salinization zones, at which the groundwater uptake will result in massive saltwater intrusion and brackish groundwater upconing. Therefore, MSLR, associated with human activities can disrupt the stability of the groundwater resources and induce more pressure on groundwater sustainability.



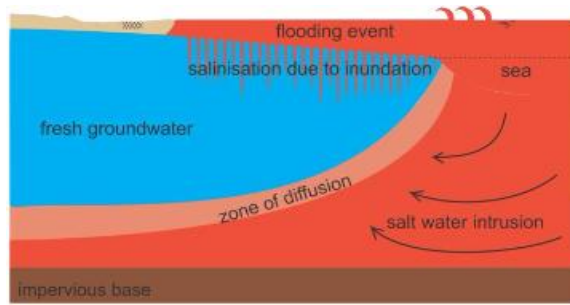


Figure 6: Effects of the MSLR on coastal aquifers

Source: Delsman, 2015 and Faneca et. al., 2015

## CHAPTER 3

# Research Methodology

### 3.1. Research Flow

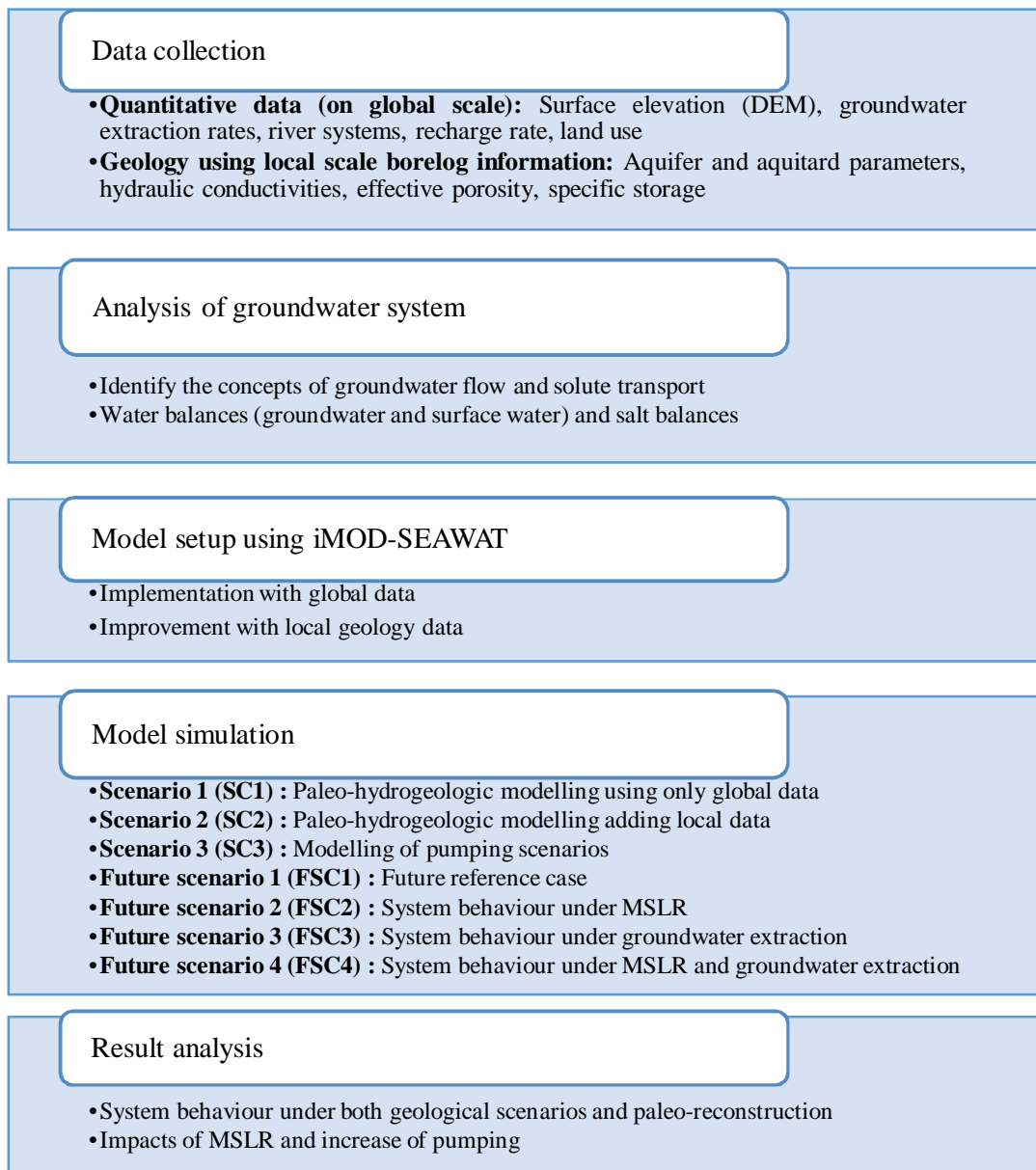


Figure 7: Research Flow

Figure 7 demonstrates the research methodology followed during the current study. It primarily consists of several steps such as data collection, analysis of groundwater system available in the deltaic region, model setup using iMOD-SEAWAT, model simulation and results analysis. Detailed descriptions of each stage are available with the following sections.

## 3.2. Global Data collection

### 3.2.1. Digital Elevation Model (DEM)

NASA Shuttle Radar Topographic Mission (SRTM) has developed ground elevation data for the whole world with a resolution of 3 arc second (approximately 90 m). It is freely downloadable from the National Map Seamless Data Distribution System, or from the United States Geological Survey (USGS) FTP site. There is another data set of 1 arc second resolution which is available for several parts of the world. The vertical error of the DEM data is reported to be less than 16 m (Jarvis et. al., 2008). Figure 8 represent the downloaded data on RRD elevation variation from SRTM.

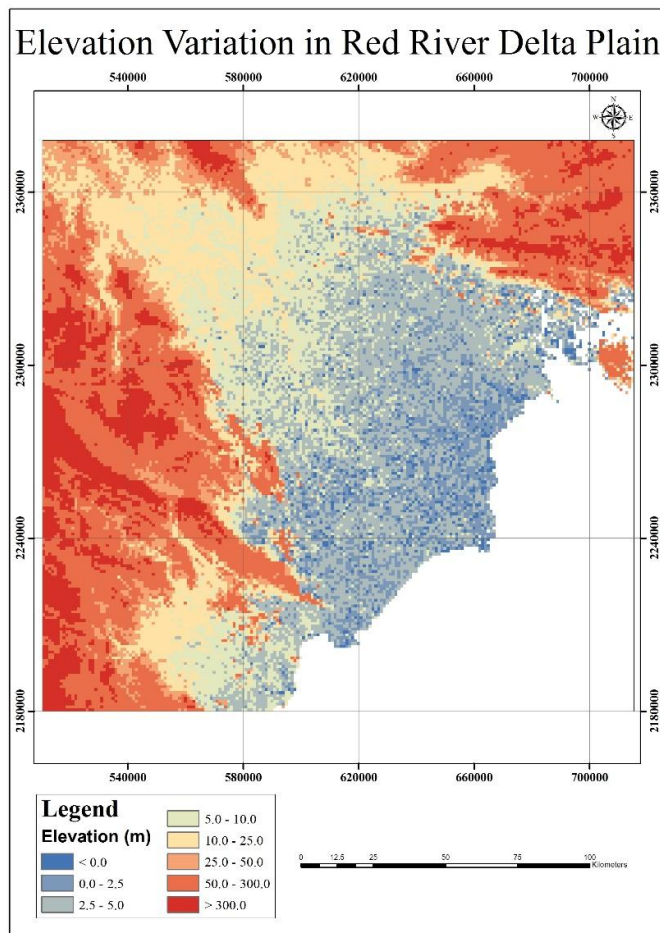


Figure 8: SRTM data on elevation variation in RRD

### 3.2.2. Ocean Bathymetry Data

General Bathymetric Chart of the Oceans (GEBCO) offers 30 arc second resolution, publicly available bathymetry data sets for the world's oceans. It is available in NetCDF, Esri ASCII, raster or INT16 GeoTIFF formats (Sandwell et. al., 2002).

SRTM-DEM and GEBCO data together furnished the necessary input information for the top layer of the model as shown in Figure 9. The RRD plain is relatively flat and lies below 3 m above mean sea level (AMSL) and much of it even does not exceed 1 m. The delta plain is surrounded by a mountain region with a maximum elevation of about 1,300 m and is composed of crystalline rocks from Palaeozoic and Mesozoic sedimentary rocks (Tran et al., 2012). Bathymetric data indicates a maximum offshore depth of 41 m below mean sea level (BMSL).

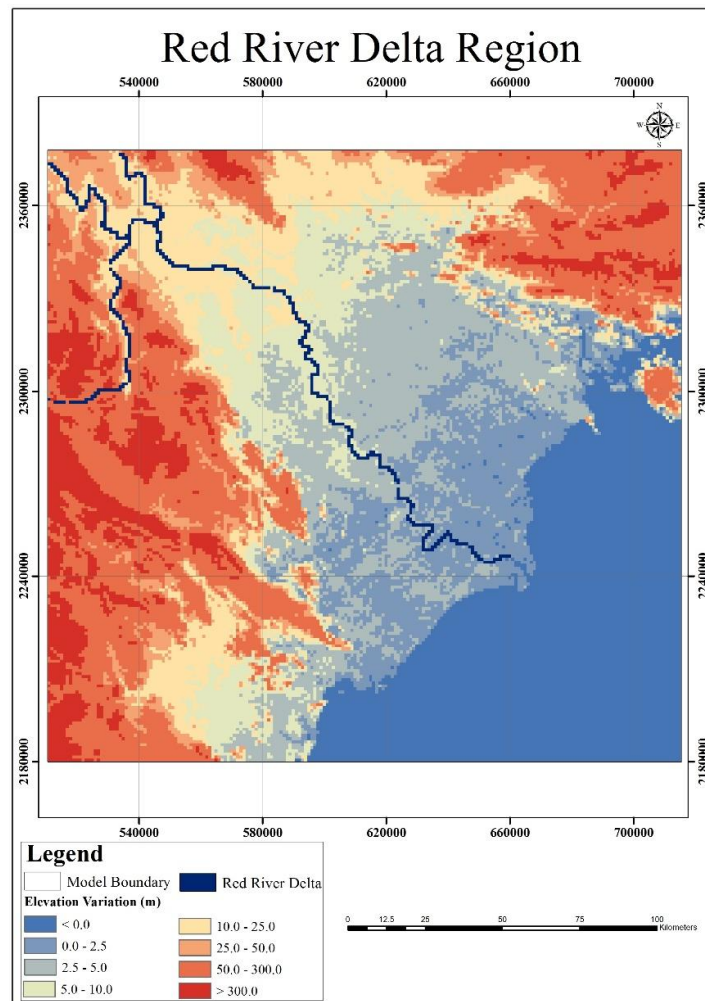


Figure 9: Model delta region

### 3.2.3. Bedrock

The depth to bedrock was estimated based on three main global datasets viz. GEBCO (General Bathymetric Chart of the Oceans), GLIM (Global Lithological Map) and regolith thickness by Daniel Zamrsky PhD researcher attached to Deltares and Utrecht University. The

existence of the unconsolidated sediments was taken into account during the estimations. Calculated depth values were interpolated following the inverse distance weighting (IDW) technique in ArcGIS and smoothed with the Focal Statistics tool available in Arc Tool Box. This process was incorporated with a  $12 \times 12$  rectangular neighbourhood, which functioned based on the average of the input cells. Resulted interpolation map of the bedrock depth variation is shown in Appendix 1, where the bottom is steeped towards the offshore with a maximum depth of 440 m BMSL while the same was demarcated to be around 50 m BMSL near the hilly regions.

### **3.2.4. River Network**

River network data can be downloaded from HydroSHEDS database (Hydrological data and maps based on SHuttle Elevation Derivatives at multiple Scales), which is available on a global scale. It is a mapping product comprising geo-referenced data at various scales, including river networks, watershed boundaries, drainage directions and flow accumulations. HydroSHEDS data are based on high-resolution elevation data obtained from SRTM where the river network data are available with 15 and 30 arc second resolutions (Lehner et. al., 2008).

RRD region has a complex hydraulic network with a significant influence from the anthropogenic activities. The major river of the plain, Red River or the Song Hong River comprises of two major tributaries; the Da and Lo Rivers in the upstream of the delta. It flows in the middle of the delta plain until the Tonkin Bay, tallying up to 216 km in its length within the delta (Figure 9). Besides these main branches, the delta contains several reaches and artificial irrigation and drainage channels, which further complicate the hydraulic system of the area (Appendix 1).

### **3.2.5. Land Use**

Land use data were downloaded via Global Land Cover Share (GLC-SHARE) database, which was developed by Food and Agriculture Organization (FAO). This data set provides major thematic land cover types derived from the “best available” high resolution national, regional and sub-regional land cover databases at a resolution of 30 arc second (1 km) and available to download in GeoTIFF format. Major thematic classes consist of artificial surfaces, cropland, grassland, tree covered area, shrubs covered area, herbaceous vegetation, aquatic or regularly flooded, mangroves, sparse vegetation, bare soil, snow and glaciers and water bodies.

RRD plain consists of several land use types such as artificial surface, crop lands, grass lands, tree covered area, shrubs, mangroves and water bodies. For this study, recharge rates were estimated depending on these classes and a fraction of the total precipitation was considered to be contributing to the net groundwater recharge. Further, precipitation and its fractions

contributing to groundwater recharge were derived from several literature studies. Wagner et al., 2011 presents monthly precipitation for the year of 2007 in Nam Dinh Province in RRD plain and these were assumed to be same for the whole RRD region. The fractions to estimate net recharge were derived from a previous research study carried out in Day River Basin (Wolf, 2015). Those values were also considered to be uniform for the entire delta plain. Calculated recharge rates are in a range of 0.02 to 0.74 mm/day. Appendix 2 provides the relevant calculations and final interpolated map.

### **3.2.6. Population Density**

Gridded Population of the World (GPW) series, now in its fourth version (GPWv4) represents the distribution of population on a global scale. It has a resolution of 30 arc second and freely available for download. This has several data types, named as population counts, population density, UN-adjusted population counts, UN-adjusted population density, land area, water area and data quality indicators. Additionally, a vector data set of the centre point locations (centroids) for each of the input administrative units and a grid of national level numeric identifiers are also included (CIESIN, 2016).

The highest population densities are recorded from the major cities in the region such as Ha Noi, Bao Ninh, Hung Yen, Thai Binh, Nam Dinh, Hai Duong, and Hai Phong. General statistics office of Vietnam also reveals similar information (Statistical Documentation and Service Centre, 2011). These population density data were used in deriving extraction rates of groundwater wells together with the aid of several other literature (Bui et al., 2011, Bui et al., 2012, Bui et al., 2012b and Norrman et al., 2015) that provide total groundwater pumping rates within the region. In this study, groundwater pumping well locations (Figure 10) were considered to be similar to those presented by Bui et al., 2011 and Bui et al., 2012. Bui et al., 2012 elaborate information on groundwater pumping in Hanoi in decades ago. According to that study, groundwater had been pumped at a rate of 200,000 m<sup>3</sup>/day in Hanoi during 1970 and it has increased enormously up to 400,000 m<sup>3</sup>/day by 1990. They have also figured out that in present, groundwater pumping rate at Hanoi has reached about 800,000 m<sup>3</sup>/day, catering for almost all the domestic water demands. Norrman et al., 2015 also considered similar pumping rates for Hanoi and stated that the groundwater pumping rate of the entire delta is more than 1 million m<sup>3</sup>/day. Future groundwater extraction rates were predicted based on the population growth rate (1.07% per year) and an individual water requirement of the region (90 l/day). All these statistical information were used to estimate future groundwater extraction rates under the different scenarios considered (Table 3 and Appendix 3).

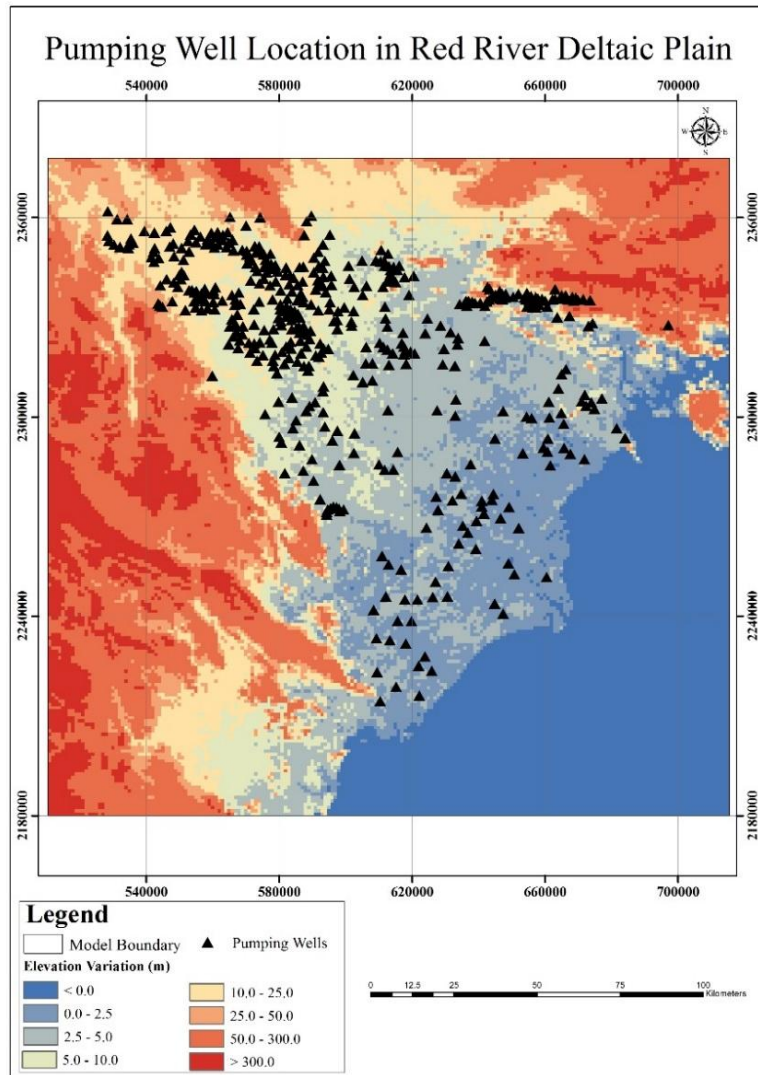


Figure 10: Pumping well locations in the deltaic plain

Table 3: Groundwater pumping rates

Year	Province	Total pumping (m³/day)	Year	Province	Total pumping (m³/day)
1970	Hanoi	200000	2010	Hai Phong	169274
1990	Hanoi	400000		Hanoi	800000
	Hai Phong	10000		Hung Yen	103664
	Nam Dinh	10000		Nam Dinh	165219
	Hai Duong	10000		Ninh Binh	81686
2010	Hai Dong	154893		Thain Binh	160939
	Bac Ninh	95545		Ha Nam	70909

### 3.3. Local Data Collection

#### 3.3.1. Geology

Winkel et al., 2011 worked on Arsenic pollution in groundwater across the RRD plain. This study provides information on several borehole logs. This dataset comprises the details of 79 borehole logs and their spatial distribution over the deltaic region is shown in Figure 11. The borehole logs were categorized according to the lithology classes, named as aquifer, clay aquitard, clay mud aquitard and limestone. However, literature on RRD plain reveals the existence of two major aquifer systems in the region; namely, Holocene and Pleistocene aquifer. Hence, the borehole log classification was modified according to the cross sections given in Winkel et al., 2011.

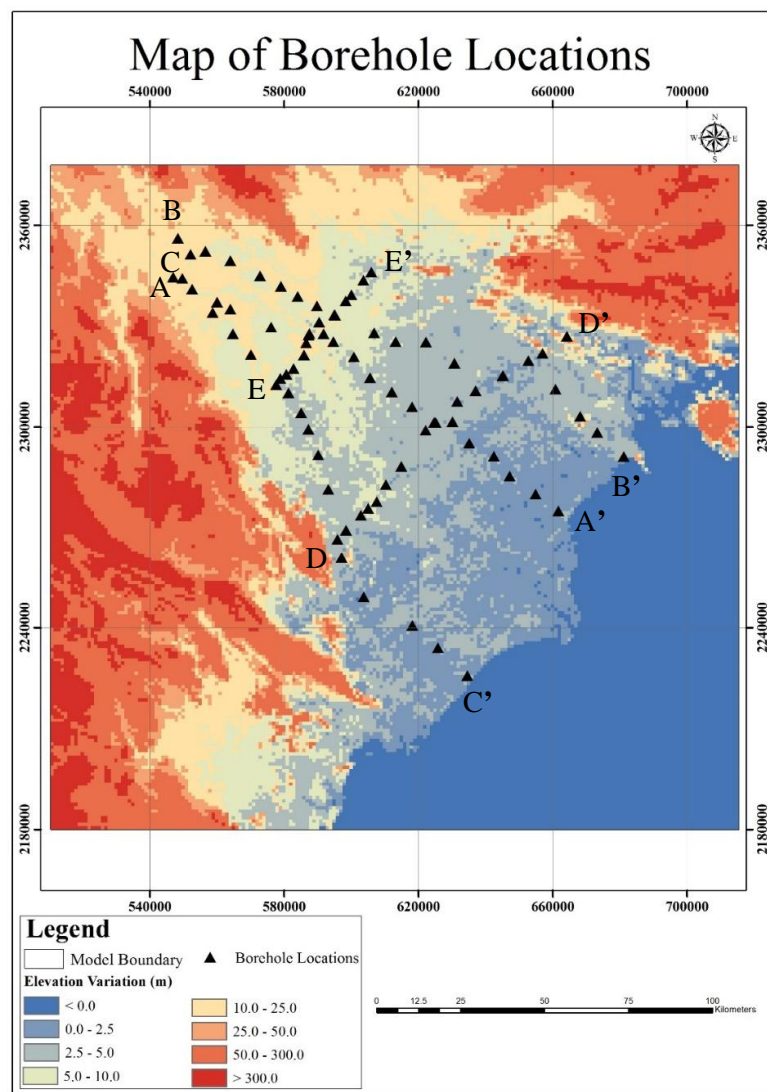


Figure 11: Map of borelogs locations

After finalizing the lithological classification of borehole logs, they were processed to interpolate three dimensionally by a tool available in iMOD-Batch mode called “3DSolid-Tool”. It utilizes the kriging technique to interpolate three dimensionally and offers the user to visualize spatial variation of geology. It can also be adapted to estimate the hydraulic conductivities in the modelled area, which is an input parameter for the LPF package. Geological variation of the model layers are attached in Appendix 4.

### 3.3.2. Aquifer Property Parameters

Aquifer property parameters were assumed for the SC1 model as the information on the global scale were absent. Therefore, hydraulic conductivity of 0.005 and 40 m/day was assumed for clay and aquifer layers, respectively. Further, vertical anisotropy factor was presumed to be 1 for clay layer and 0.5 for the sand aquifer.

Further, the literature available (Wagner et. al., 2011; Van Pham and Lee, 2014) provided relevant values for the other scenario models as listed below.

Table 4: Model inputs of hydraulic conductivity, vertical anisotropy factor, specific storage and porosity values

<b>Hydraulic Conductivity (m/day)</b>	
Holocene Aquifer	1.62
Pleistocene Aquifer	7.75
Holocene Clay	0.003
Pleistocene Clay	0.003
Limestone	1.13
Bed rock	0
<b>Vertical Anisotropy Factor</b>	10
<b>Specific Storage</b>	0.0021
<b>Effective Porosity</b>	0.3

Table 5 below summarise the sources of data collection in both global and local scale.

Table 5: Sources of data collection

<b>Digital Elevation Model (DEM)</b>	SRTM
<b>Ocean Bathymetry Data</b>	GEBCO
<b>Bedrock</b>	An estimation using GEBCO, GLIM and regolith thickness data
<b>River Network</b>	HydroSHEDS
<b>Land Use</b>	Global Land Cover Share database
<b>Population Density</b>	GPWv4
<b>Borehole Log Data</b>	Winkel et al., 2011

<b>Aquifer property parameters</b>	Wagner et. al., 2011; Van Pham and Lee, 2014
<b>Pumping data</b>	Bui et al., 2011; Bui et al., 2012; Bui et al., 2012b; Norrmann et al., 2015

## 3.4. Model setup and Simulation

### 3.4.1. Initial Model Setup

A 3D variable-density groundwater flow model was initiated by defining the model boundary as illustrated in Figure 9. It covers the RRD plain and the surrounding mountainous regions, extending across a total area of 40 590 km<sup>2</sup>. The model developed has a resolution of 1 km, where its grid comprises 198 rows, 205 columns and 10 model layers with variable thickness. These thicknesses of the model layers, ranging from 2 – 134 m, have the largest values in mountainous regions, whereas the offshore maximum thickness is about 35 m (Figure 12). The current study also considers a system so offshore to the present land-sea interphase due to the aim of paleo-reconstruction modelling and to test the possible geology influences on the saline distribution.

During the study, regions with an elevation higher than 300 m were neglected in the model because the research is primarily focused on the groundwater aquifer systems in the low-lying delta plain. Further, they were considered as higher storage potentials. Under the IBOUND condition of the flow model, grid cells representing these mountainous regions were defined as inactive in each layer for the whole modelling procedure. Furthermore, offshore cells were distinct with a constant concentration in ICBOUND condition for the first layer in the transport model. Area of interest in IBOUND and ICBOUND inputs are shown in Figure 13.

Subsequently, model inputs were converted into a uniform coordinate system viz. WGS 84, UTM Zone 48 N and all the inputs were finally transformed into iMOD-SEAWAT supportive formats of IDF and IPF.

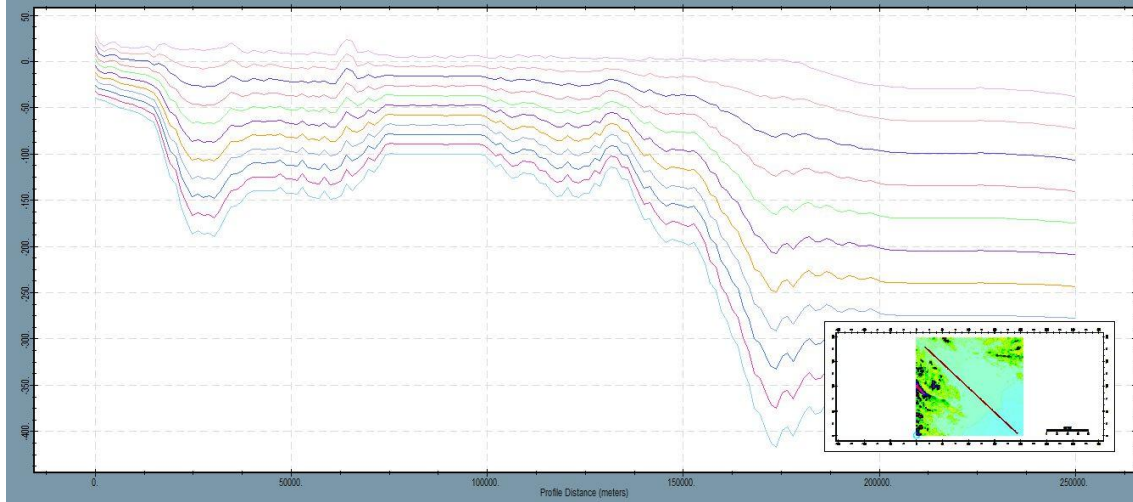


Figure 12: Variable thickness layers in the model

Initial model setup was limited for globally available data sets and commenced with a basic flow and transport model packages. A head dependent boundary was defined for the active cells following the mountainous regions, as they are the primary sources of recharging for territory. Offshore model boundary and the low-lying deltaic plain boundaries were also considered as head dependent flux boundaries. Initial head values were derived from the DEM data set and the initial concentrations of fresh and saltwater were considered as 1 and 35 g/l, respectively. Since good quality geological information is sparse at global scale, the preliminary global model was simulated assuming an existence of a clay aquitard in the first layer and a homogeneous aquifer system in the following layers. River network was also included in the model, together with a uniform recharge rate of 1 mm/day.

The basic global data model was simulated for 100 years and the model velocities were tried to reduce in order to develop a faster model for longer time scale simulations. Several steps were followed to improve the model speed and the model stability to facilitate the paleo-reconstruction scenario with-in the available time period. Defining uniform inactive regions while removing isolated cells, smoothening the input heads and changing the head dependent boundary conductance values were the main procedures adopted to obtain a much faster and stable model. Paleo-hydrogeologic modelling was initiated after such a model was successfully setup for the study domain.

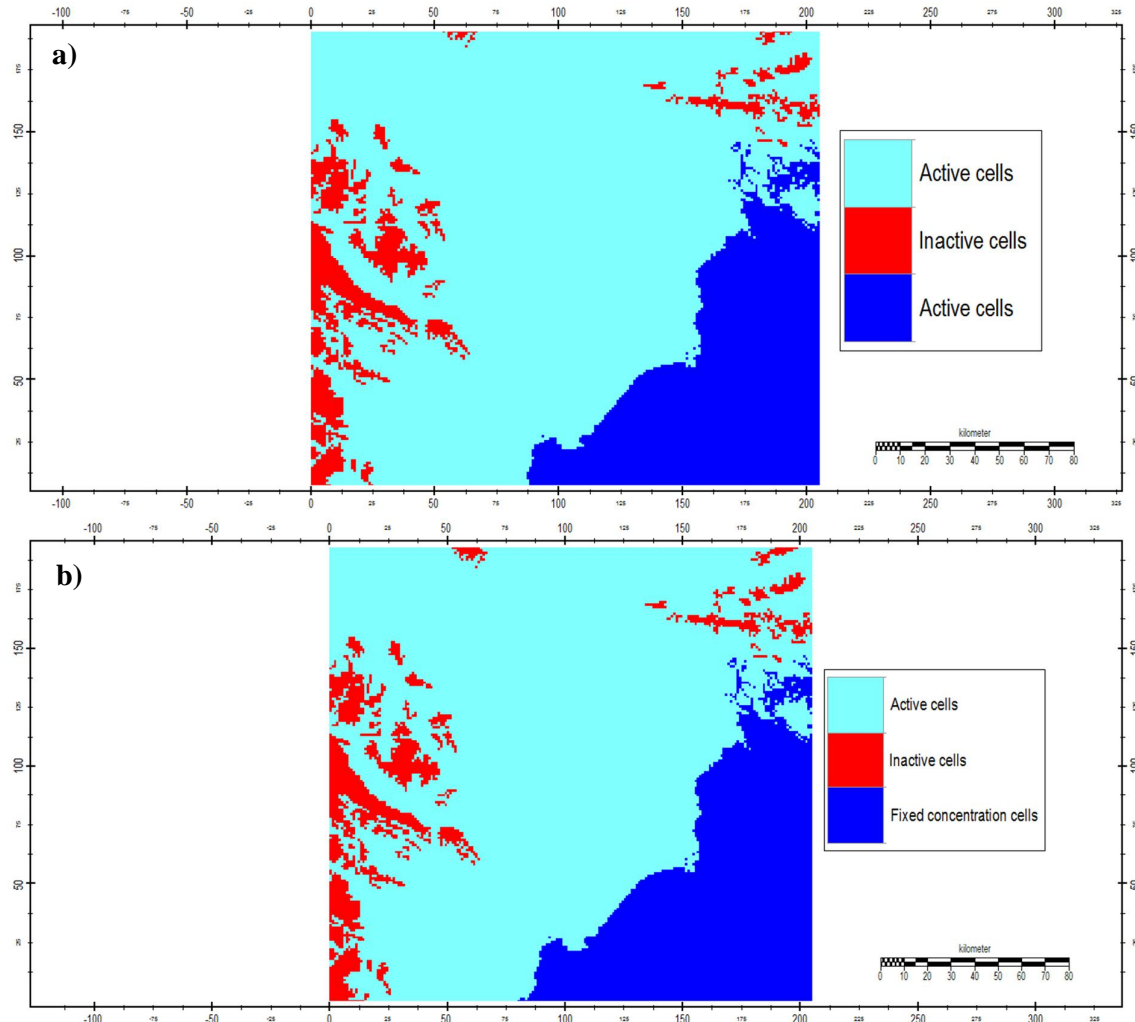


Figure 13: Active, inactive and fixed concentration cells in the model domain

a) IBOUND condition b) ICBOUND condition

### 3.4.2. Paleo – Hydrogeologic Modelling with Only Global Data (SC1)

Paleo-hydrogeologic modelling was commenced by defining a reference year, at which the salinity distribution is more or less known or is certain to not to influence the present salinity distribution. Surface elevations were assumed to be as same as the present and current DEM data was utilized for the paleo-reconstruction modelling. Larsen et al., 2017 emphasise that the sea level rise during 8.5 to 6.5 kyrs ago was the governing period for the development of Holocene deltas. Considering all these factors, paleo-hydrogeologic modelling for RRD was started from 14 kyrs ago, where the salinity distribution is assumed to be known. During this study, eustatic sea level fluctuation during the late Holocene period was modelled with 7 diverse models by defining 7 stress periods as described in Table 6.

Table 6: Paleo-hydrogeologic model details

Stress Period	Sea Level	Model Duration (years)	Moment of Time
<b>SP0</b>	< - 41 m BMSL	0 (represent the initial moment)	-14 kyrs ago
<b>SP1</b>	< - 41 m BMSL	1000	-13 kyrs ago
<b>SP2</b>	- 39 m BMSL	2000	-11 kyrs ago
<b>SP3</b>	- 10 m BMSL	2000	-9 kyrs ago
<b>SP4</b>	0 m	2000	-7 kyrs ago
<b>SP5</b>	+ 5 m AMSL	3000	-4 kyrs ago
<b>SP6</b>	0 m	4000	Present day

As illustrated in Figure 5, sea level was lower than 41 m BMSL (Table 6) before 14 kyrs ago, implying that the study area was totally occupied by fresh groundwater. Yet, a saltwater wedge should exists underneath the surface and it was assumed to be presented from the second layer onwards for the SP0 model. It was defined in accordance with the Sink Source Mixing package. Head dependent boundary concentration values implied the existence of saltwater wedge.

In the paleo-modelling, the Red River and its main tributaries were extrapolated offshore by considering the elevation variations in the plain, allowing the river network to flow over the whole model domain. River network data downloaded from HydroSHEDS database also consists of several irrigation channels. These artificial channels were removed from the RIV package during the paleo-hydrogeologic models. Geology of the region was assumed to be as described under section 3.4.1. Recharge and drainage packages were remained unchanged from the description in the same section. Uniform and relatively high recharge rate (1 mm/day) was assumed over the modelled region, selected in accordance to the timescales considered in the models.

As mentioned in Table 6, SP0 model was simulated for a very short period of time, so that it would represent the initial situation. Henceforth, SP1 paleo-reconstruction model was developed from 14 kyrs with 1 kyrs of modelling period. This model accounted for the concentration and groundwater head distribution obtained from the SP0 model. It is then followed by the SC2 model, which started 13 kyrs ago, where the sea level is assumed to be around 39 m BMSL. Hence, the IBOUND and ICBOUND boundary conditions were changed accordingly. Sea level overtopping was introduced by mainly changing the general head boundary conditions of the first layer. The river network data was modified accordingly. Groundwater heads and concentrations variations were inserted from the outputs of the SP1 model and the transient state was considered for the next 2 kyrs simulation. The described process was continued for all the other models until the present day concentration and head distribution were obtained by using only the globally available data.

### **3.4.3. Paleo – Hydrogeologic Modelling with Local Data (SC2)**

Paleo-reconstruction modelling procedures described under section 3.4.2 were developed by using only the globally available data. Hereon, the model was advanced by introducing localized geology data. iMOD 3DSolid-Tool interpolation on borehole logs (section 3.3.1) was used under the Layer Property Flow package with actual aquifer property parameter values collected from the available literature (Table 4). All the other parameters were kept unchanged when compared to the paleo-hydrogeologic models described in section 3.4.2. With this improved geological information, the same stress periods mentioned in Table 6 were simulated.

### **3.4.4. Modelling the Current Status of Delta (SC3)**

Paleo-hydrogeologic model results from section 3.4.3 were applied to develop a model for the present aquifer systems. Available literature suggest that there are enormous pumping activities carried out within the RRD plain, and these were taken into account for the modelling work corresponding during this step. Section 3.2.6 reveals more information on groundwater pumping rates and its estimations are presented in Appendix 3. Subsequently, calculated recharge rates (Appendix 2), which were assessed based on land use variation (section 3.2.5) were also added to the model. However, governed by the availability of information, SC3 models were simulated only for the years of 1970, 1990 and 2010.

### **3.4.5. Testing for Future Scenarios (FSC)**

To estimate the influences of several future forcing combinations, a reference model (FSC1) was developed, where the pumping rates were assumed to be unchanged for the next 100 years. Hence, the pumping rates used in year 2010 were kept constant for the reference model with a uniform sea level.

Population growth, intense agriculture, urbanization and industrialization will escalate the groundwater pumping within RRD. Available pumping rates in the years of 1970, 1990 and 2010 support the above proposition. Therefore, the pumping rates were adjusted in accordance to the population growth rate in the FSC2 model setups. Appendix 3 particularly describes the calculations, where it is estimated to have a fixed increased groundwater pumping rate (~ 50%) for the next 100 years.

According to the literature, RRD plain will face a sea level rise of about 1 m during the next 100 years, which will eventually disturb the groundwater aquifer systems in the region. Hence, another model was developed by considering only this phenomenon while maintaining a constant pumping rates. Therefore, the groundwater extraction rate will remain as in year 2010, while sea level overtopping would be the only environment changing with respect to

the reference model (FSC3). Head dependent boundaries were changed in accordance to the sea level increase. Thus, the comparison will be productive to estimate the impacts of MSLR in the delta plain.

Finally, RRD model was tested with respect to both the future predicted MSLR of 1 m and increased groundwater pumping rates (similar to what explained earlier) (FSC4). Hence, the model would indicate the impacts on aquifer systems with respect to MSLR and groundwater pumping rates considered. Table 7 below summarises the FSC model setups.

Table 7: Description of tested FSC models

<b>Model Name</b>	<b>Sea Level (m AMSL)</b>	<b>Groundwater Pumping Rates</b>
<b>FSC1</b>	0	Similar to the rate in year 2010
<b>FSC2</b>	0	~ 50% increase
<b>FSC3</b>	+1	Similar to the rate in year 2010
<b>FSC4</b>	+1	~ 50% increase

## **CHAPTER 4**

# **Results and Discussion**

## **4.1. Interpretation of Geological Distribution**

Winkel et al. 2011 published borehole log classifications for the RRD plain as described in Section 3.3.1. They were modified according to the literature to demarcate the Holocene and Pleistocene aquifer systems separately. It was problematic to demarcate the divisions of upper and lower Holocene aquifer or clay systems as well as the upper and lower Pleistocene aquifer systems. Therefore, the lithology was modified to have only five classes as Holocene clay, Pleistocene clay, Holocene aquifer, Pleistocene aquifer and limestone. Moreover, these borehole logs did not provide details on the bedrock. Therefore, it was assumed that the final lithology of each borehole log continues until the estimated bedrock. Geological interpolation results for each layer is mentioned in Appendix 4.

Figure 14 represents the geological variation along line A-A' in accordance with Figure 11. Figure 14-a shows the geological interpretation used in Winkel et al. (2011), while, Figure 14-b demonstrates the 3DSolid-Tool results. With Figure 14-b, it is also conceivable to observe the geology distributions followed by the modelled layers. According to Figure 14-a, inland regions have less total aquifer volume compared to the total volume near the coast. Throughout the entire cross section, Holocene clay aquitard layer exists above the Pleistocene clay layer. The 3DSolid-Tool interpolation also resulted in providing similar information about aquifer volumes along the same cross section, while indicating the existence of Holocene clay layer on top layer almost all over the region.

Despite that, the distribution patterns of Pleistocene clay and Holocene aquifer system are obviously doubtful. Borehole log A8 provides information until 15 m BMSL, reporting the existence of Holocene clay and Holocene aquifer. Since, the assumption of continuity of the final lithology class until the bedrock due to the lack of information has developed a different Holocene aquifer pattern as displayed in Figure 14-b. Further close to the coast, a Pleistocene aquifer is sandwiched in between two Pleistocene clay formations. However, this clay patch was neglected in the developed model as it is in between layer 2 and 3. Henceforth, it emphasizes the importance of increasing the number of layers for further developments.

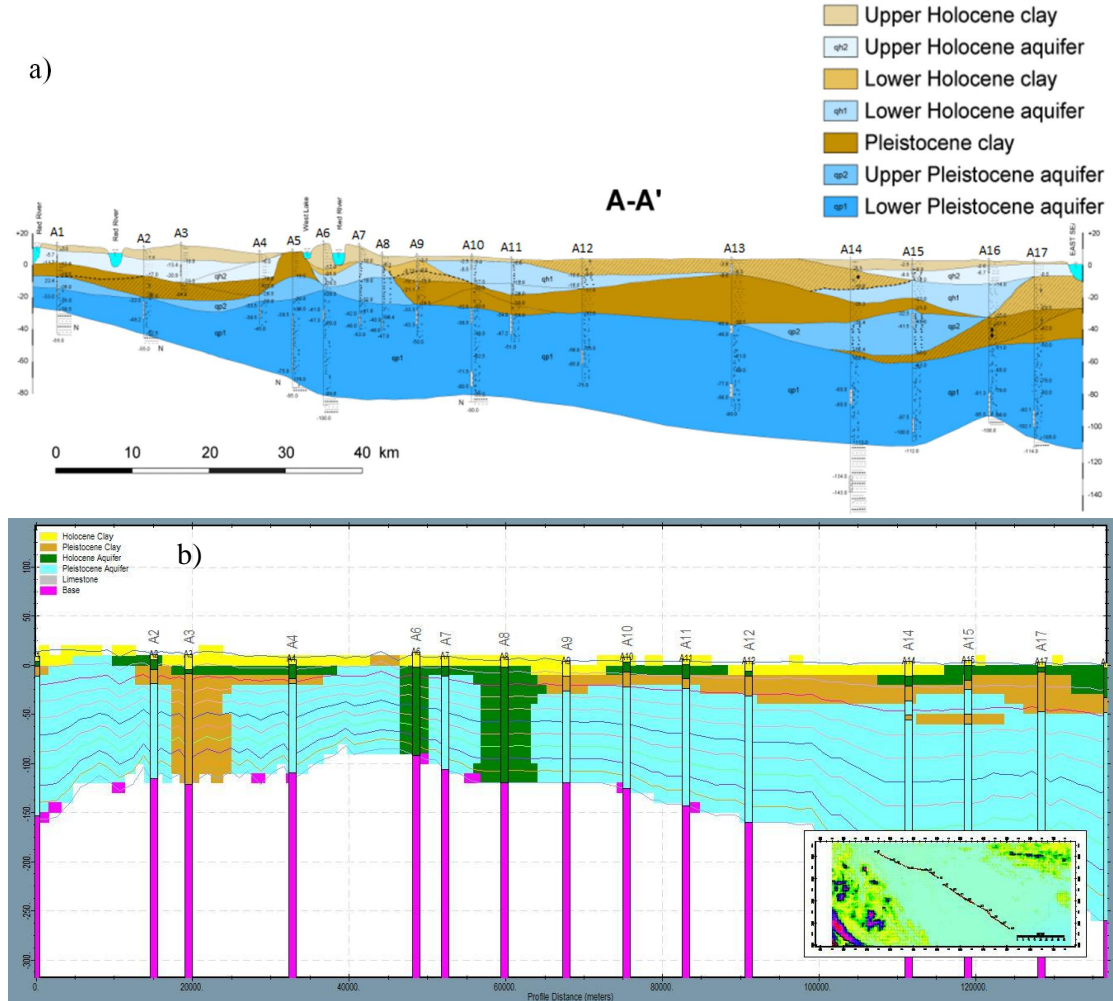


Figure 14: Geology variation along line A-A' a) Winkel et al., 2011 b) 3DSolid-Tool results

Figure 15 compares the geology distribution considered by Winkel et al. (2011) with the 3DSolid-Tool output along line C-C'. Distribution of Holocene clay patterns are almost the same in both cross sections. However, it is visible that between C1 and C3, continuity of Holocene aquifer was disturbed in the 3DSolid-Tool interpolation. C2 borehole log reveals information on Holocene aquifer, which is neglected during the interpolation. Therefore, the aquifer layer is not continuous. A similar situation can be observed between C3 and C5 borehole logs, where the continuity of Pleistocene clay layer was disturbed. Another such instance occurs at borehole log C10, where the lithology information is available only until 40 m BMSL. However, the interpolation was conducted assuming the continuity of the final lithology type until the bed rock, which resulted in a continuous Pleistocene clay layer around borehole log C10.

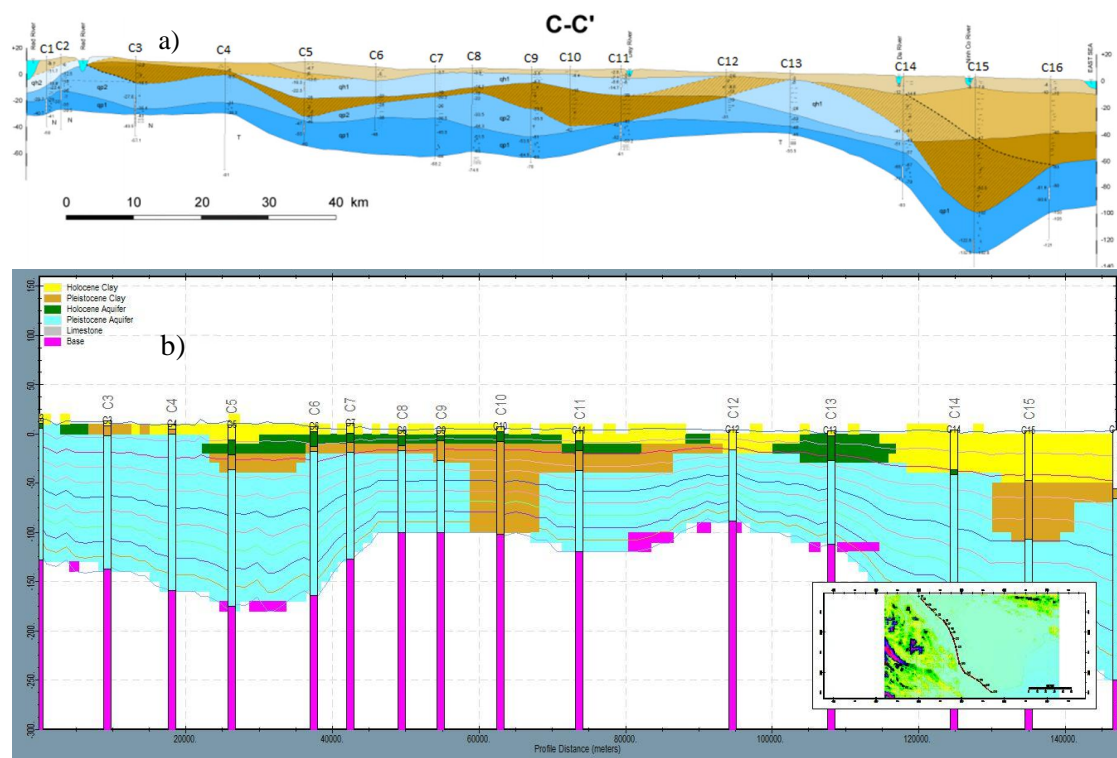


Figure 15: Geology variation along line C-C' a) Winkel et al., 2011 b) 3DSolid-tool results

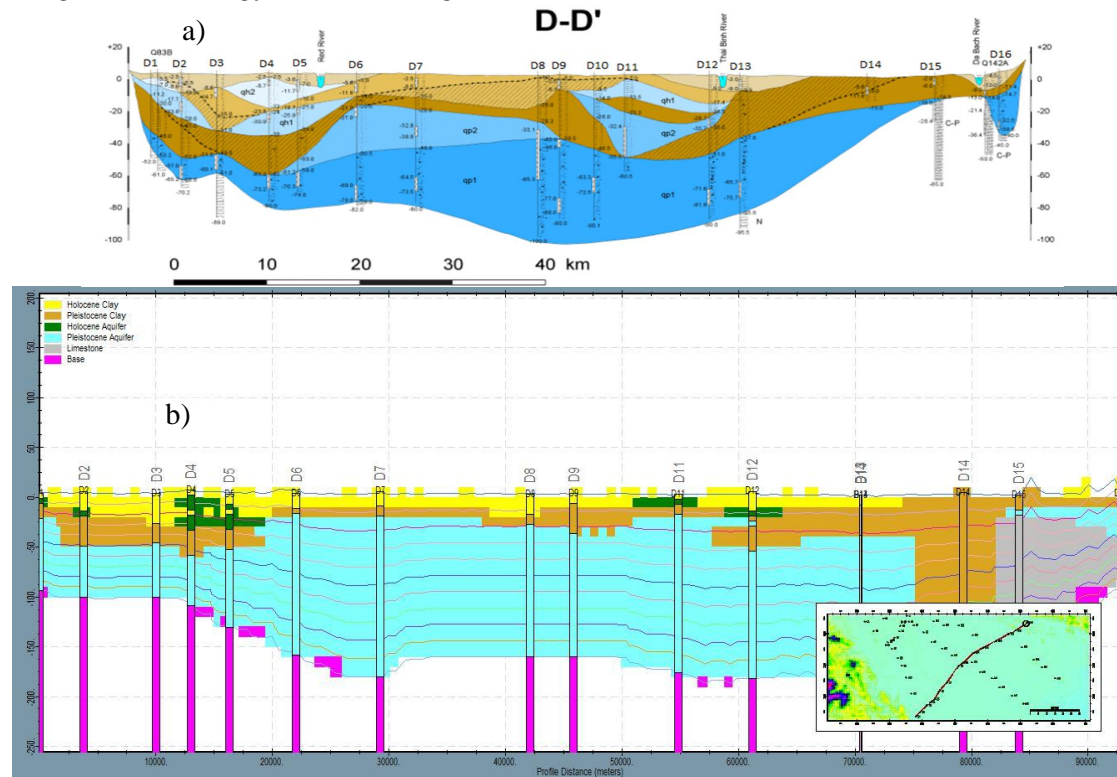


Figure 16: Geology variation along line D-D' a) Winkel et al., 2011 b) 3DSolid-tool results

The above figure (Figure 16) compares the geological variation across the line D-D', where the existence of the limestone layer is visible. According to the Wagner et al (2011), northern parts of Vietnam has several limestone patches that are commonly subjected to extensive karst dissolution. Figure 16 illustrates the limestone layer interpolation by the 3DSolid-Tool within the model region.

## 4.2. Development of the Basic Model

The development of a 3D variable-density groundwater flow model in the RRD Vietnam was commenced with the concept of achieving a stable model with less computational time. The model consists of several inactive regions as described in Section 3.4, which were needed to be carefully selected in order to stabilize the model and limit computational time. Implementation of inactive regions was necessary due to the existence of mountainous regions that are not a part of the area of concern. Therefore, regions having an elevation higher than 300 m AMSL was considered as inactive. This process resulted in a model domain as displayed in Figure 13. It contained some isolated cells along with inactive cells that caused non-convergence issues in the simulations. It could increase the unnecessary detection and model analysis time. Hence, the isolated cells were carefully removed to improve the model stability. Figure 17 represents the modified model domain that was used in all the later models developed during this study.

Proper selection of active and inactive cells improved the model stability and also reduced the computational time for a certain extent. Theoretically, larger velocities are generated by significant head differences, which ultimately result in large computational time. At the beginning, larger velocities were observed in the boundaries as shown in Figure 18-a. It is clear that the higher velocities were formed in the active – inactive region boundary, which needed to be modified. Therefore, the initial heads introduced on these boundaries were smoothed and the relevant conductance values were changed accordingly. Especially the general head boundary conductance for the active – inactive boundary was reduced to a value of  $0.001 \text{ m}^2/\text{day}$ , implying that the initial head values will be same as the elevation variation in the DEM. River conductance values were also reduced to produce a realistic surface water infiltration and absorption to and from the subsoil. With all these changes, model velocities were reduced to the values that are presented in Figure 18-b. These modifications reduced the model run time to about one eighth of that of the initial model. Hence, it provided the necessary inputs and environment to simulate the paleo-hydrogeologic models.

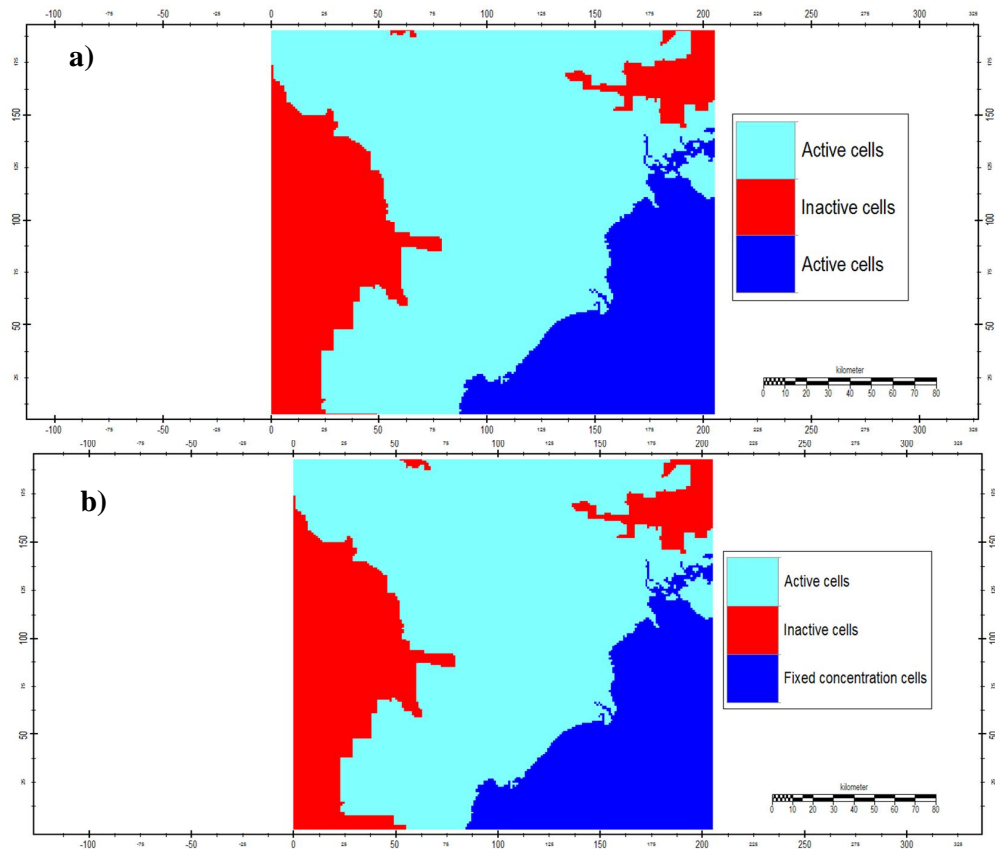


Figure 17: Improved model boundary conditions; a) IBOUND b) ICBOUND

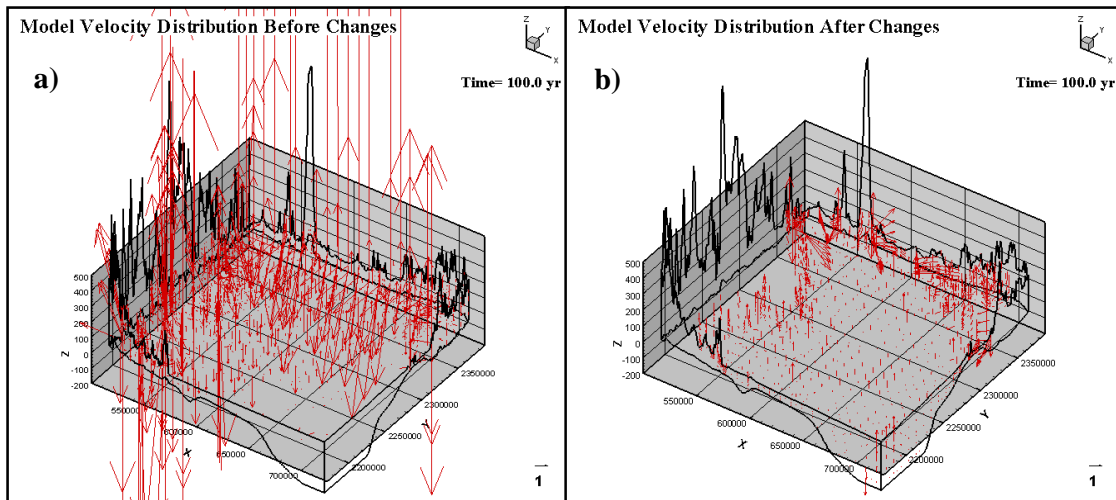


Figure 18: a) Velocity distribution of the model with initial conditions b) Velocity distribution of the model with changes

## 4.3. Paleo – hydrogeologic Modelling

### 4.3.1. SP0 Model Results

At the beginning of SP0 model simulation under both SC1 and SC2 conditions, it was assumed to have the influence of saltwater wedge from layer 2 onwards, while the top layer was defined as fresh for the entire region. The model simulated for a relatively short period under steady state conditions that represent the initial situation of the region (Figure 19). It clarifies the concept of introducing the saltwater intrusion wedge to the system. Moreover, during this step, both scenarios resulted in a similar output. Hence, the commencement of both modelling procedures were identical.

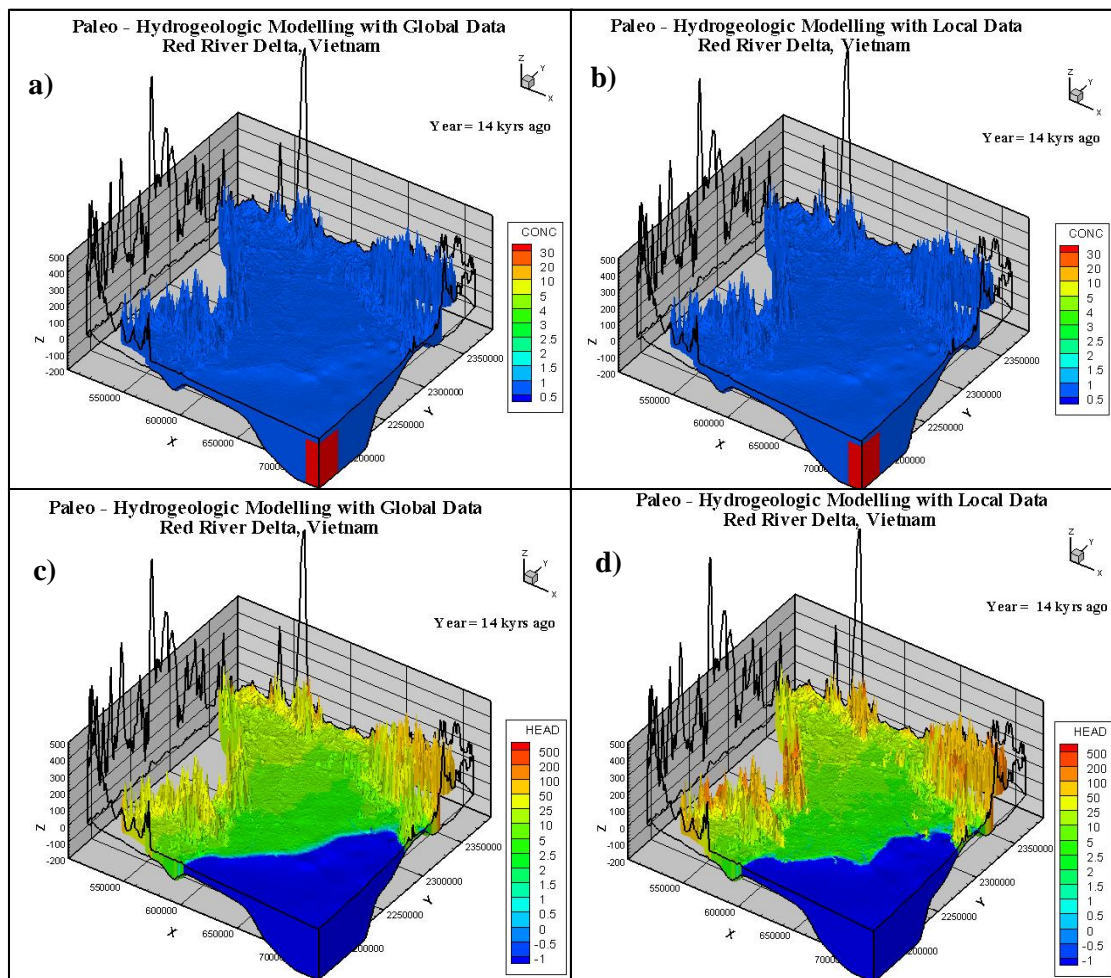


Figure 19: Concentration variation 14 kyrs ago for a) SC1 b) SC2  
Groundwater head distribution 14 kyrs ago for c) SC1 d) SC2

#### 4.3.2. SP1 Model Results: 14 - 13 kyrs before present

The SP1 model was simulated with the same parameters as SP0. Hence, the SP0 model outputs were introduced to the SP1 model. The model developed the initial saltwater wedge as shown in Figure 20-a and Figure 20-c. In both scenarios, it is observed that the growth of saltwater wedge is increasing as the depth increases. Under SC1 model, saltwater intrudes up to a maximum distance of about 4 km inland in the lower layers, while in SC2, the same distance is observed to be about 3 km.

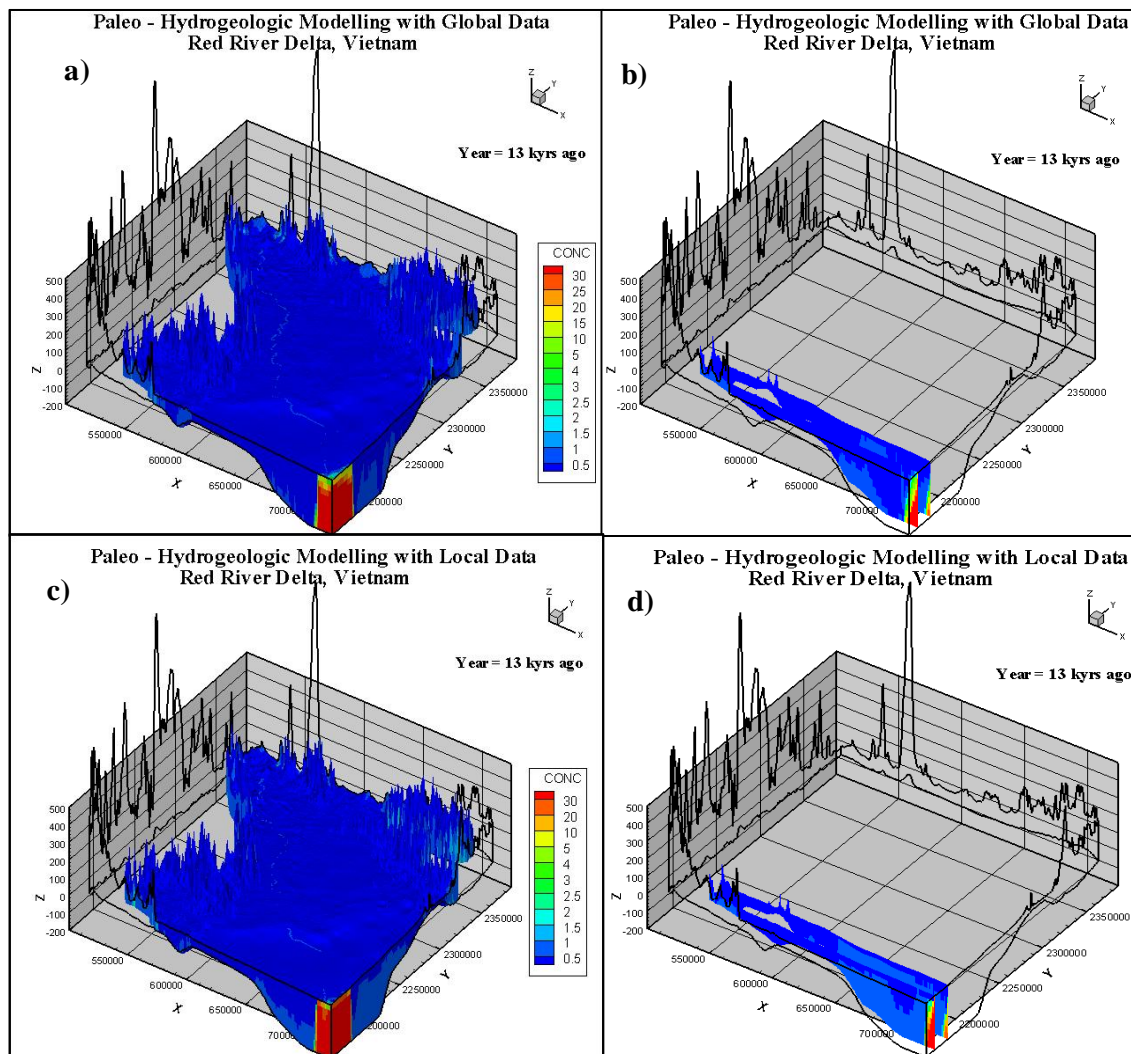


Figure 20: a) Concentration distribution of SC1 model; 13 kyrs ago b) Saltwater wedge development of SC1 model ( $y = 2190447$  and  $y = 2205447$ )  
c) Concentration distribution of SC2 model; 13 kyrs ago d) Saltwater wedge development of SC2 model ( $y = 2190447$  and  $y = 2205447$ )

The volume of saltwater is higher in the SC1 model, which implies a rapid mixing in the system. As a result of density driven transport, both model results illustrate an increase of salinity level in the top most layers. Yet, SC2 model comparatively has higher saline concentrated water in the top most layer due to the higher hydraulic conductance in the region. Hence, the salinity mixing and saltwater wedge development show minor dissimilarities for the two scenarios. Figure 20-b and Figure 20-d enclose two cross sections in the region, where the saltwater wedge development can clearly be observed. Lateral development of saltwater wedge is less in SC2 in both cross sections compared to SC1, which can be attributed to the impacts of geological variations introduced. However, the groundwater head distribution under both scenarios is similar to Figure 19-c and Figure 19-d.

#### 4.3.3. SP2 Model Results: 13 – 11 kyrs ago

SP1 model results were used as inputs to the SP2 models that demonstrate the groundwater system behaviour for the previous 13 - 11 kyrs. Sea water overtopping in the corner over a small area was introduced to the models to resemble the MSLR, given that the sea level has reached 39 m BMSL by this time (Table 6). Figure 21-a and Figure 21-c shows the model results in terms of concentration variation of SC1 and SC2, respectively. In these figures, the saltwater – freshwater mixing zone is visible. For both the models, it was found that the maximum saltwater wedge width is similar to that of the SP1 model results (~3 km). Thus, the salinity variation in SC1 and SC2 models are very much similar. Figure 21-b and Figure 21-d show the development of saltwater wedge with two cross sections drawn identically to that of Figure 20. They also have a similar distribution of saltwater. According to the results of section 4.1, this region has a Pleistocene aquifer. Hence, the geological variation in the referred section is similar in both models and hence have developed identical salinity distributions. In both models, number of cells with salinity or brackish water have increased.

Groundwater head distributions also found to be similar for both the model (Figure 19-c and Figure 19-d), indicating that the model has reached a steady state situation where the groundwater heads are uniform.

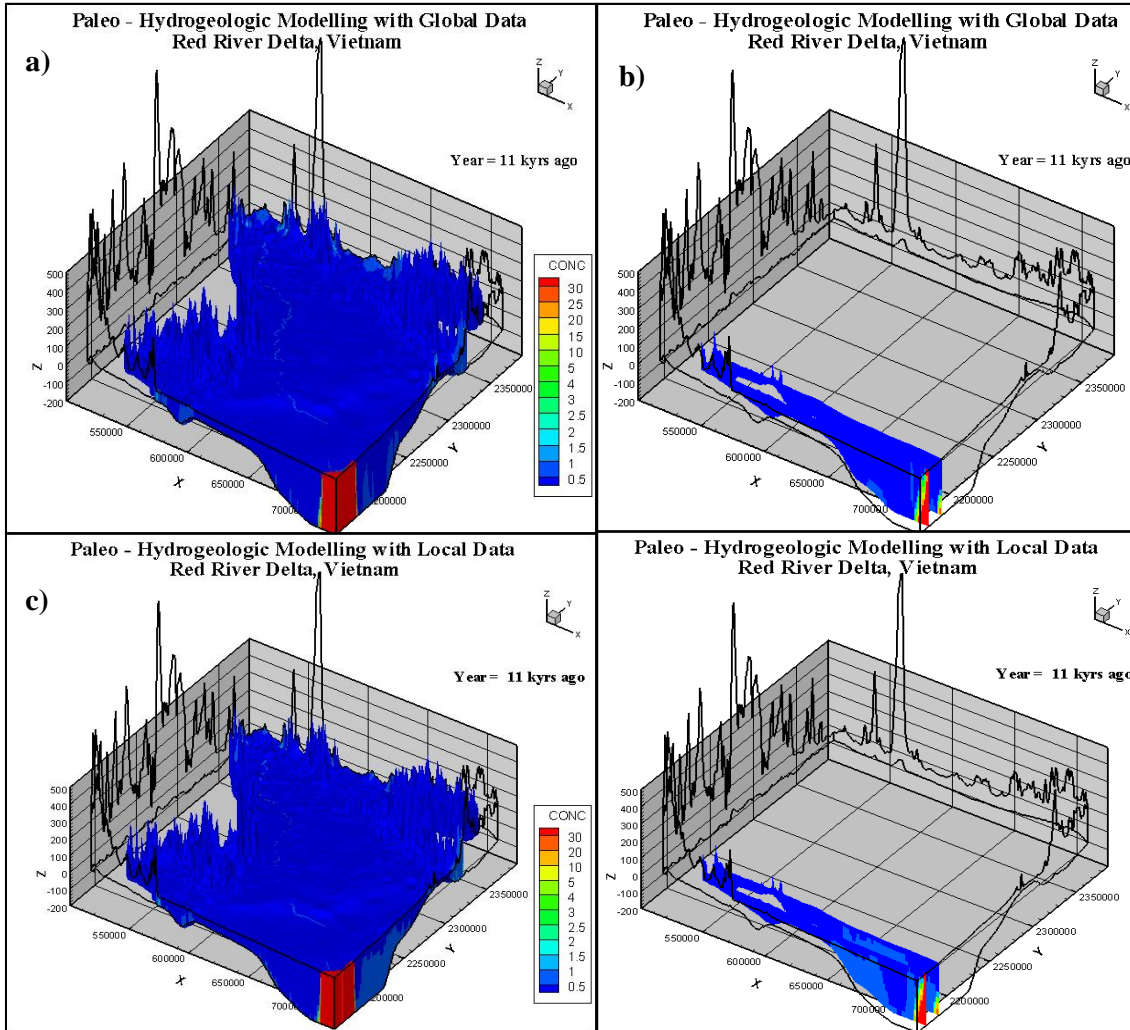


Figure 21: a) Concentration distribution of SC1 model; 11 kyrs ago b) Saltwater wedge development of SC1 model ( $y = 2190447$  and  $y = 2205447$ )  
c) Concentration distribution of SC2 model; 11 kyrs ago d) Saltwater wedge development of SC2 model ( $y = 2190447$  and  $y = 2205447$ )

#### 4.3.4. SP3 Model Results: 11 – 9 kyrs ago

Following the paleo-reconstruction modelling, SP3 models were simulated for another 2 kyrs which describe the groundwater system behaviour during 9 kyrs ago. Groundwater head distribution was identical to previous models for both SC1 and SC2 cases and the relevant concentration variation is shown in Figure 22-a and Figure 22-c, respectively. By the time of SP3 model, sea level had stretched more inland, where the regions below -10 m were inundated. It was observed that the sea level overtopping in the delta region together with natural advection and dispersion processes have developed saline conditions, even several tens of meters below the surface. This phenomenon is growing rapidly in SC1 model

compared to that of SC2. Hence, the sea water overtopping in SC1 model resulted in uniformly developed brackish groundwater wedge underneath.

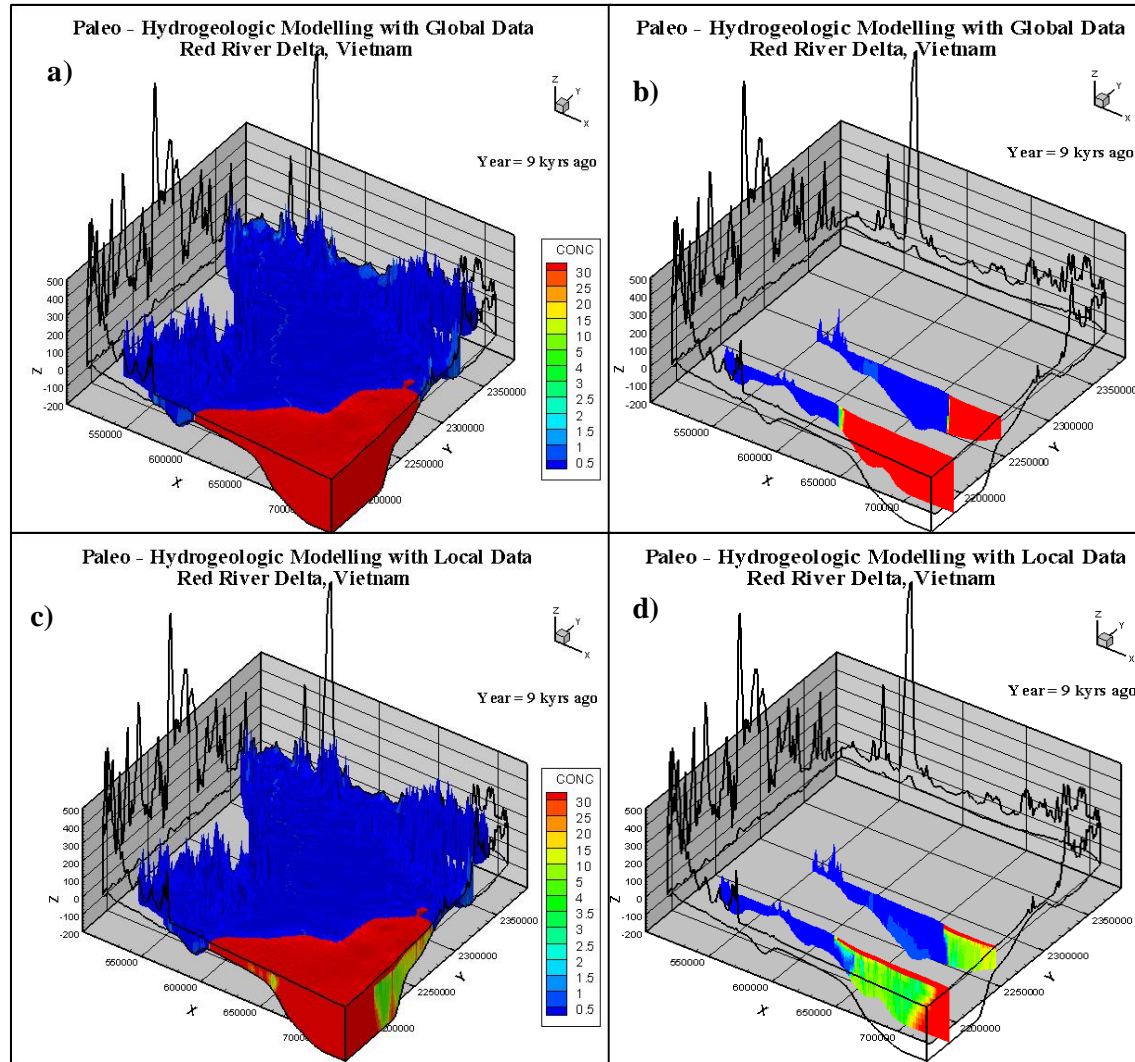


Figure 22: a) Concentration distribution of SC1 model; 9 kyrs ago b) Seawater over topping of SC1 model ( $y = 2206133$ ,  $y = 2258582$ )  
c) Concentration distribution of SC2 model; 9 kyrs ago d) Seawater fingering of the SC2 model ( $y = 2206133$ ,  $y = 2258582$ )

However, for the SC2 model, evolution of brackish water is found to be more uneven. Regions with clay aquitards were observed to have saltwater due to the diffusive transport, while the aquifer regions have developed brackish concentrations due to the density driven transport fluxes (Figure 22-b and Figure 22-d) (Post et. al, 2013). In Figure 22-b, it can be observed that the groundwater below the overtopped sea has become salty, whereas in Figure 22-d, brackish groundwater extent is appeared to be quite limited. As a result of the improved

geology and layer property values adopted in the relevant model, Figure 22-d indicates the saltwater fingering process that has taken place in SC2 model. In the SC1 model, given hydraulic conductivity values, in conjunction with its simple geological profile have created larger density driven groundwater flows and mixing. Consequently, the natural fingering process and saline– brackish water mixture in the offshore areas couldn't be observed.

#### **4.3.5. SP4 Model Results: 9 – 7 kyr ago**

Around 7 kyr ago, sea level in RRD region had reached the current offshore position and this situation was modelled in SP4. The results shown in Figure 23-a illustrate a minor scale saltwater intrusion closer to the coastal regions and aligned with the Red River and its main tributaries. This situation is detached under SC2 results. Hence, a cross section was drawn along these regions to estimate the groundwater flow paths as shown in Figure 23-b and Figure 23-d. It can be implied that there are upward flows along these regions, which have caused saltwater intrusion on the top layers. Moreover, upward flows are higher in SC1 model compared to that in SC2. Thus, the transportation of the underlying saline groundwater on to the top layer can be observed in SC1 model.

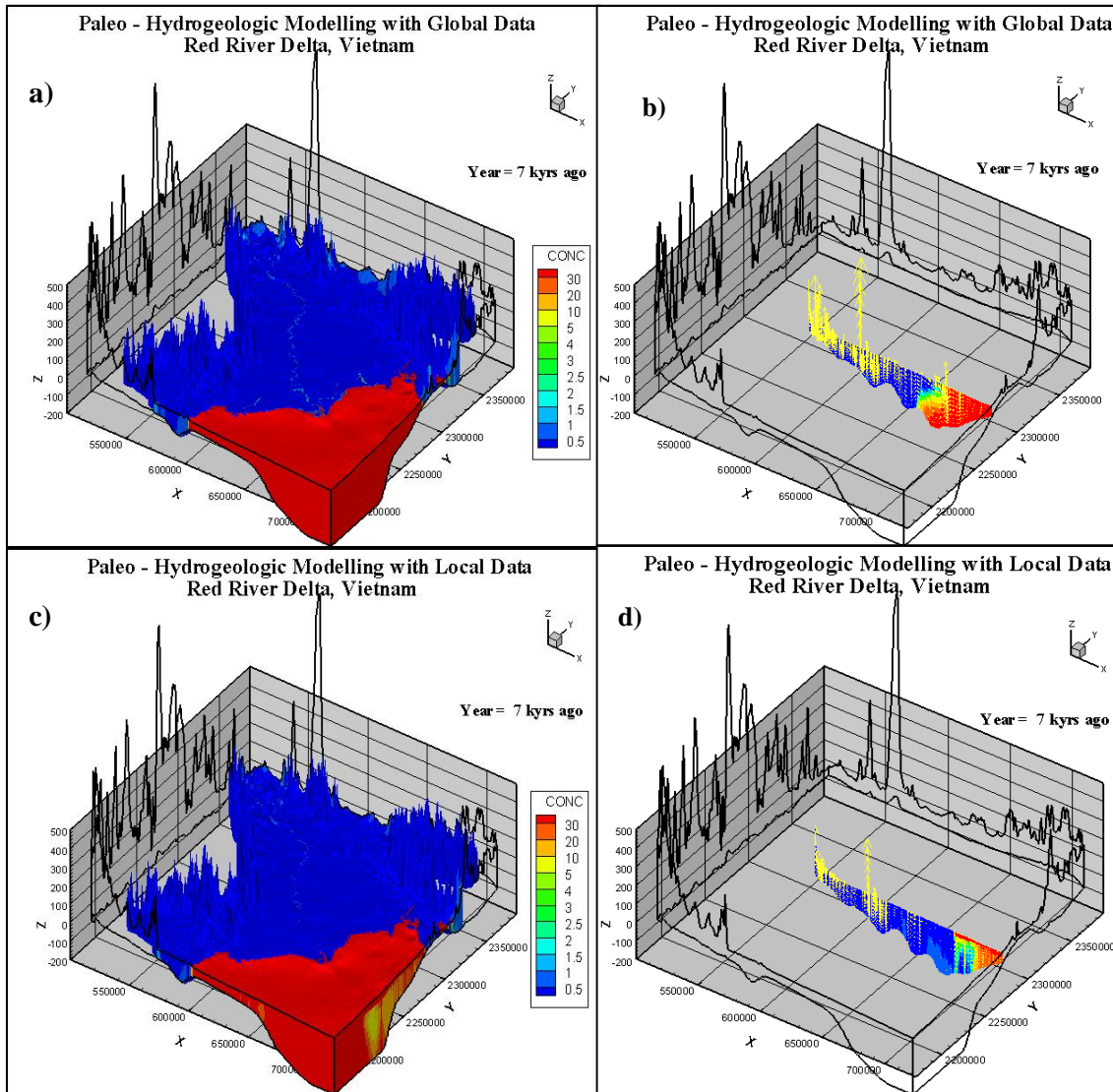


Figure 23: a) Concentration distribution of SC1 model; 7 kyrs ago b) Seawater over topping of SC1 model ( $y = 2283955$ )  
c) Concentration distribution of SC2 model; 7 kyrs ago d) Seawater fingering of the SC2 model ( $y = 2283955$ )

Groundwater head distribution for both scenarios are presented in Figure 24, where the head distribution within the landside is quite similar to that illustrated in Figure 19, but the head distribution in offshore side indicates a slight increment compared to the previous results. In Figure 24-b, it is possible to observe the impacts of geological formations on groundwater head distribution.

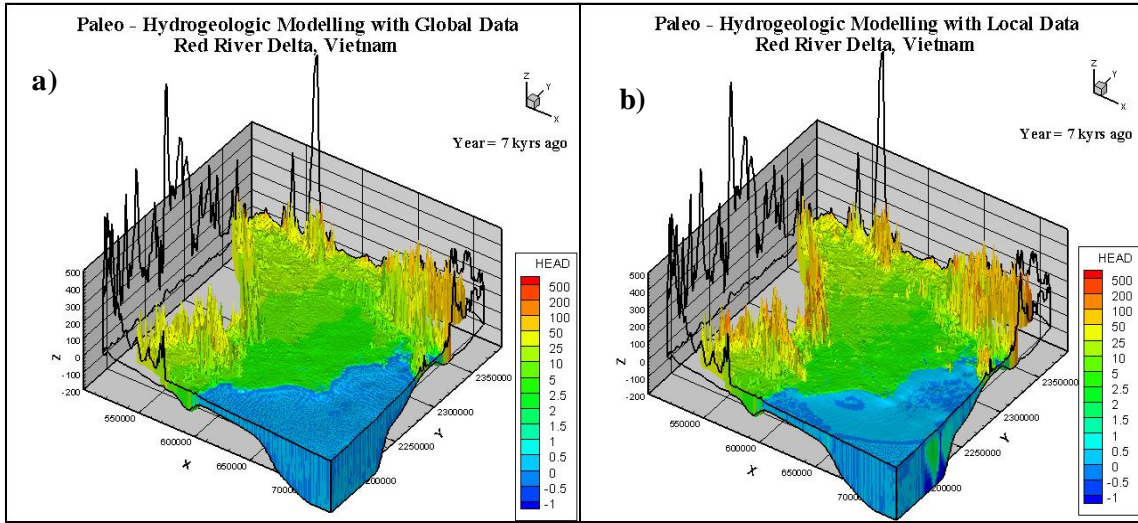


Figure 24: a) Groundwater head distribution in SC1 model; 7 kyrs ago b) Groundwater head distribution in SC2 model; 7 kyrs ago

#### 4.3.6. SP5 Model Results: 7 – 4 kyrs ago

According to the eustatic sea level fluctuation in the Holocene era, sea level reached a high stand of about 5 m before 4 kyrs ago and this phenomenon was simulated with SP5 models, where the local sea level grasped more closely to Hanoi, capital city of Vietnam. Sea level overtopping into far inlands probably would have decreased the available freshwater volume in the delta plain. Further, it can entrap saltwater even few meters away from the current coast line which can be problematic with the ongoing groundwater abstractions.

Figure 25 represents the concentration distributions of the model results at the end of SP5 and relevant cross sections to understand the level of salinity distribution within the inland areas. Cross section at  $y=2325446.82$  E is drawn across Hanoi city (Figure 25-b and Figure 25-d), where it can be observed that the saline groundwater is trapped few kilometres away in both scenarios. Hence, there is a potential risk of getting saline intrusion to far inlands of the RRD plain due to both the saline paleo groundwater and ongoing groundwater pumping activities. Those risk levels will be scrutinized later in section 4.4 and 4.5.

Cross section at  $y=2,257,294$  E was plotted mainly to differentiate the implications of the addition of geological information to the model. Figure 25-d shows the sea water fingering process and the salty – brackish mixing regions that are not visible in SC1 results (Figure 25-b). The addition of real time geological information advances the model to represent the natural sea water mixing phenomenon.

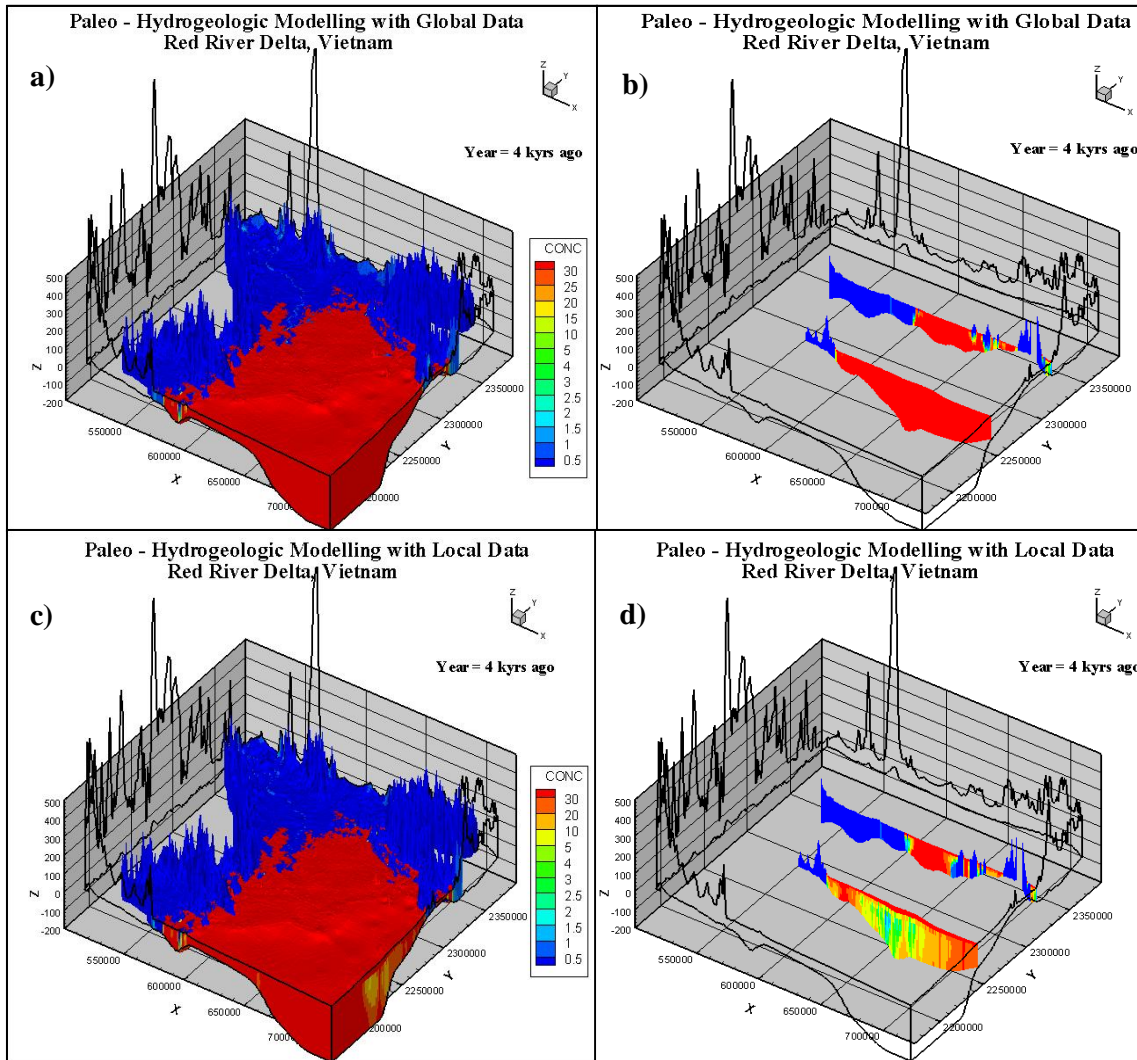


Figure 25: a) Concentration distribution of SC1 model; 4 kyrs ago b) Seawater over topping of SC1 model ( $y = 2257294$  and  $y = 2325446.82$ )

c) Concentration distribution of SC2 model; 4 kyrs ago d) Seawater fingering of the SC2 model ( $y = 2257294$  and  $y = 2325446.82$ )

Furthermore, Figure 26 demonstrates the groundwater head distribution over 4 kyrs ago. It is visible that the groundwater heads have increased in the deltaic plain with respect to the sea level high stand. It is also possible to observe the impacts of geological formations on groundwater head distribution.

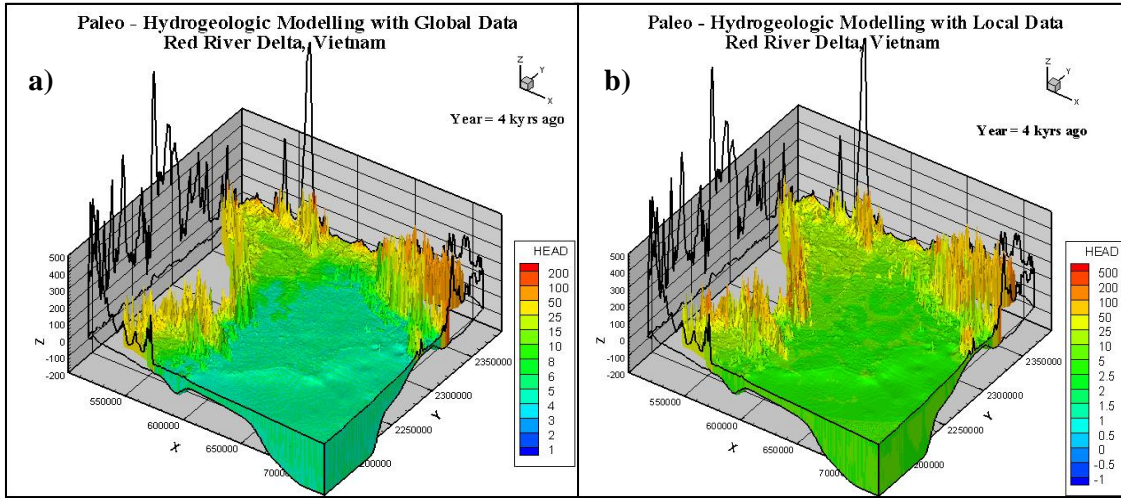


Figure 26: a) Groundwater head distribution in SC1 model; 4 kyrs ago b) Groundwater head distribution in SC2 model; 4 kyrs ago

#### 4.3.7. SP6 Model Results: 4 – 0 kyrs ago

Concluding the paleo-reconstruction modelling, SP6 model was simulated from 4 kyrs ago to present day, which would provide the information on current aquifer systems and their status within RRD plain. Groundwater head distribution (Figure 27) is found to be more or less similar to the same illustrated in Figure 24 while Figure 28 shows the concentration distributions of the region under both scenarios.

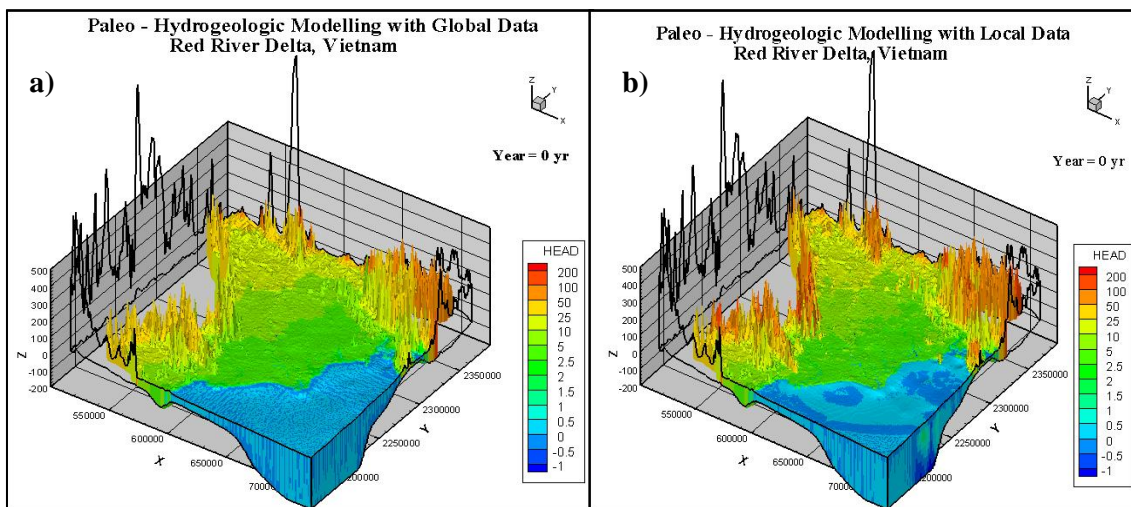


Figure 27: Present day groundwater head distribution a) SC1 b) SC2

In Figure 28-a, it is possible to visualize the impacts of sea level high stand. Saline regions on the top surface are a result of the SP5 model. Meanwhile, Figure 28-b display a cross section

of the region, where saline groundwater is trapped in far inlands compared to the current offshore state. As a result of the paleo-hydrogeologic modelling for 14 kyr, it is possible to determine the level of salty paleo groundwater entraps within far inlands of the RRD region. According to the SC2 model results, still there exist regions with saline groundwater in deep offshore areas, while SC1 model results indicate totally brackish offshore water. The introduction of local geological information has developed diverse impacts in the model as this saline groundwater mixing region is located under a clay aquitard. Hence, it can be interpreted that the diffusive transport of brackish water from the relatively low permeable layer is quite minimum.

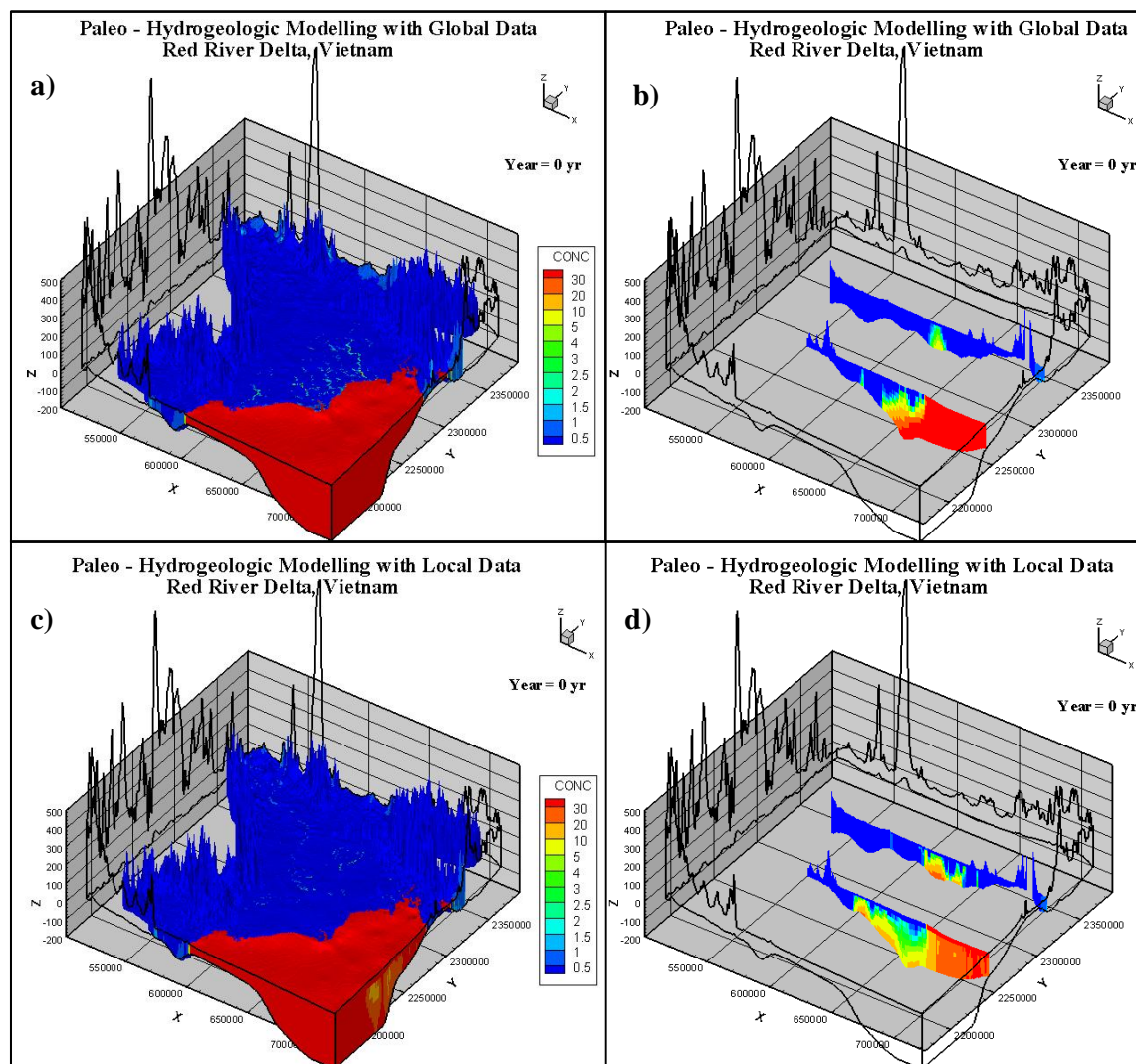


Figure 28: a) Concentration distribution of SC1 model b) Salty paleo water trapped in SC1 model ( $y = 2257294$  and  $y = 2325446.82$ )  
 c) Concentration distribution of SC2 model d) Salty paleo water trapped in SC2 model  
 ( $y = 2257294$  and  $y = 2325446.82$ )

Figure 28-b and Figure 28-d represent the concentration distribution of the same cross sections, which were used in Figure 25-b and Figure 25-d, respectively. Comparison of these two cross sections indicates the impacts of eustatic sea level fluctuation in RRD region and the trapped salty paleo groundwater in the deltaic region. But also in combination with the impacts of geology, SC2 shows much more brackish groundwater inland. Therefore, it can be concluded that the consideration of paleo-hydrogeologic changes in salinity modelling immensely important for the RRD case.

#### **4.4. Comparison of Paleo–hydrogeologic Models**

According to the SC1 model results, the saltwater intrusion distance was estimated as 70 km, while SC2 model resulted in 85 km for the same. Hence, the models have resulted in developing a saltwater wedge which are in the same range as per the results published by other researches. Tran et al. (2012) have estimated the saltwater intrusion to be 50 – 75 km, while Larsen et al. (2017) have mentioned that paleo sea water with a concentration of 19.6 g/l can be found at 75 km to the inland of RRD. Both results from SC1 and SC2 models of this research study indicate that saline-paleo groundwater with 19.6 g/l concentration can be found at a distance of about 34 and 60 km inland.

Total fresh groundwater volume under each stress period for both scenarios are calculated for the area of interest using MATLAB considering a threshold of 1 g/l to categorize the fresh and saltwater. Figure 29 represents the fresh groundwater volume variation in both scenarios during the paleo-hydrogeologic modelling. The overall figure demarcates the depletion of total fresh groundwater volume in the study region due to the sea-level rise. Sea level high stand that occurred 4 kyrs ago has caused the highest impact on fresh groundwater availability for both cases. Furthermore, during 7 kyrs ago and currently the sea level is at the same location. The influence of eustatic sea level high stand decreased the total fresh groundwater volume in present in SC1 and SC2 compared to 7 kyrs ago. However, aforementioned stages have the highest difference in fresh groundwater estimation between SC1 and SC2 models. But, simple geology assumed in SC1 generates a rapid recovery compared to SC2. Moreover, Figure 30 presents the fresh groundwater volume variation in each aquifer type under SC2.

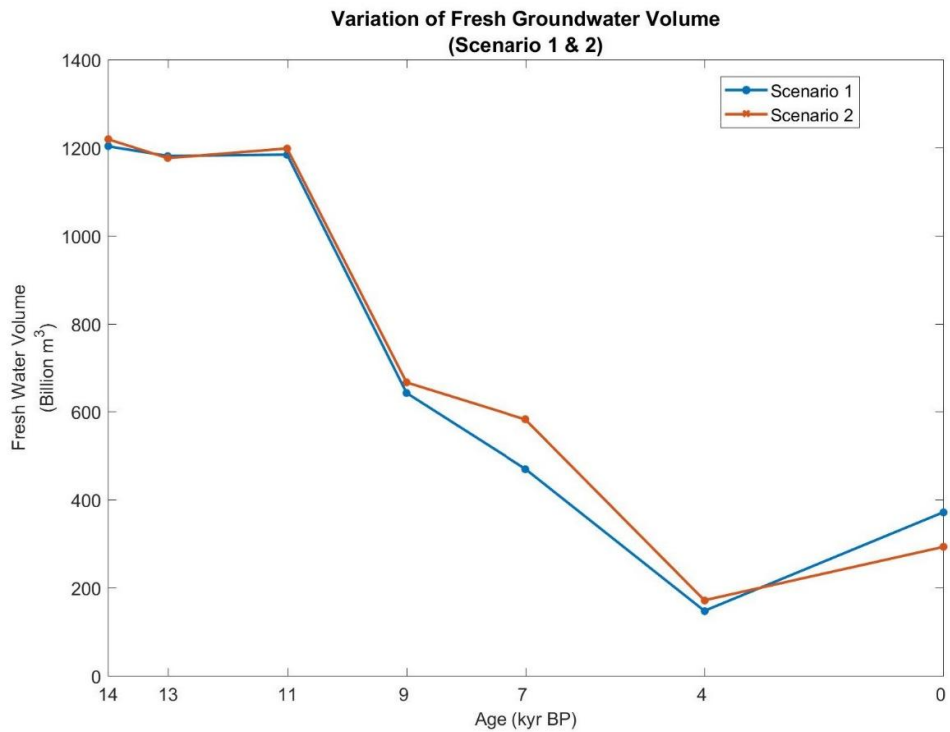


Figure 29: Total fresh groundwater volume variation under scenario 1 and 2

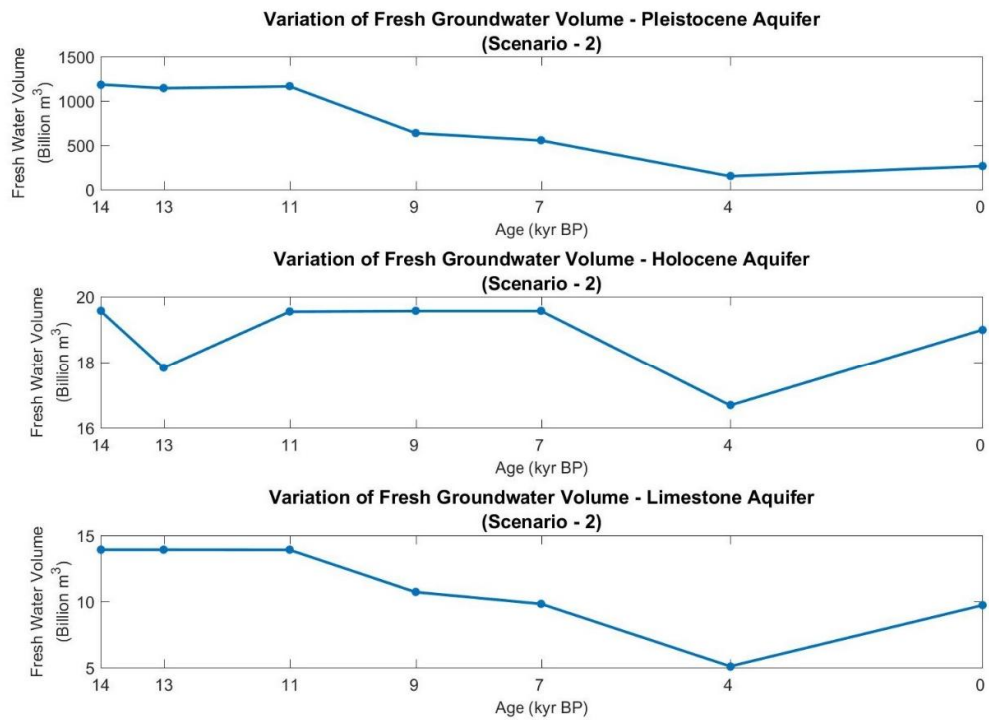


Figure 30: Freshwater volume variation under scenario 2

Table 8 tabulates the available fresh groundwater volumes under each stress period for both scenarios. It is noticeable that the initial fresh groundwater volumes are equal in both cases, while at the final step of SC1 records a higher volume. Freshwater volume difference in SP6 models is around 78.7 Billion m<sup>3</sup>. This difference is due to introduction of local geology to the models. Yet, the SC1 model provides a reasonable estimation for the paleo-reconstruction modelling in RRD plain.

Table 8: Fresh groundwater volume variation in paleo-reconstruction modelling under SC1 and SC2

Moment of time	SC1 (Billion m <sup>3</sup> )	SC2 (Billion m <sup>3</sup> )			Total Freshwater Volume	
		Pleistocene Aquifer	Holocene Aquifer	Limestone Aquifer		
SP0	14 kyrs ago	1218.9	1185.4	19.6	13.9	1218.9
SP1	13 kyrs ago	1181	1144.3	17.8	13.9	1176
SP2	11 kyrs ago	1183.9	1164.5	19.5	13.9	1197.9
SP3	9 kyrs ago	642.6	663.3	19.6	10.7	696.6
SP4	7 kyrs ago	470	553	19.6	9.8	562.8
SP5	4 kyrs ago	147.6	149.9	16.7	5.1	171.7
SP6	Present day	371.5	264.2	18.9	9.7	292.8

According to the iMOD-SEAWAT output on mass budget of SP6 models under both scenarios determines that the change of storage (out-in) in SC1 as a decrease of 358,018 m<sup>3</sup>/day while SC2 model implies an increase of storage from a 390,623 m<sup>3</sup>/day. Further, the head dependent boundary inflow accounts for 6,377,665,536 m<sup>3</sup>/day and 1,508,590,976 m<sup>3</sup>/day under SP1 and SP2 models respectively. The inflow from the head dependent boundaries composes of inflow from the land boundary, seawater inflow and natural recharge. Head dependent boundary outflow is estimated as 4,334,757,376 and 1,012,602,688 m<sup>3</sup>/day for each model. Moreover, the net recharge (recharge-drainage) calculations estimate a rate of 3,815,407,616 m<sup>3</sup>/day and 3,175,233,536 m<sup>3</sup>/day in both SC1 and SC2 models respectively.

#### 4.5. Current Status of Red River Delta, Vietnam

Massive scale groundwater pumping is taking place in the RRD as shown in Table 3, which has been added to the model during the next steps to demarcate the current aquifer status. Results of the SC2 paleo-hydrogeological models were utilized for this analysis and thus, the geological distribution of the region has been taken into account.

Paleo-reconstruction model results were considered to provide information of the year 1920. Hence, 1920 was considered as the initial status for the current modelling series. Consequently, 50 years of groundwater extraction in Hanoi was considered with a rate of

819.67 m<sup>3</sup>/day from each extraction well (Appendix 3). According to Van Pham and Lee (2014); large scale groundwater pumping takes place from the Pleistocene aquifer system. Hence, the extractions were assumed to be from the Pleistocene aquifer in model layer 5. Figure 31 displays the concentration and head distribution in year 1970, corresponding to the aforementioned groundwater pumping activities. Head distribution (Figure 31-b) has been slightly reduced compared to the resulted head distribution from SP6 model under SC2. When compared with Figure 28-c, saline concentration cells can be observed on the top layers closer to the coastal region, indicating that saline-paleo groundwater has reached upper layers as a result of continuous pumping.

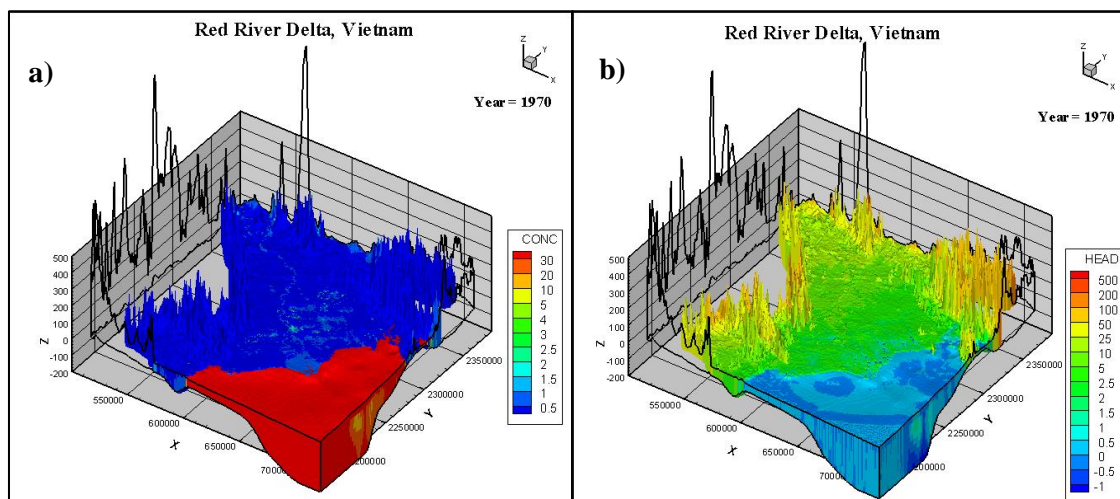


Figure 31: a) Concentration variation and b) groundwater head distribution in 1970

Groundwater extractions were then increased from about 53% in total, in which, it was assumed that the groundwater abstraction in Hanoi was continuous from the Pleistocene aquifer in model layer 5, while the other cities extract groundwater from the Pleistocene aquifer in model layer 3.

Figure 32 illustrates the concentration and groundwater head distribution in 1990. Compared to the reference year of 1920, growth of saline intrusion in the surface layer has increased by 1990, whereas the groundwater head distribution shows a slight decrease.

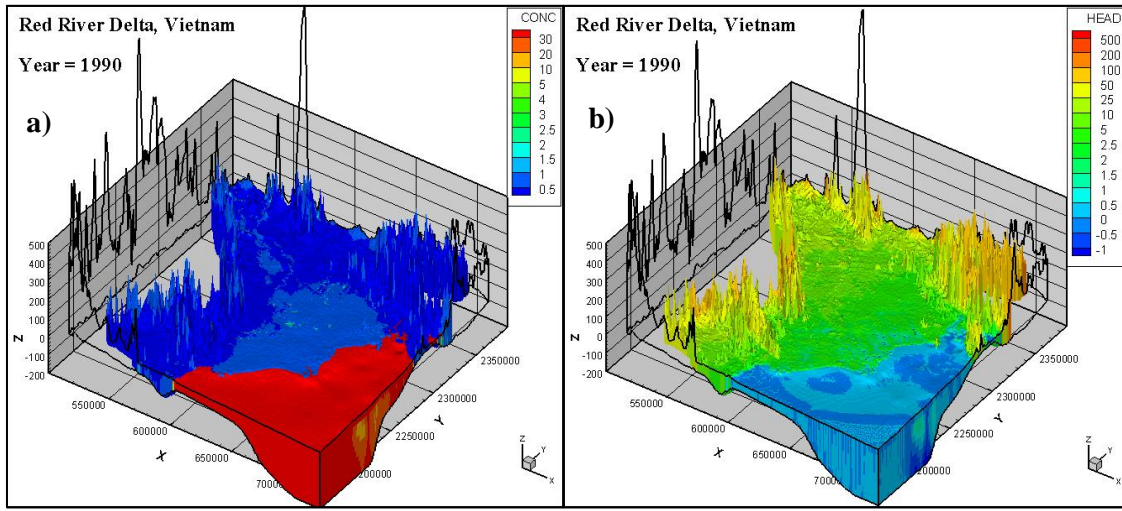


Figure 32: a) Concentration variation and b) groundwater head distribution in 1990

Over again, groundwater extraction rates were increased (Appendix 3) where the model results represent the groundwater system in 2010. It is assumed that the major groundwater extractions continue from the Pleistocene aquifer in model layer 7, while the minor extractions take place from the Pleistocene aquifer in model layer 5. Figure 33 shows the groundwater concentration and head distribution in 2010 with the impacts of increased groundwater extractions. In comparison with Figure 32-a, Figure 33-a shows the growth of salinity level closer to the top layers, where groundwater heads are further decreased.

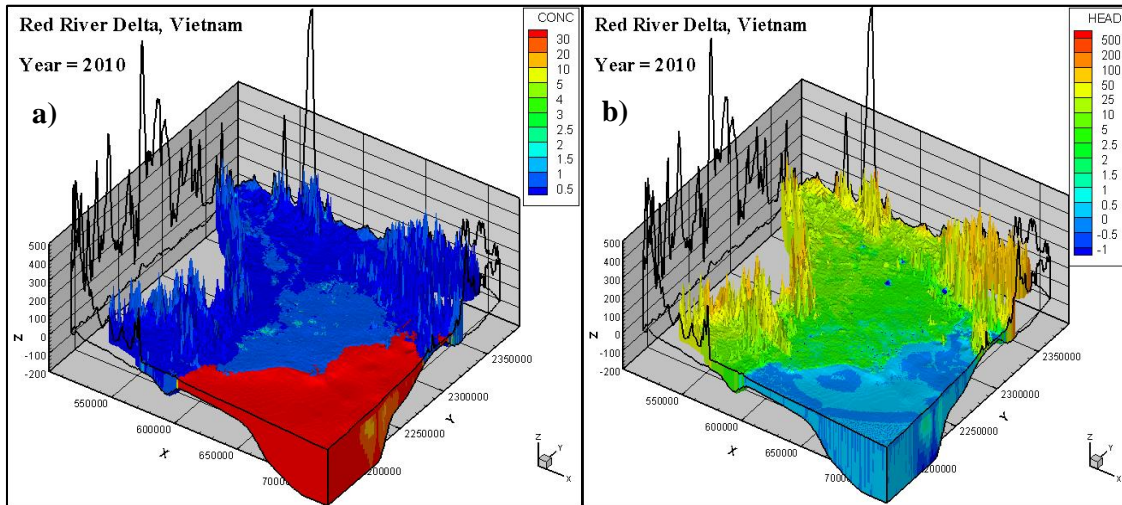


Figure 33: a) Concentration variation and b) groundwater head distribution in 2010

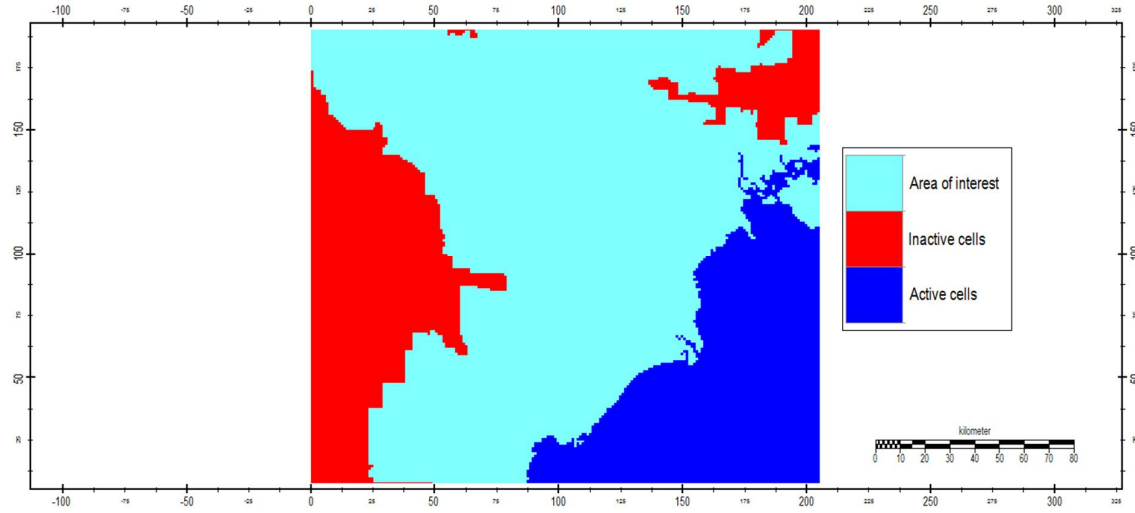


Figure 34: Area of interest in estimating fresh groundwater volumes

Figure 35 characterises the total fresh groundwater volume variation in the area of interest (Figure 34) of the simulated models from 1920 to 2010. The graphs below illustrates the pumping induced threats in the delta plain. A depletion in fresh groundwater storage in the Pleistocene aquifer can be observed, whereas the storage of the other two types of aquifers remain constant. This implies that the Pleistocene aquifer system is under an emerging threat due to the escalating pumping activities.

According to Van Pham and Lee (2014); Holocene aquifer system is abandoned by the residents of the vicinity due to its poor water quality. Furthermore, Holocene aquifer is principally distributed in model layer 1 is isolated by an underlying Pleistocene clay layer. Hence, many have suggested that the interactions between Holocene and Pleistocene aquifer systems are minimum (Van Pham and Lee 2014; Tran et al., 2012; Nghi et al., 1991 and Pham et al., 2015). Thus, the fresh groundwater storage in Holocene aquifer system remains relatively stable. Limestone aquifer system also resides sustainable due to its natural conditions.

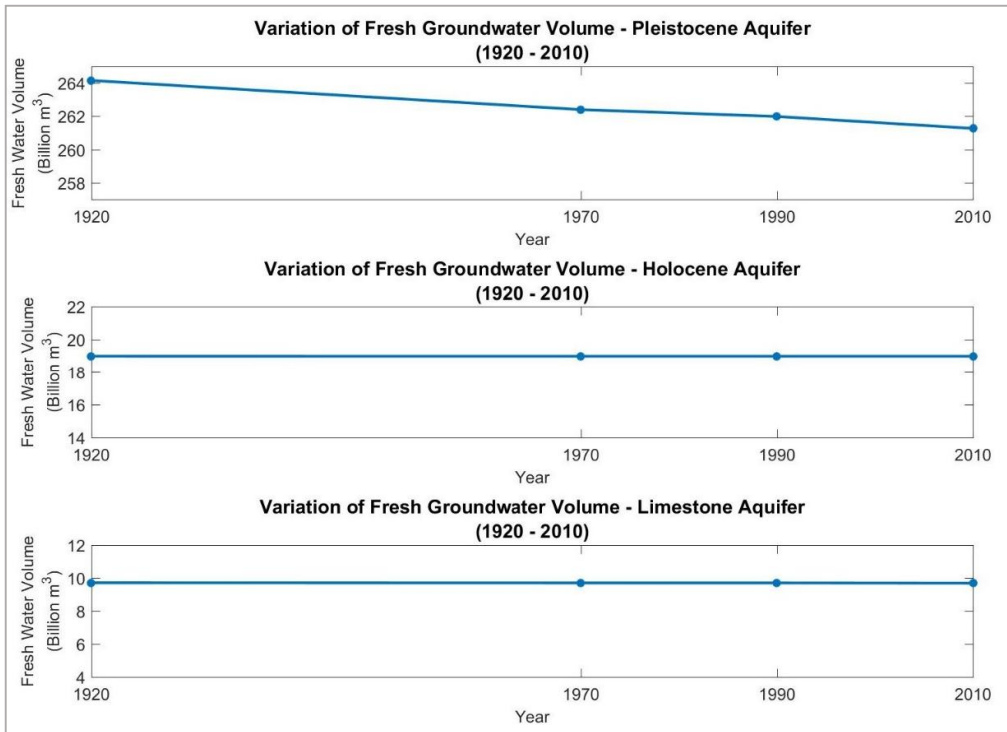


Figure 35: Total fresh groundwater volume variation in each aquifer type from 1920 to 2010

Bui et al. (2012a) stated that a pumping induced cone of depression has already been developed under Hanoi which could cause future threats. This study results also indicate the development of a cone of depression in Hanoi. Figure 36 represents the growth of pumping induced cone of depression in 2010 in model layer 7 (with respect to the reference year). In Hanoi, groundwater heads have decreased throughout the modelled years as an impact of massive pumping activities. Figure 36-c shows the groundwater head difference in model layer 7, where a maximum head depletion of 27 m is recorded under the city of Hanoi. Hence, the average groundwater depletion rate in the Pleistocene aquifer can be estimated as 0.3 m/year where Bui et al., 2011 stated a declination rate of 0.2 m/year.

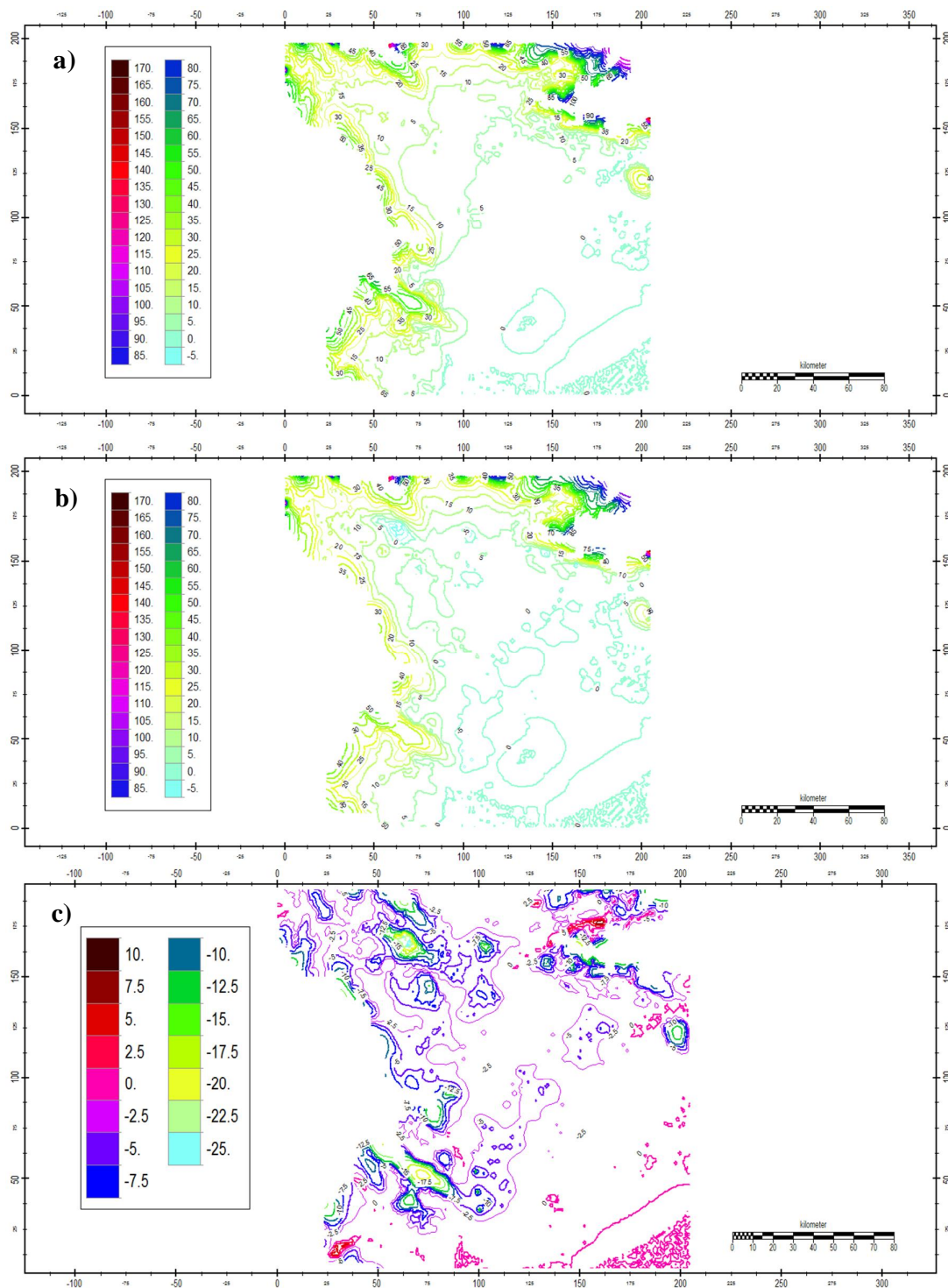


Figure 36: Development of pumping induced cone of depression a) Groundwater head distribution in model layer 7 in 1920 b) Groundwater head distribution in model layer 7 in 2010 c) Head difference in model layer 7 (2010-1920)

Furthermore, the contour maps of groundwater head also suggest that the coastal cities like Nam Dinh and Thai Binh (Figure 1) are under emerging threats. Van Pham and Lee (2014) reported a groundwater head depletion of about 4 – 8 m in these regions for the period of 1995 – 2011. The current study also estimates a depletion of about 5 – 7.5 m for the model period.

From the output results of 2010 model salinity was found 85 km inland from the coast. Hence, it clarifies that the longitudinal distribution of salinity in the system hasn't changed when compared to the estimations from the paleo-reconstruction model. Yet, the salinity level has increased in the surface layers as a result of the saline-paleo groundwater trapped in lands.

## 4.6. Simulation for Future Scenarios

### 4.6.1. Reference Case (FSC1)

A “reference model” (FSC1) was developed as the preliminary step in future scenario assessment. Hence, the groundwater pumping rates estimated for the year 2010 were kept constant and the model was simulated for 100 years. All the other parameters remained unchanged so that the diverse scenarios can be compared with respect to the reference model.

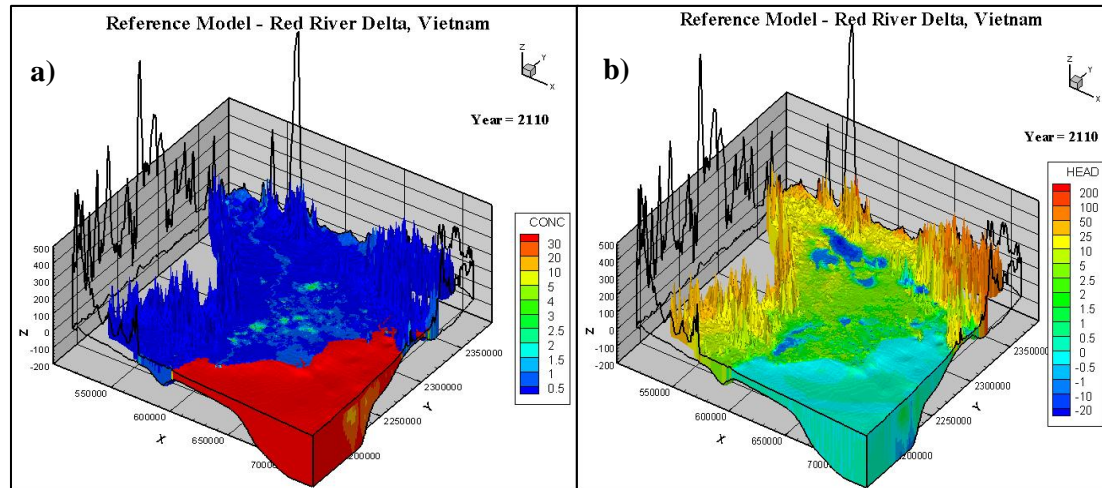


Figure 37: a) Concentration distribution in 2110 according to FSC1 b) Head distribution in 2110 according to FSC1

Figure 37 reveals the predicted concentration and groundwater head distribution in the year of 2110 for the FSC1 model. Increasing state of salinity intrusion in the next 100 years is clearly visible with the current rate of pumping (Figure 37-a, with respect to Figure 33-a). Groundwater heads have decreased drastically around Hanoi, Nam Dinh, Thai Binh and Hai Phong provinces.

#### 4.6.2. Increase in Groundwater Extraction Rates (FSC2)

In terms of future scenario assessment, an increase in groundwater pumping rates was assumed with in relation to the current population growth in RRD region (Annex 3). Figure 38 illustrates the concentration and groundwater head variation by 2110 with increased groundwater extraction rates. In comparison to Figure 37, it shows a significant increase in salinity in the deltaic plain, which can be attributed to the combined effect of paleo salty groundwater and pumping activities. Consequently, a major decrease in groundwater heads can also be observed in the region (Figure 38-b), indicating the development of the cone of depression. Maximum drop in heads is estimated to be around 85 m under Hanoi territory.

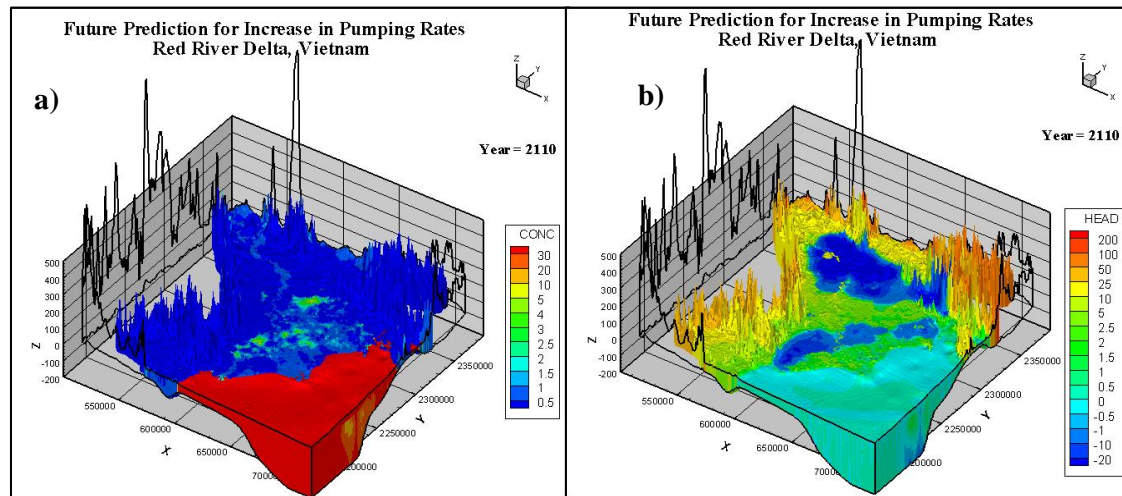


Figure 38: a) Concentration variation in 2110 under FSC2 b) Groundwater head variation in 2110 under FSC2

Figure 39 illustrates the salinity increase and severe decrease of groundwater heads of FSC2 with respect to FSC1. Figure 39-b evidently indicates the growth of pumping induced cone of depression in Hanoi region. Groundwater head depletion is around 7 m with regards to FSC1.

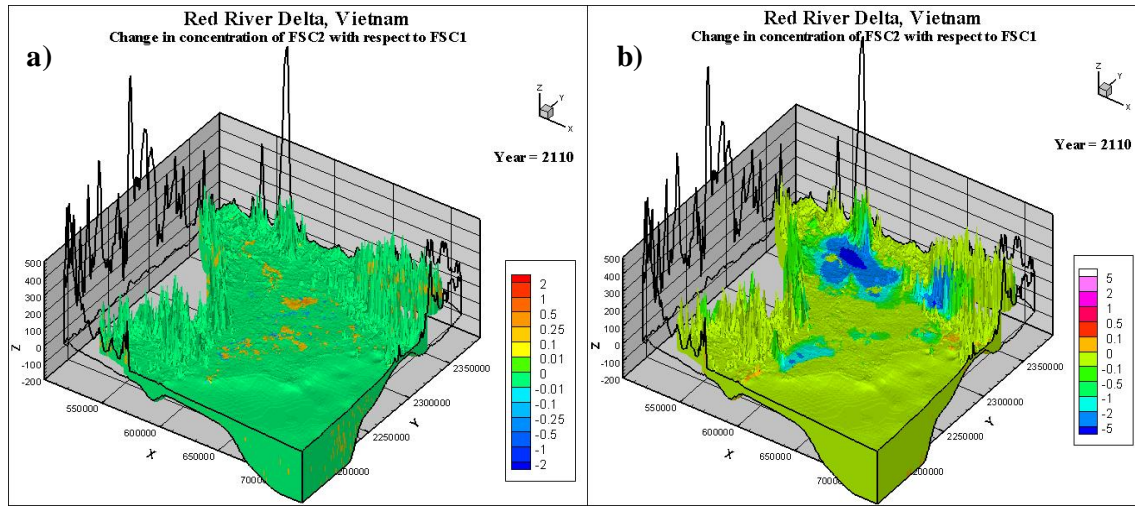


Figure 39: a) Groundwater concentration and b) head distribution change in FSC2 with respect to FSC1

#### 4.6.3. Impacts on Predicted MSLR (FSC3)

Figure 40 presents the results obtained by considering only the impacts of MSLR of the region (FSC3). Resulting concentration and groundwater head distribution are more alike with FSC1 results (Figure 37), whereas the offshore head distribution has been changed due to the sea level overtopping. Therefore, Figure 40 indicates that MSLR has less influences on the groundwater aquifer systems in the region.

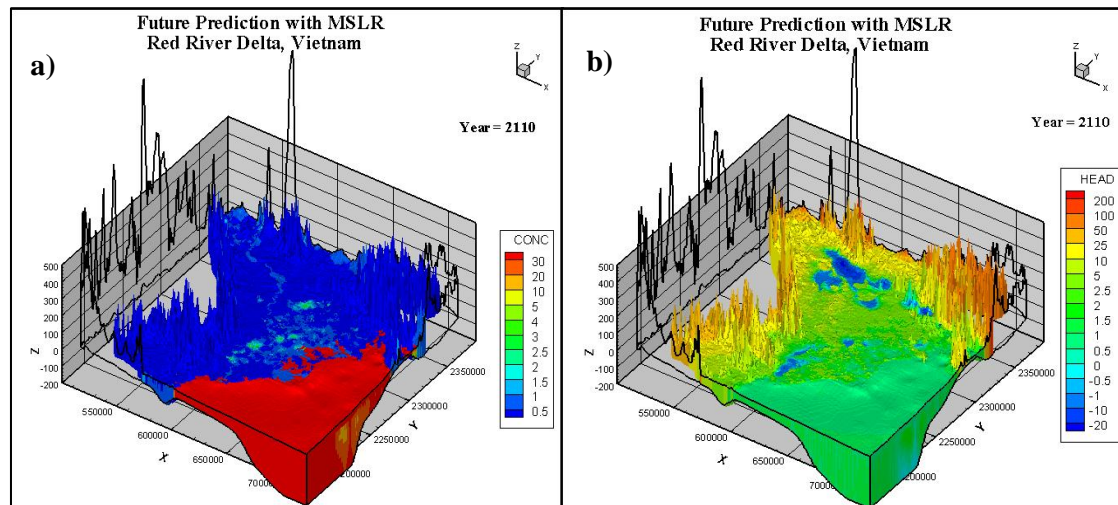


Figure 40: a) Concentration variation in 2110 with MSLR b) Groundwater head variation in 2110 with MSLR

Aforementioned phenomenon is further proved by Figure 41 which represents the impacts on FSC3 model with regard to FSC1. Groundwater head distribution in the area of the interest indicated minor changes. So, the cone of depression developed in FSC1 has not been further advanced. This is in agreement with the findings presented in Van Pham and Lee (2014). However, sea level overtopping could decrease the fresh groundwater volume as shown in Figure 41-a.

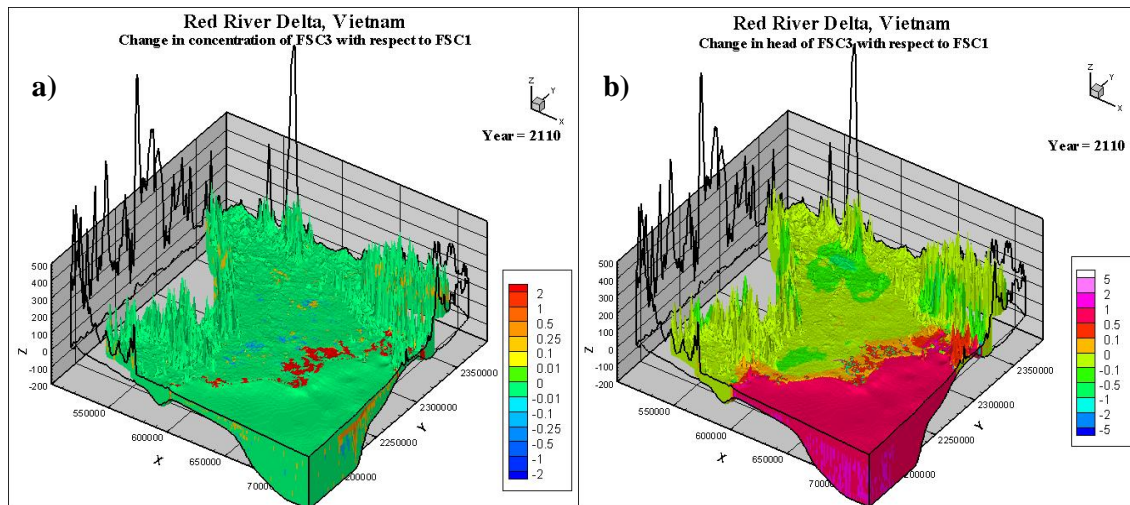


Figure 41: a) Concentration and b) groundwater head distribution change in FSC3 with respect FSC1

#### 4.6.4. Increase in Groundwater Extraction Rates along with Predicted MSLR (FSC4)

During this step, the increase in groundwater extraction rates and the predicted MSLR were considered together (FSC4) which can be stated as the most probable environment to occur in the future. Figure 42 displays the concentration variation and the groundwater head distribution in the model outputs. It can be observed that the concentration variation in Figure 42-a is similar to that displayed in Figure 38-a, whereas the head distribution in the deltaic plain is similar to that shown in Figure 38-b. Figure 43-a represents the impacts on groundwater concentration in FSC4 with regards to FSC1 where sea level overtopping has influenced the fresh groundwater availability. Moreover, Figure 43-b proves that the head distribution in the area of interest is similar with FSC2 (Figure 38-b).

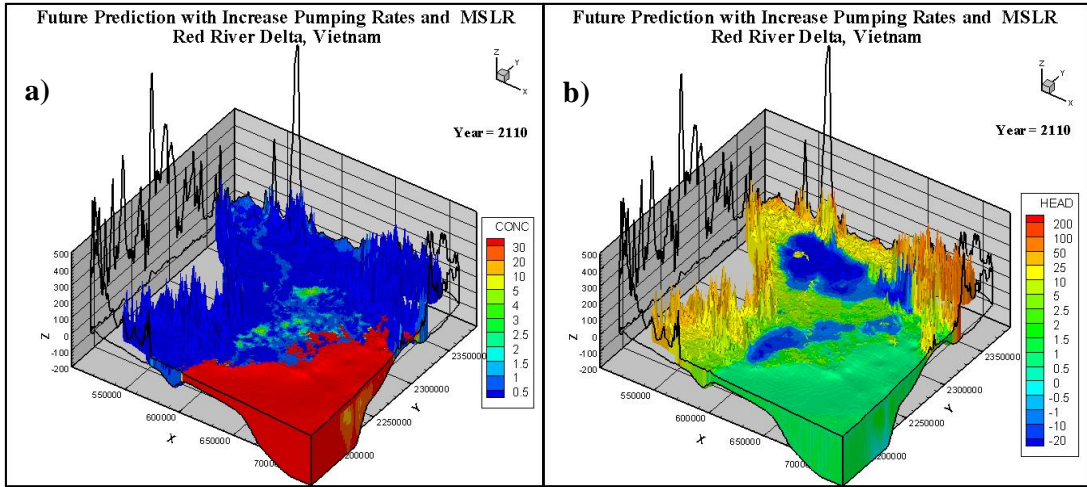


Figure 42: a) Concentration variation in 2110 with increase in pumping rates and MSLR  
b) Head variation in 2110 with increase in pumping rates and MSLR

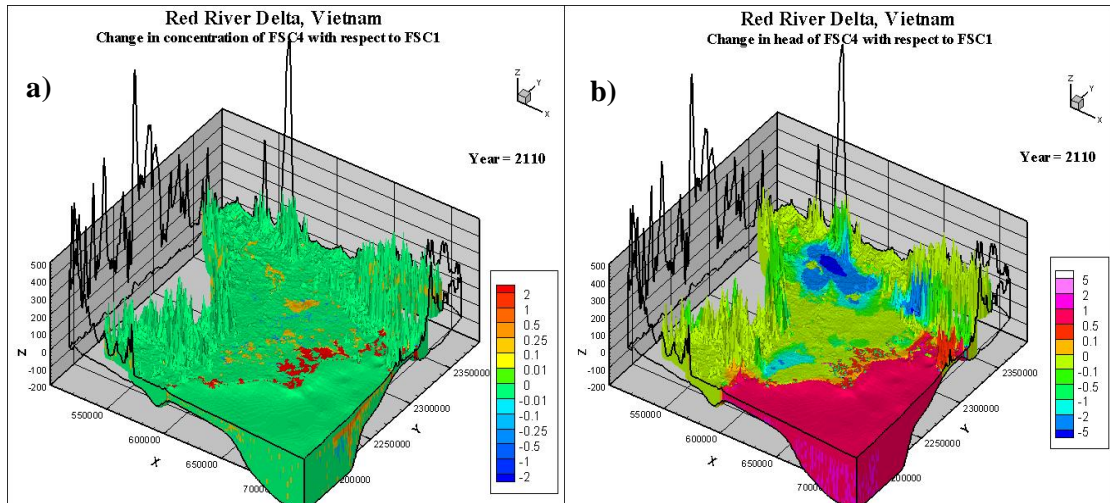


Figure 43: a) Concentration and b) groundwater head distribution change in FSC4 with respect FSC1

#### 4.6.5. Future Scenario Comparison

Groundwater head and concentration distributions of the considered future scenarios indicate a higher sensitivity for the increase in the pumping rates, whereas MSLR has less influence on the same. Appendix 5 involves several cross sections along Hanoi and Nam Dinh provinces under each simulation, which clarify the influences of pumping and MSLR on the same. Hence, it can be considered that the salty paleo water trapped under the deltaic plain causes the salinity intrusion in the region under the influence of excessive groundwater extractions.

Figure 44 presents the fresh groundwater volume variation with respect to the reference model for each tested scenario. The increase in pumping rates develops a diminution in fresh

groundwater availability in the Pleistocene aquifer, while the sea level overtopping also develops a similar situation. Impacts of both scenarios drastically reduce the freshwater volume in the aquifer system as shown in Figure 44-a. Holocene and limestone aquifers are mostly stabilize under natural conditions and hence the tested future scenarios will not considerably affect them.

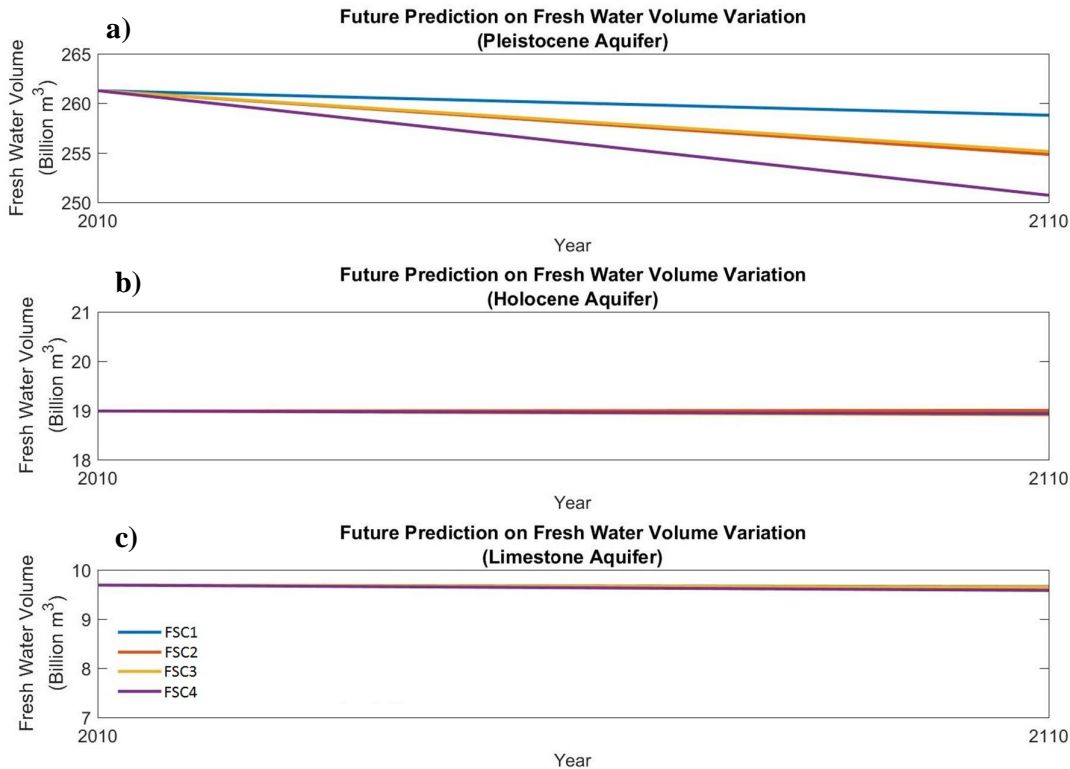


Figure 44: Total freshwater volume variation under tested future  
 a) Pleistocene Aquifer  
 b) Holocene Aquifer c) Limestone Aquifer

## **CHAPTER 5**

# **Conclusions and Recommendations**

## **5.1. Conclusions**

Development of a 3D variable-density groundwater flow and transport model for the RRD in Vietnam with iMOD-SEAWAT, an open-source software which couples MODFLOW and MT3DMS will enable the assessment of the groundwater systems in the region under the influences of climate change driven and anthropogenic forcing at a macro time scale.

Though there was a possibility of retrieving data from the National Centre for Water Resources Planning and Investigation (NAWAPI) in Vietnam, the current model was initiated with globally available data (SC1). The conceptual model was originally developed with the curiosity to measure the extent that a similar research can reach with only global data. Further, the addition of local data (SC2) while increasing the complexity of the model in later steps was used to estimate the precision of the global data model.

3DSolid-Tool in graphical user interface of iMOD was utilized to develop the geological distribution in the study region via several borehole logs. It is noticeable that the geology interpolation in the deltaic region resulted in producing several deviations to the geological profiles found in the literature due to the uncertainty of the borehole logs classification and also due to the lack of borehole logs in the entire study region. Moreover, the interpolation emphasised the significant importance of the number of model layers on the outcome. Layer thickness variation in the deltaic plain and the offshore conclude increasing the number of model layers up to about 40 layers where the model layer thickness around coast would reach a maximum of 10 m.

Addressing the first research question, SC1 and SC2, both simulations imply similar impacts on fresh groundwater volume with regards to eustatic sea level fluctuation where the highest impact corresponds with the sea level high stand. However, final total freshwater volumes of each model were calculated as 371.5 and 292.8 billion m<sup>3</sup> for SC1 and SC2 respectively. Moreover, SC1 and SC2 models determine that the paleo-saltwater exists about 70 and 85 km away from the coast correspondingly.

Research question 2 examined the reliability of utilization of the global data for data scarce region which is being addressed by the comparison of SC1 and SC2 models. The fresh

groundwater recovery under SC2 is less than SC1 indicating the influence of local geology. Simple geology assumed in SC1 model has developed faster salt-fresh groundwater mixing fluxes comparison to SC2. Simulation results under SC1 paleo-reconstruction models conclude the plausibility to construct a 3D variable density groundwater flow model and to estimate the fresh-saltwater wedge. However, the SC2 model revealed more realistic progressions such as fingering process with sea level overtopping.

Later, groundwater pumping scenarios were introduced to the SC2 model for the years of 1970, 1990 and 2010 in order to estimate the current state of RRD region. Results of these models indicate a decrease in Pleistocene aquifer's freshwater storage by about 3 billion m<sup>3</sup> at the end of the year 2010. Further, they indicate a pumping-induced cone of depression under the city of Hanoi. Groundwater head depletion in the region was estimated to be around 27 m. Coastal cities like Nam Dinh and Thai Binh were found to be under severe threats because of the drastic reduction of their groundwater heads. Salinity concentration mainly increases with the extractions in the delta plain as an impact of trapped saline paleo-groundwater. Hence, conducting a paleo-hydrogeologic modelling assist to conclude the current status of the groundwater system of the RRD. Considering the recently published research works, it can be concluded that the SC2 model provides more reliable estimations for the paleo-reconstruction modelling.

A reference model of unchanged groundwater pumping (FSC1), increment of groundwater pumping by ~ 50% (FSC2), MSLR by 1 m (FSC3) and both MSLR rise and pumping increase (FSC4) are the tested future scenarios to answer the final research questions stated in Chapter 1. Groundwater heads rapidly decrease with the predicted increase in groundwater pumping rates compared to the increase in MSLR. Correspondingly, upconing of trapped paleo-saltwater is observed more with rising groundwater extractions. More importantly, the increased pumping rates and MSLR together result in the highest fresh groundwater volume depletion in the RRD where the resources' management plans should be developed considering this phenomenon.

## **5.2. Recommendation**

- Calibrating the 3D variable-density groundwater flow and coupled salt transport model with actual contemporary quantity and quality data will increase the accuracy of the conceptual model developed with global data sets and published literature on geological data.
- Lithology classes used in the model should be improved to accommodate the complex geological changes undergone by the RRD during the Holocene period.
- Paleo-reconstruction models under SC1 used significantly larger horizontal and vertical hydraulic conductivity values. Simulating the models again with the conductivity values used in SC2 model might indicate the fingering processes under SC1 simulations.
- Reducing the uncertainties in the adopted salt transport parameter values will significantly enhance the model reliability (e.g. longitudinal dispersivity values).
- Locations of pumping wells and pumping rates were estimated fully depending on available literature resources which might add uncertainties to the model estimations. Therefore, collecting some real time data with groundwater pumping will accurate the model estimations.

# References

- Bear, J., Cheng, A.H.D., Sorek, S., Ouazar, D. and Herrera, I. eds., 1999. Seawater intrusion in coastal aquifers: concepts, methods and practices. (Vol. 14). Springer Science & Business Media.
- Brakenridge, G.R., Syvitski, J.P.M., Overeem, I., Higgins, S.A., Kettner, A.J., Stewart-Moore, J.A., Westerhoff, R., 2013. Global mapping of storm surges and the assessment of coastal vulnerability. *Nat. Hazards* 66, 1295–1312. doi:10.1007/s11069-012-0317-z
- Bui, D. Du, Kawamura, A., Tong, T.N., Amaguchi, H., Nakagawa, N., 2012a. Spatio-temporal analysis of recent groundwater-level trends in the Red River Delta, Vietnam. *Hydrogeol. J.* 20, 1635–1650. doi:10.1007/s10040-012-0889-4
- Bui, D. Du, Kawamura, A., Tong, T.N., Amaguchi, H., Nakagawa, N., Iseri, Y., 2011. Identification of aquifer system in the whole Red River Delta, Vietnam. *Geosci. J.* 15, 323–338. doi:10.1007/s12303-011-0024-x
- Bui, D. Du, Kawamura, A., Tong, T.N., Amaguchi, H., Trinh, T.M., 2012b. Aquifer system for potential groundwater resources in Hanoi, Vietnam. *Hydrol. Process.* 26, 932–946. doi:10.1002/hyp.8305
- Dasgupta, S., Laplante, B., Meisner, C., Wheeler, D., Yan, J., 2009. The impact of sea level rise on developing countries: A comparative analysis. *Clim. Change* 93, 379–388. doi:10.1007/s10584-008-9499-5
- Delsman, J.R. 2015. Saline groundwater - surface water interaction in coastal lowlands. <http://hdl.handle.net/1871/52796>
- Delsman, J.R., Hu-A-Ng, K.R.M., Vos, P.C., De Louw, P.G.B., Oude Essink, G.H.P., Stuyfzand, P.J., Bierkens, M.F.P., 2014. Paleo-modeling of coastal saltwater intrusion during the Holocene: An application to the Netherlands. *Hydrol. Earth Syst. Sci.* 18, 3891–3905. doi:10.5194/hess-18-3891-2014
- Dzung, N.X., Nagothu, U.S., Rafoss, T., Borrell, A. and Huy, B., 2014. Climate change and impacts on rice production in Vietnam: Pilot testing of potential adaptation and mitigation measures.
- Faneca Sanchez, M., Bashar, K., Janssen, G.M.C.M., Vogels, M., Snel, J., Zhou, Y., Stuurman, R., Oude Essink, G.H.P., 2015. SWIBANGLA : Managing salt water intrusion impacts in coastal groundwater systems of Bangladesh 153.
- Hien, L.T., Quy, P.N., Viet, N.T., 2010. Assessment of Salinity Intrusion in the Red River under the Effect of Climate Change. *J. Civ. Eng. Archit.* 4, 1–6.
- Hijioka, Y., E. Lin, J.J. Pereira, R.T. Corlett, X. Cui, G.E. Insarov, R.D. Lasco, E. Lindgren, and A. Surjan, 2014. Asia. In Climate Change 2014: Impacts, Adaptation, and Vulnerability. Part B: Regional Aspects. Contribution of Working Group II to the Fifth Assessment Report of the Intergovernmental Panel on Climate Change
- Jarvis, A., Reuter, H.I., Nelson, A., Guevara, E. 2008. Hole-filled SRTM for the globe Version 4. available from the CGIAR-CSI SRTM 90m Database

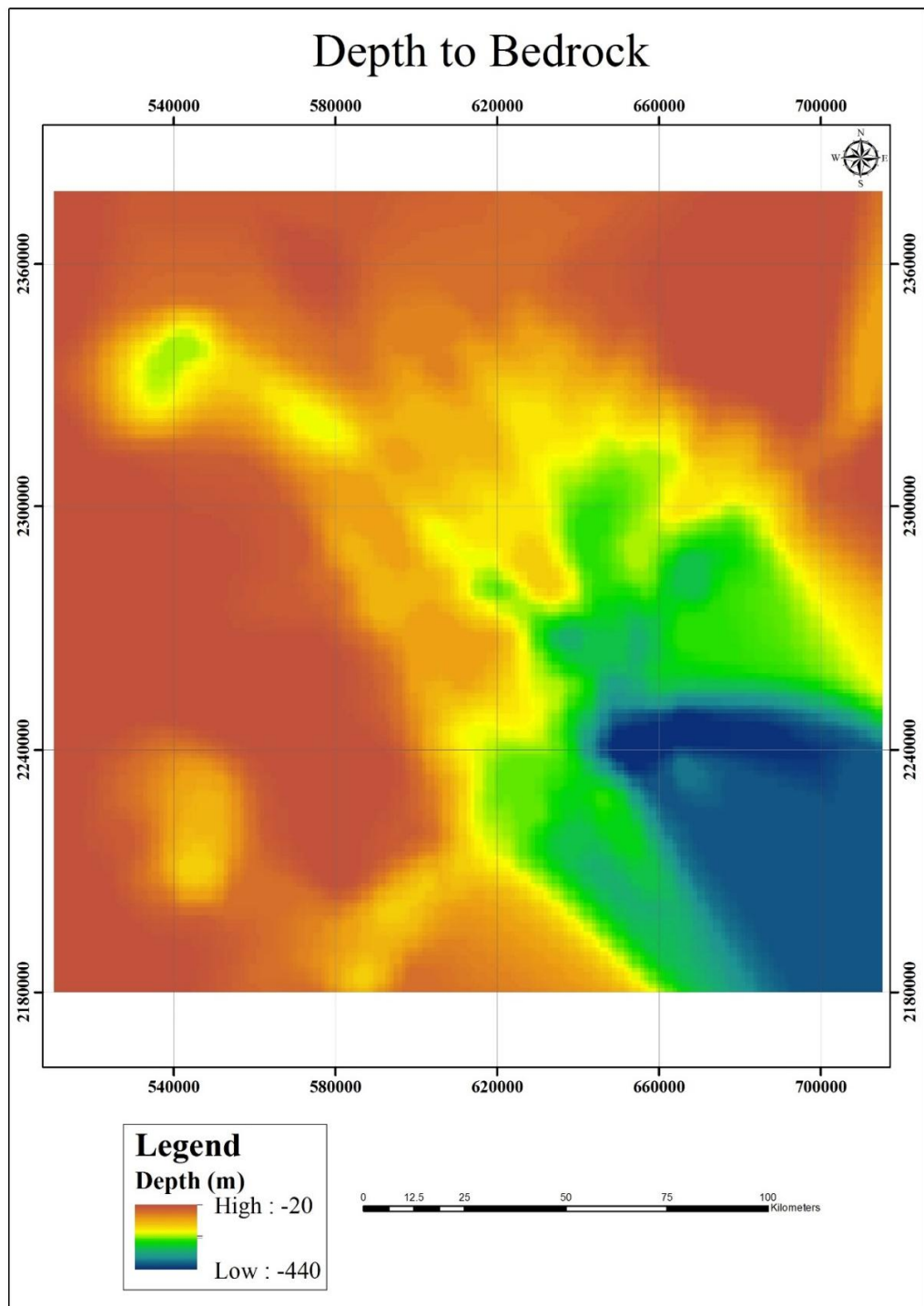
- (<http://srtm.csi.cgiar.org>)
- Kim, K.Y., Chon, C.M. and Park, K.H., 2007. A simple method for locating the fresh water–salt water interface using pressure data. *Groundwater*, 45(6), pp.723-728
- Larsen, F., Tran, L.V., Van Hoang, H., Tran, L.T., Christiansen, A.V. and Pham, N.Q., 2017. Groundwater salinity influenced by Holocene seawater trapped in incised valleys in the Red River delta plain. *Nature Geoscience*, 10(5), pp.376-381.
- Lehner, B., Verdin, K., Jarvis, A. 2008. New global hydroprahy derived from spaceborn elevation data. *Eos, Transactions*, 89 (10): 93-94. Data available at: <http://www.hydrosheds.org/>
- Li, Z., Saito, Y., Matsumoto, E., Wang, Y., Tanabe, S., Vu, Q.L., 2006. Climate change and human impact on the Song Hong (Red River) Delta, Vietnam, during the Holocene. *Quat. Int.* 144, 4–28. doi:10.1016/j.quaint.2005.05.008
- Minderhoud, P. S. J., Erkens, G., Van Hung, P., Vuong, B. T., Erban, L. E., Kooi, H., & Stouthamer, E. 2017. Impacts of 25 years of groundwater extraction on subsidence in the Mekong delta, Vietnam. *Environmental Research Letters*, 12, 13. <https://doi.org/10.1088/1748-9326/aa7146>
- Neumann, J.E., Emanuel, K.A., Ravela, S., Ludwig, L.C. and Verly, C., 2015. Risks of coastal storm surge and the effect of sea level rise in the Red River Delta, Vietnam. *Sustainability* 7, no. 6: 6553-6572
- Nghi, T., Ngo Quang Toan, Do Thi Van Thanh, Nguyen Dinh Minh, Nguyen Van Vuong, 1991. Quaternary sedimentation of the principal deltas of Vietnam. *J. Southeast Asian Earth Sci.* 6, 103–110. doi:10.1016/0743-9547(91)90101-3
- Nguyen, T.T., Kawamura, A., Amaguchi, H., Nakagawa, N., 2011. Interactions Between the Red River and Groundwater of Confined Aquifer in Hanoi , Vietnam. Japan Society of Hydrology and Water Resources. Session ID: 10
- Nguyen, H.N., 2008. Human Development Report 2007 / 2008 Flooding in Mekong River Delta Vietnam. *Hum. Dev. Rep.* 4.
- Nohara, D., Kitoh, A., Hosaka, M. and Oki, T., 2006. Impact of climate change on river discharge projected by multimodel ensemble. *Journal of Hydrometeorology*, 7(5), pp.1076-1089
- Norrman, J., Sparrenbom, C.J., Berg, M., Dang, D.N., Jacks, G., Harms-Ringdahl, P., Pham, Q.N., Rosqvist, H., 2015. Tracing sources of ammonium in reducing groundwater in a well field in Hanoi (Vietnam) by means of stable nitrogen isotope ( $\delta^{15}\text{N}$ ) values. *Appl. Geochemistry* 61, 248–258. doi:10.1016/j.apgeochem.2015.06.009
- Oude Essink, G.H.P., 2001. Improving fresh groundwater supply - Problems and solutions. *Ocean Coast. Manag.* 44, 429–449. doi:10.1016/S0964-5691(01)00057-6
- Pham, N.Q., Tran, L.T., Larsen, F., Gerber, C., Purtschert, R., 2015. Groundwater Recharge for Pleistocene Aquifer in the Southwest of Red River Delta, Vietnam.
- Post, V.E., Groen, J., Kooi, H., Person, M., Ge, S. and Edmunds, W.M., 2013. Offshore fresh groundwater reserves as a global phenomenon. *Nature*, 504(7478), pp.71-78

- Queensland Government 2016. Impacts of salinity.  
<https://www.qld.gov.au/environment/land/soil/salinity/impacts/>
- Rhoodles, D., Kandiah, A. and Mashali, A.M., 1992. The use of saline waters for crop production-FAO irrigation and drainage paper 48
- Sandwell, D.T., Gille, S.T., and Smith, W.H.F., 2002. Bathymetry from Space. Oceanography, Geophysics, and Climate, Geoscience Professional Services, Bethesda, Maryland. 24pp.
- Statistical Documentation and Service Centre - General Statistics Office of Vietnam, 2011, “Area, population and population density in 2011 by province”
- Szabo, S., Brondizio, E., Renaud, F.G., Hetrick, S., Nicholls, R.J., Matthews, Z., Tessler, Z., Tejedor, A., Sebesvari, Z., Foufoula-Georgiou, E., da Costa, S., Dearing, J.A., 2016. Population dynamics, delta vulnerability and environmental change: comparison of the Mekong, Ganges–Brahmaputra and Amazon delta regions. *Sustain. Sci.* 11, 539–554. doi:10.1007/s11625-016-0372-6
- Tran, L.T., Larsen, F., Pham, N.Q., Christiansen, A. V., Tran, N., Vu, H. V., Tran, L. V., Hoang, H. V., Hinsby, K., 2012. Origin and extent of fresh groundwater, salty paleowaters and recent saltwater intrusions in Red River flood plain aquifers, Vietnam. *Hydrogeol. J.* 20, 1295–1313. doi:10.1007/s10040-012-0874-y
- Van Pham, H., Lee, S.-I., 2014. Assessment of seawater intrusion potential from sea-level rise and groundwater extraction in a coastal aquifer. *Desalin. Water Treat.* 3994, 1–15. doi:10.1080/19443994.2014.971617
- Waelbroeck, C., Labeyrie, L., Michel, E., Duplessy, J.C., McManus, J.F., Lambeck, K., Balbon, E., Labracherie, M., 2002. Sea-level and deep water temperature changes derived from benthic foraminifera isotopic records. *Quat. Sci. Rev.* 21, 295–305. doi:10.1016/S0277-3791(01)00101-9
- Wagner, Frank, Dang Tran Trung, Hoang Dai Phuc, and Falk Lindenmaier, 2011, “Assessment of Groundwater Resources in Nam Dinh Province”, Final Technical Report of improvement of Groundwater Protection in Vietnam, Ha Noi
- Winkel, L.H.E., Trang, P.T.K., Lan, V.M., Stengel, C., Amini, M., Ha, N.T., Viet, P.H., Berg, M., 2011. Arsenic pollution of groundwater in Vietnam exacerbated by deep aquifer exploitation for more than a century. *Proc. Natl. Acad. Sci.* 108, 1246–1251. doi:10.1073/pnas.1011915108
- Wolf, M. 2015. Effects of Land Use Change on Groundwater Recharge A Case Study in the Day River Basin, Vietnam, Master’s Thesis. Water Science and Management, Faculty of Geosciences, Utrecht University
- World Health Organization (WHO), 1996, “Guidelines for drinking water quality”, 2nd Edition, vol. 2, Health criteria and other supporting information, 1996, (pp 940–949) and Addendum to vol 2, 1998 (pp 281–283), World Health Organization. Geneva
- World Bank Group, 2016, “Vietnam”, <http://www.worldbank.org/en/country/vietnam>
- Yang, J., Graf, T., Ptak, T., 2015. Impact of climate change on freshwater resources in a heterogeneous coastal aquifer of Bremerhaven, Germany: A three-dimensional modeling

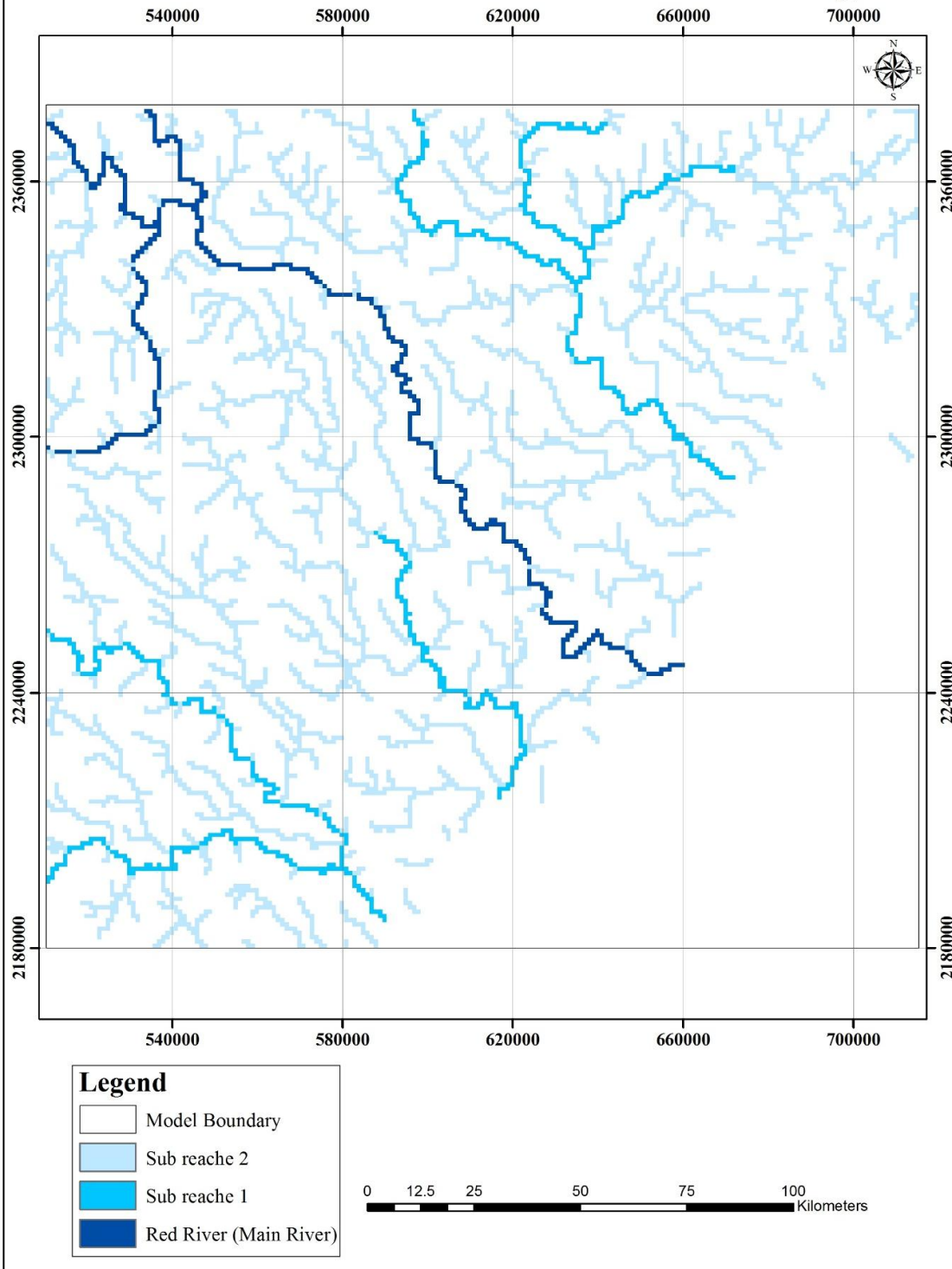
study. J. Contam. Hydrol. 177–178, 107–121. doi:10.1016/j.jconhyd.2015.03.014

## Appendices

## Appendix 1:



## River Network in Red River Delta Region



## Appendix 2: Recharge Rate Estimation

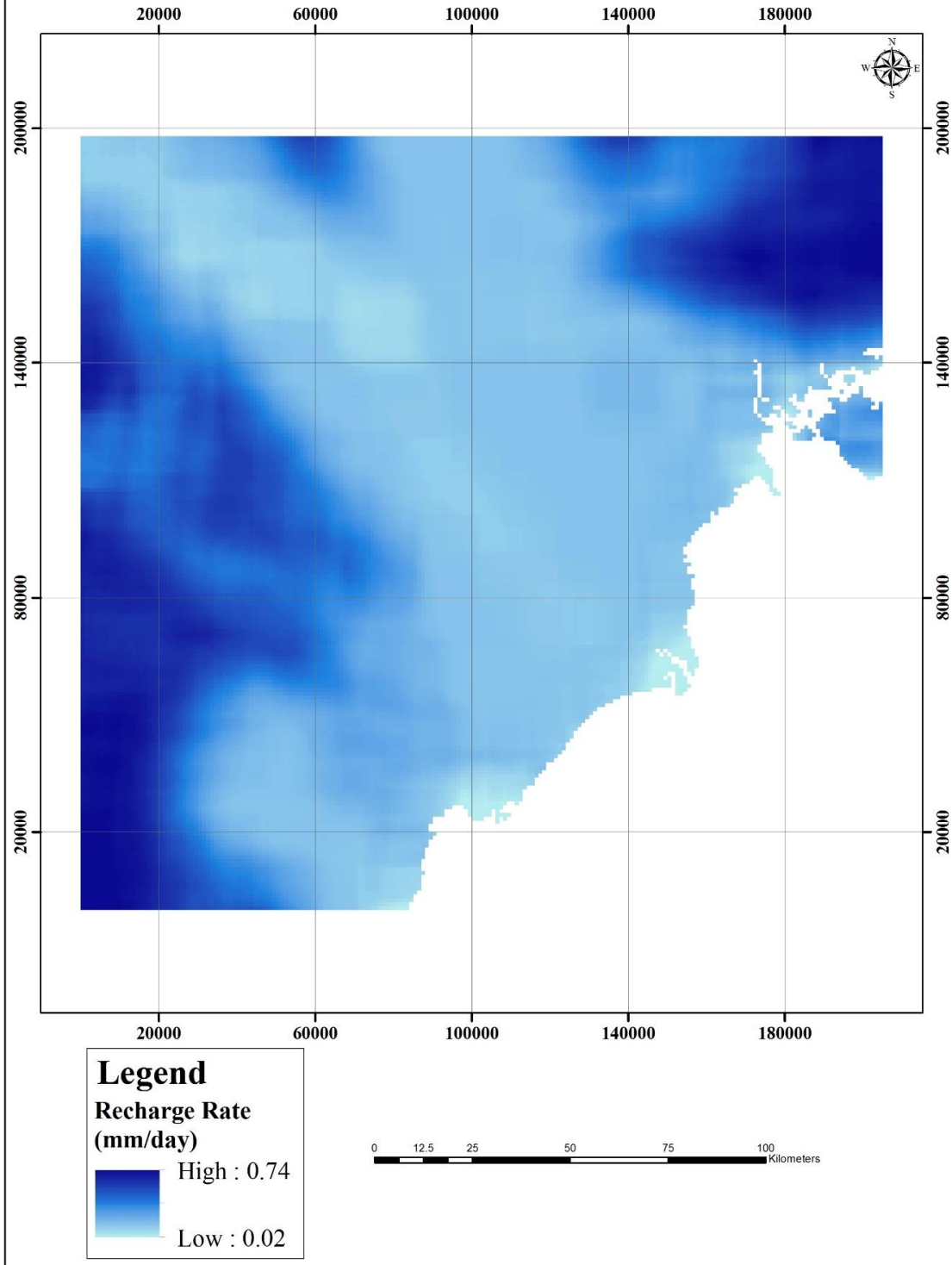
Estimating the fractions from Wolf, 2016

Type	Available land use type from GLC-SHARE	Land use type used by Wolf, 2016	Fractions derived from Wolf, 2016				Percentage Used	
			Dry Season		Wet Season			
			Min	Max	Min	Max		
1	Artificial surface	Residence – high density	0	0.1	0.6	1.8	0.625	
2	Crop lands	Paddy field	1.5	5.3	7.9	25.5	10.05	
3	Grass lands	Pasture (grass)	4.3	23.1	20.3	42.6	22.575	
4	Tree covered area	Evergreen forest	4	19.4	13.4	42.1	19.725	
5	Shrubs	Shrub-land	2.5	11	11.3	34.8	14.9	
6	Mangroves	Mangroves	3	10.6	9.3	30	13.225	

Net recharge rates calculation

Source: Wagner et al., 2011 (mm)	Precipitation in 2007						Recharge for each land use type (mm)
	1	2	3	4	5	6	
January	5	0.03	0.505	1.13	1	0.75	0.66
February	9	0.054	0.909	2.034	1.8	1.35	1.188
March	34	0.204	3.434	7.684	6.8	5.1	4.488
April	30	0.18	3.03	6.78	6	4.5	3.96
May	87	0.522	8.787	19.662	17.4	13.05	11.484
June	71	0.426	7.171	16.046	14.2	10.65	9.372
July	204	1.224	20.604	46.104	40.8	30.6	26.928
August	421	2.526	42.521	95.146	84.2	63.15	55.572
September	186	1.116	18.786	42.036	37.2	27.9	24.552
October	144	0.864	14.544	32.544	28.8	21.6	19.008
November	4	0.024	0.404	0.904	0.8	0.6	0.528
December	7	0.042	0.707	1.582	1.4	1.05	0.924
Total	1202	7.212	121.402	271.652	240.4	180.3	158.664
Recharge Rate (mm/day)		<b>0.02</b>	<b>0.33</b>	<b>0.74</b>	<b>0.66</b>	<b>0.49</b>	<b>0.43</b>

## Recharge Flux in Red River Delta Regions

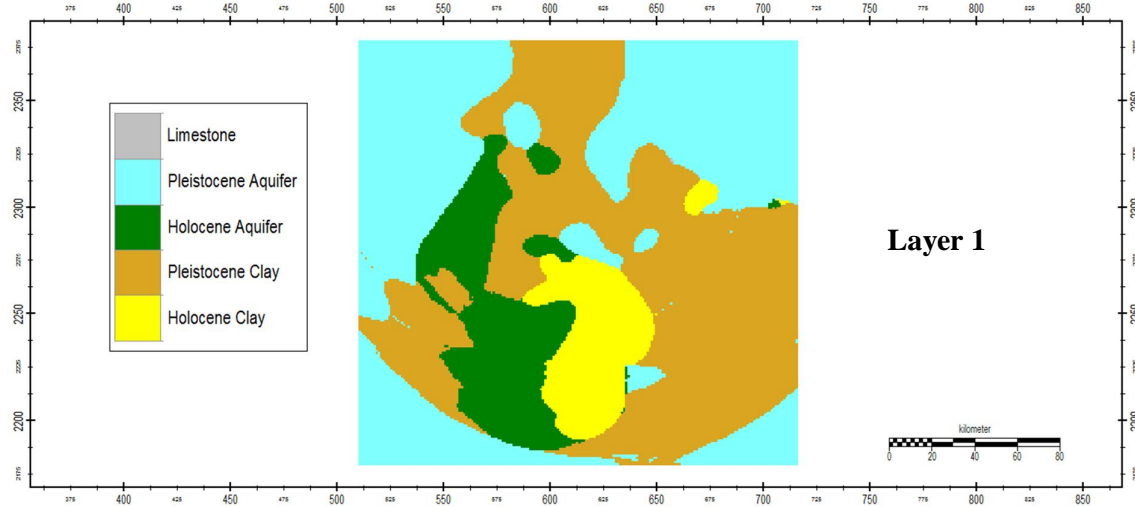


### Appendix 3: Estimation of Pumping Rates

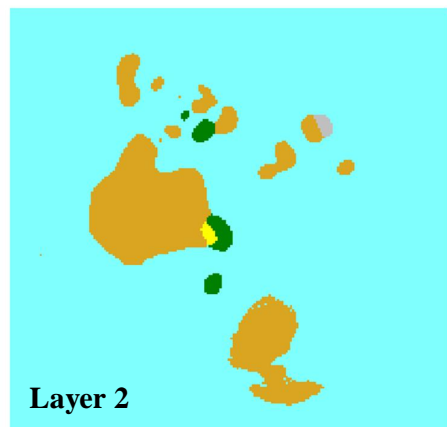
	Population in 2010 (*1000)	Population in 2110 (*1000)
<b>Hai Dong</b>	1718.9	3558.123
<b>Bac Ninh</b>	1060.3	2194.821
<b>Ha Nam</b>	786.9	1628.883
<b>Hai Phong</b>	1878.5	3888.495
<b>Hanoi</b>	8877.9	18377.253
<b>Hung Yen</b>	1150.4	2381.328
<b>Nam Dinh</b>	1833.5	3795.345
<b>Ninh Binh</b>	906.5	1876.455
<b>Thain Binh</b>	1786	3697.02

			Pumping rate per well (m <sup>3</sup> /day)			
Year	Province	No. of Wells	1970	1990	2010	2110
1970	Hanoi	244	819.6721311			
<b>Total pumping in 1970 = 200 000 m<sup>3</sup>/day</b>						
1990	Hanoi	244		1639.344262		
	Hai Phong	30		333.3333333		
	Nam Dinh	18		555.5555556		
	Hai Duong	68		147.0588235		
<b>Total pumping in 1990 = 430 000 m<sup>3</sup>/day</b>						
2010	Hai Duong	68			2277.830674	
	Bac Ninh	27			3538.708061	
	Ha Nam	22			3223.120947	
	Hai Phong	30			5642.47551	
	Hanoi	244			3278.688525	
	Hung Yen	22			4712.007037	
	Nam Dinh	19			8695.750121	
	Ninh Binh	4			20421.49607	
	Thai Binh	26			6189.96003	
<b>Total pumping in 2010 = 1 802 128.8 m<sup>3</sup>/day</b>						
2110	Hai Duong	68				4715.109495
	Bac Ninh	27				7325.125687
	Ha Nam	22				6671.86036
	Hai Phong	30				11679.92431
	Hanoi	244				6786.885246
	Hung Yen	22				9753.854566
	Nam Dinh	19				18000.20275
	Ninh Binh	4				42272.49687
	Thai Binh	26				12813.21726
<b>Total pumping in 2110 = 3 730 406.8 m<sup>3</sup>/day</b>						

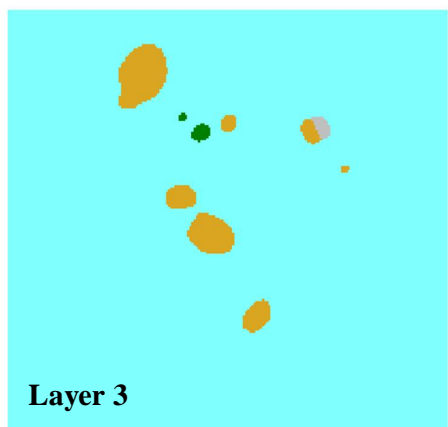
## Appendix 4: Geological Distribution in Model Layers



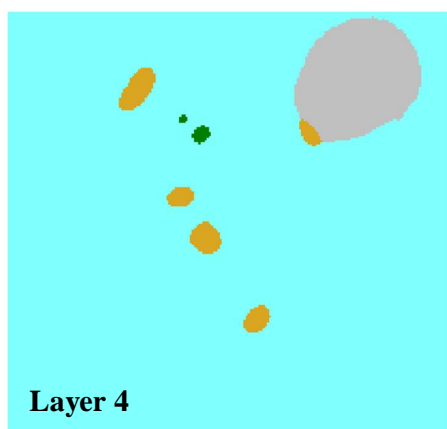
Layer 1



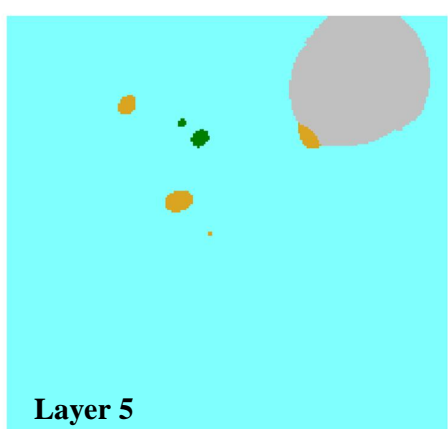
Layer 2



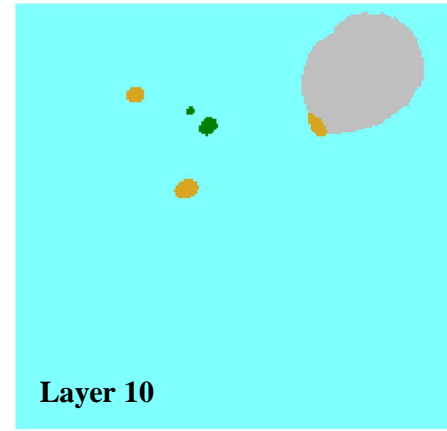
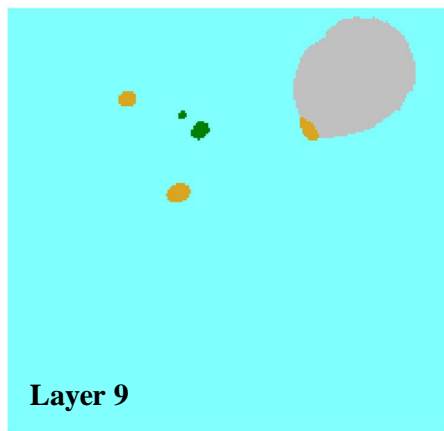
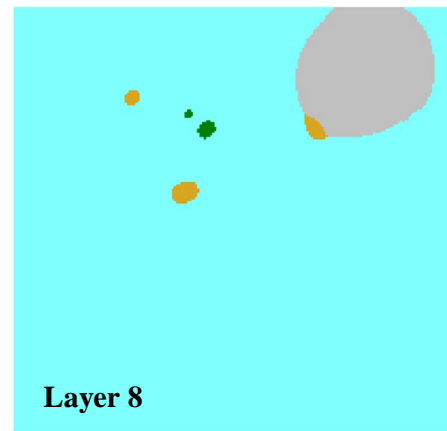
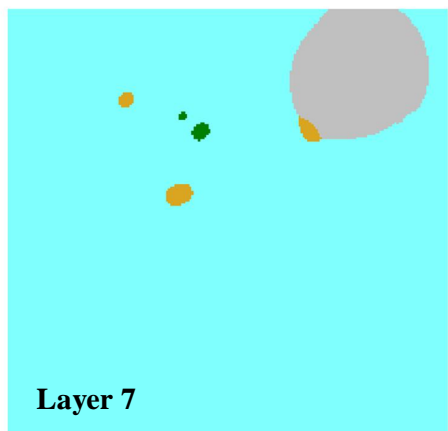
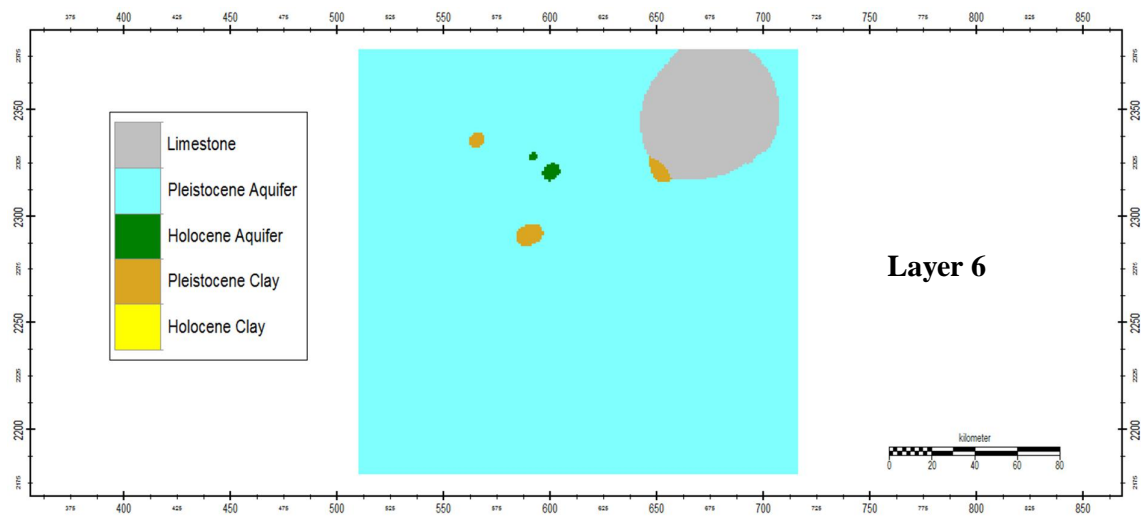
Layer 3



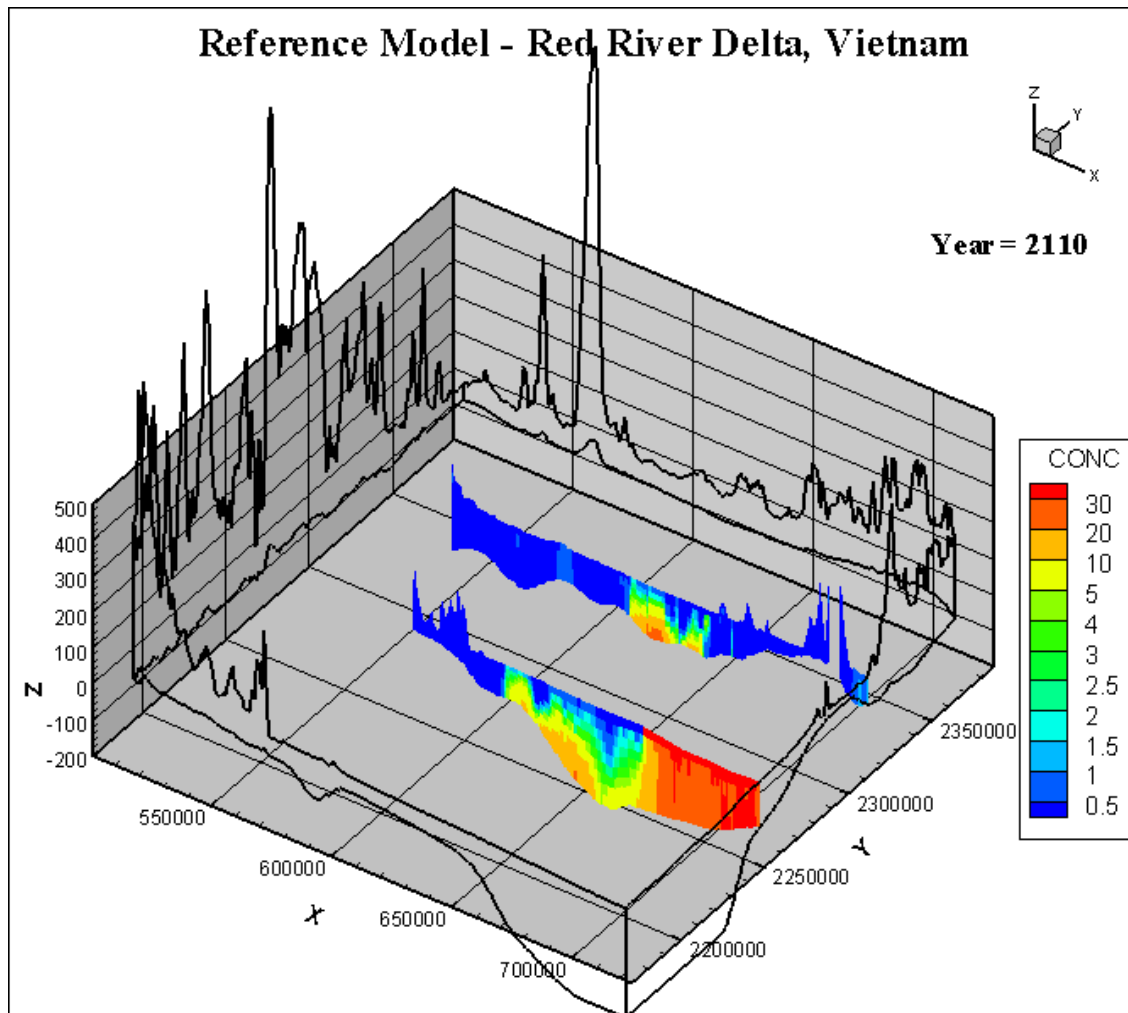
Layer 4



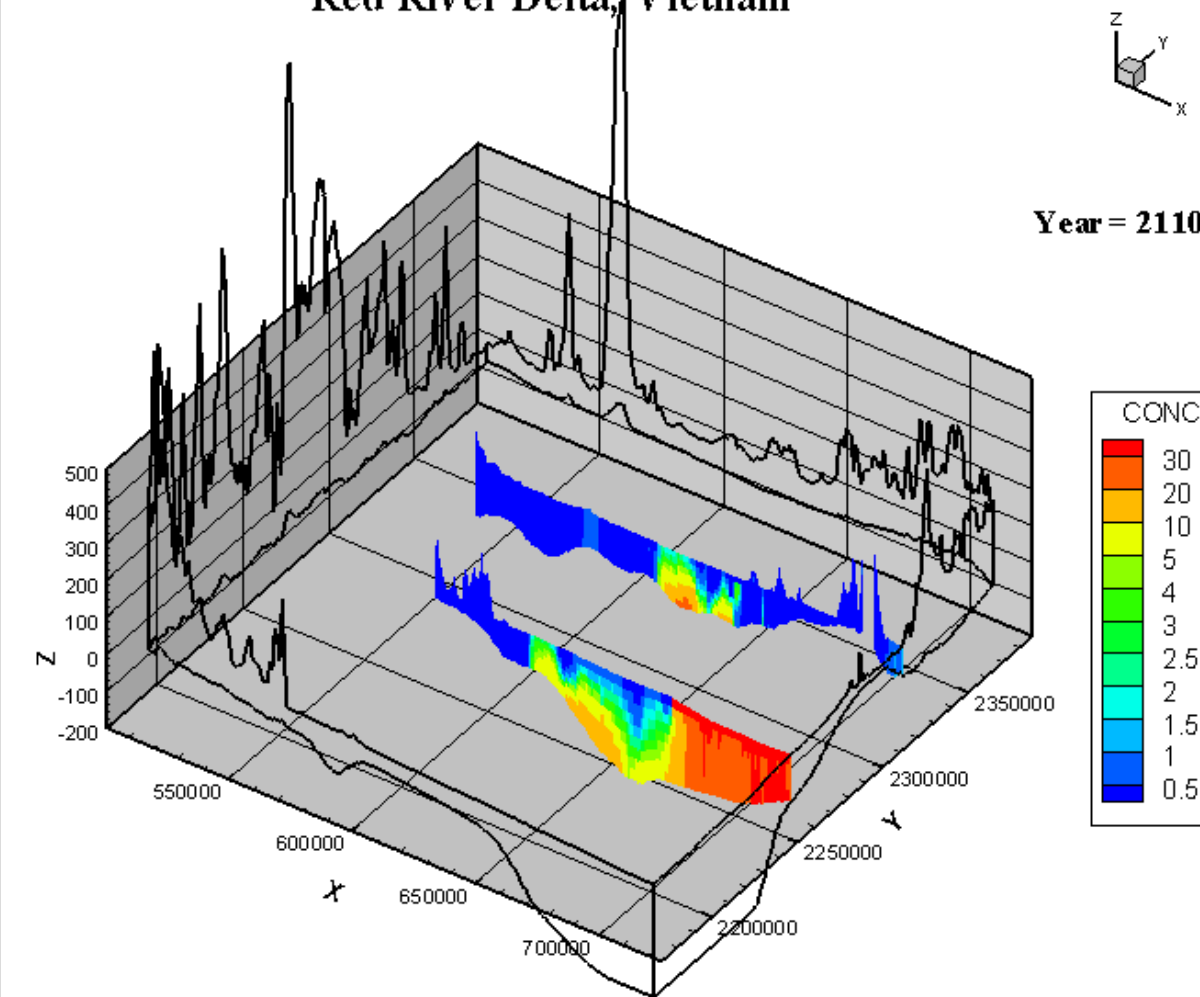
Layer 5



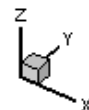
## Appendix 5: Future Scenario Simulation



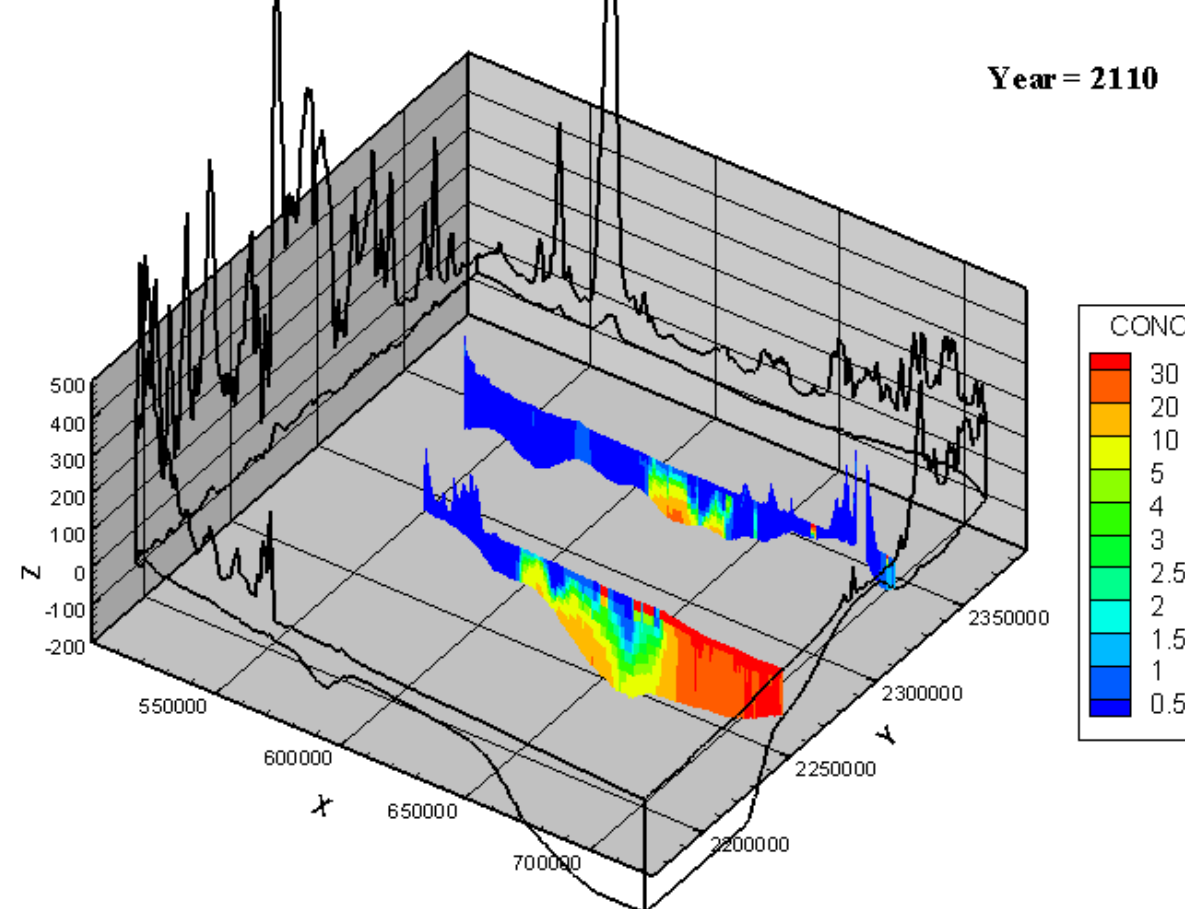
## Future Prediction for Increase in Pumping Rates Red River Delta, Vietnam



## Future Prediction with MSLR Red River Delta, Vietnam



Year = 2110



## Future Prediction with Increase Pumping Rates and MSLR Red River Delta, Vietnam

